Physics Reports 489 (2010) 89–159

Contents lists available at ScienceDirect

Physics Reports

journal homepage: www.elsevier.com/locate/physrep

Theoretical aspects of the magnetocaloric effect

N.A. de Oliveira *, P.J. von Ranke

Instituto de Física Armando Dias Tavares- Universidade do Estado do Rio de Janeiro, Rua São Francisco Xavier 524, Rio de Janeiro, 20550-013, RJ, Brazil

ARTICLE INFO

Article history:
Accepted 29 October 2009
Available online 4 December 2009
editor: D.L. Mills

Keywords:
Magnetocaloric effect
Magnetism
Spins Hamiltonians
Band models
Metals and alloys

ABSTRACT

The magnetocaloric effect is the heating or cooling of magnetic materials when subjected to magnetic field variation. It is characterized by the temperature change (ΔT_{ad}) in an adiabatic process and by the entropy change (ΔS_{iso}) in an isothermal process. The renewed interest in the magnetocaloric effect can be attributed to Brown's work concerning the near room temperature magnetic refrigerator and Pecharsky and Gschneidner's discovery of the giant magnetocaloric effect near room temperature in $Gd_5Si_2Ge_2$. After these pioneering works, the magnetocaloric effect has been intensively studied in a great number of magnetic materials. Despite this intense study, the underlying physics behind the magnetocaloric effect is not yet completely understood. In this report, we discuss the theoretical aspects of the magnetocaloric effect in rare earth metals and their alloys as well as in transition metal based compounds. In particular, we discuss the effects of pressure, doping, anisotropy and magnetoelastic interaction on the magnetocaloric potentials ΔS_{iso} and ΔT_{ad}. The magnetocaloric effect in rare earth based compounds is discussed by using model Hamiltonians of interacting localized magnetic moments, including the crystalline electrical field interaction and the magnetoelastic coupling. The discussion of the magnetocaloric effect in transition metal based compounds is made by using model Hamiltonians based in the framework of the band theory. The results discussed in this report reveal important aspects of the magnetocaloric effect as well as point out some new perspectives on this area of research.

Contents

1. Introduction 90
2. Thermodynamics of the magnetocaloric effect 91
   2.1. Alternative determination of the magnetocaloric potentials 92
   2.2. Alternative processes for entropy change 96
3. Magnetic refrigeration 97
4. Magnetocaloric effect in rare earth compounds 99
   4.1. Theoretical formulation 99
      4.1.1. Magnetic Hamiltonian 100
      4.1.2. Crystalline lattice Hamiltonian 104
      4.1.3. Calculations without crystalline electrical field 106
   4.2. Application to Gd based compounds 107
   4.3. Application to RAl_2 compounds 109
   4.4. Application to RNi_2 compounds 112
   4.5. Application to RNi_5 compounds 112
   4.6. Anisotropic magnetocaloric effect: Application to $DyAl_2$ 114

* Corresponding author.
E-mail address: Nilson@uerj.br (N.A. de Oliveira).

0370-1573/$ – see front matter © 2009 Elsevier B.V. All rights reserved.
doi:10.1016/j.physrep.2009.12.006

4.7. Magnetocaloric effect in the two energy level model ... 117
4.8. Application to $Gd_5Si_2Ge_2$ ... 121
4.9. Alternative description of the magnetoelastic coupling ... 123
5. Magnetocaloric effect in transition metal based compounds ... 126
5.1. General formulation ... 126
5.2. Magnetic heat capacity and magnetic entropy ... 128
5.3. Total entropy and the magnetocaloric effect ... 129
5.4. Systematic study ... 129
5.5. Application to real compounds ... 131
6. Magnetocaloric effect in RCo_2 compounds ... 134
6.1. Theoretical formulation ... 134
6.2. Application to $ErCo_2$, $HoCo_2$, and $DyCo_2$ ... 136
7. Magnetocaloric effect in rare earth doped compounds ... 142
7.1. Theoretical formulation ... 142
7.2. Application to $(Tb_{1-c}Ho_c)Ni_2$ ... 145
7.3. Application to $(Ho_{1-c}Er_c)Co_2$ ... 146
8. Magnetocaloric effect in antiferromagnets and ferrimagnets ... 148
8.1. Theoretical formulation ... 149
8.2. Systematic study ... 151
9. Conclusions and perspectives ... 155
Acknowledgments ... 155
References ... 155

1. Introduction

The magnetocaloric effect, firstly discovered by Warbourg [1] in 1881, is the heating or cooling of magnetic materials subjected to magnetic field variation. The heating/cooling process through the magnetic field variation can be roughly described in the following way: when the magnetic field is adiabatically applied to a usual ferromagnetic material, their magnetic moments become ordered, so that the magnetic part of the total entropy is reduced. Therefore, in order to keep constant the total entropy in the adiabatic process, the crystalline lattice entropy should increase. As a result, the material heats up. An opposite effect occurs, i.e., the material cools down, if the magnetic field is adiabatically removed.

The magnetocaloric effect is characterized by the entropy change in an isothermal process (ΔS_{iso}) and by the temperature change in an adiabatic process (ΔT_{ad}) upon magnetic field variation. The magnetocaloric potential ΔT_{ad} can be directly measured by using a thermometer, or indirectly by using specific heat data. On the other hand, the magnetocaloric potential ΔS_{iso} can only be obtained indirectly by using specific heat or magnetization data. It should be mentioned that the determination of ΔS_{iso} using magnetization data via the relation $\Delta S_{iso} = \int (\partial M/\partial T)\mathrm{d}B$ is effective for compounds with second order phase transition. However, there is much controversy over the use of this relation to determine the isothermal entropy change in compounds with first order phase transition. This aspect is addressed in the next section of this report.

The magnetocaloric effect can be used for some technological applications. For instance, the magnetocaloric effect can be applied for the physical treatment of some types of cancer [2]. Such an application relies on the existence of biocompatible magnetic nanoparticles that are mainly absorbed by cancerous cells. Thus, it is supposed that these magnetic nanoparticles heated via magnetic field variation, can kill the cancerous cells without damage to the healthy ones. This application of the magnetocaloric effect still needs much multidisciplinary effort to be used in humans. At the present time, the main application of the magnetocaloric effect is in magnetic refrigeration. Magnetic refrigeration is an environmental friendly technology, because magnetic compounds are used as the cooling materials and water or non poisonous fluids are used as heat exchanger. It is expected that magnetic refrigerators operate with an energy saving of up to 30% as compared with the conventional vapor cycle refrigerators. The process of cooling using magnetic field variation was independently proposed in 1926/1927, by Debye [3] and Giauque [4], through a process called adiabatic demagnetization. This process was demonstrated for the first time in the history of physics, a few years later when in 1933 Giauque and MacDougall [5] reached temperatures as low as 0.25 K. However, the great step towards room temperature magnetic refrigeration was only given in 1976, when Brown [6] developed a magnetic refrigerator using metallic gadolinium as a magnetic refrigerant. In his prototype magnetic refrigerator, Brown obtained a temperature reduction from 319 K to 272 K for a magnetic field variation from 0 to 7 T. After Brown's work, much effort has been done in order to make room temperature magnetic refrigeration feasible.

The magnetocaloric effect has been intensively studied in the last forty years, and much experimental data have been reported in the literature. For an overview on the experimental data of the magnetocaloric effect, we suggest the References [7–15]. The magnetocaloric effect has been mostly studied in rare earth metals and their alloys. The reference material for the magnetocaloric potentials is metallic gadolinium. In this material, the magnetocaloric potentials ΔS_{iso} and ΔT_{ad}, at the transition temperature around 292 K, upon magnetic field variation from 0 to 5 T are approximately 10 J/(kg K) and 10 K respectively. In 1997, Pecharsky and Gschneidner [16,17] discovered a very large value of the magnetocaloric potential ΔS_{iso} in the compound $Gd_5Si_2Ge_2$, which undergoes a first order phase transition near room

temperature. They have shown that the peak in the isothermal entropy change in $Gd_5Si_2Ge_2$ around 273 K, upon magnetic field variation from 0 to 5 T is about 20 J/(kg K). Due to this large value of the isothermal entropy change, as compared with the one found in metallic gadolinium, this effect was called giant magnetocaloric effect. Since the discovery of the giant magnetocaloric effect in $Gd_5Si_2Ge_2$, the search for new magnetic materials with large values of the magnetocaloric potentials has attracted the attention of scientists all over the world. Pecharsky and Gschneidner showed that the series of compounds $Gd_5(Si_xGe_{1-x})_4$ for $x < 0.5$ also exhibit the giant magnetocaloric effect [18,19]. Many other papers [20–41] have been published on the magnetocaloric effect in the series of compounds $Gd_5(Si_xGe_{1-x})_4$ and $Tb_5(Si_xGe_{1-x})_4$. The magnetocaloric effect has also been studied in transition metal based compounds [43–71], amorphous materials [72–83], nanocomposites and molecular clusters [84–89]. For instance, there are available experimental data of the magnetocaloric potentials in the pure metals Fe, Co and Ni [42]; in the compounds MnAs [43–48] ; $MnFeP_{1-x}As_x$ [49–51], $La(Fe_xM_{1-x})_{13}$(M = Co, Si) [52–61]; in Heusler alloys [62–66] and in manganites [67–71]. It is worth mentioning that the giant magnetocaloric effect has also been found in the compounds MnAs; $MnFeP_{0.45}As_{0.55}La(Fe_xSi_{1-x})_{13}$ and in Heusler alloys.

The behavior of the magnetocaloric potential ΔS_{iso} depends on the particularity of the magnetic state. For instance, in usual ferromagnets undergoing a second order phase transition, such as Gd; RAl_2 and RNi_2 (R = rare earth), the magnetocaloric potential ΔS_{iso} exhibits a peak around the magnetic ordering temperature and goes down smoothly, outside the region of the magnetic phase transition. In ferromagnets undergoing a first order phase transition, such as $Gd_5(Si_2Ge_2)$; MnAs; $MnFeP_{0.45}As_{0.55}$ and $La(Fe_xSi_{1-x})_{13}$, the magnetocaloric potential ΔS_{iso} exhibits a sharp peak around the magnetic ordering temperature and goes down quickly, farther way. The inverse magnetocaloric effect, i.e., negative values in the $-\Delta S_{iso}$ curves, has been observed in the paramagnetic compounds $PrNi_5$ [90], $TmPO_4$ [91] and $HoVO_4$ [92]; in the antiferromagnetic compounds NiMnIn [62–64]; NiMnSb [65]; $Ni_2Mn_{1-x}Cu_xGa$ [66]; $ErRu_2Si_2$ [93]; $CoMnSi_{1-x}Ge_x$ [94]; $Mn_{1.82}V_{0.18}Sb$ [95]; $CeFe_2$ [96] and in the manganite $Pr_{1-x}Ca_xMnO_3$ [69]. The table-like behavior, i.e., a plateau in the ΔS_{iso} curve, has been observed in the compound $(Gd_{1-x}Er_x)NiAl$ [97] and in the nanocrystalline sample $Pr_{0.65}(Ca_{0.6}Sr_{0.4})_{0.35}MnO_3$ [98]. In addition, a double peak has been observed in the ΔS_{iso} curve of the compound Gd_3Al_2 [99].

The magnetocaloric effect has also been studied from the theoretical point of view and much experimental data have been explained [100–128]. Important aspects of the magnetocaloric effect such as: crystalline electrical field [90,100] magnetoelastic coupling [101], spins fluctuations [102,103] and electron correlations [104] have already been addressed in the literature. However, despite the great success of the theoretical papers in explaining the experimental data, the physics behind the magnetocaloric effect is not yet completely understood.

In this report, we theoretically discuss the magnetocaloric effect in crystalline bulk compounds, taking into account the origin of their magnetism. The magnetocaloric effect in rare earth based compounds, is described by model Hamiltonians of localized interacting magnetic moments, in which the mean field approximation is used to treat the two-body exchange interaction. On the other hand, the theoretical description of the magnetocaloric effect in transition metal based compounds is made in the framework of the band theory, by considering the electron–electron interaction and the magnetoelastic coupling. This report is organized as follows: in Section 2, we discuss the thermodynamics of magnetism and the magnetocaloric effect. In Section 3, we briefly illustrate the application of the magnetocaloric effect in magnetic refrigeration. Section 4 is devoted to the study of the magnetocaloric effect in rare earth based compounds. In Section 5, we present the theoretical discussion of the magnetocaloric effect in transition metal based compounds. In Section 6, we discuss the magnetocaloric effect in the Laves phase intermetallic compounds RCo_2. Section 7 deals with the magnetocaloric effect in rare earth doped compounds. Finally, in Section 8 we discuss the magnetocaloric effect in antiferromagnets and ferrimagnets.

2. Thermodynamics of the magnetocaloric effect

In order to discuss the thermodynamics of the magnetocaloric effect in a solid material, it is necessary to know the total entropy under the action of an applied magnetic field. Generally speaking, the total entropy of a magnetic material is made up of the contributions from the crystalline lattice (S_{lat}), from the conduction electrons (S_{el}), from the atomic magnetic moments (S_{mag}) and from the atomic nucleus (S_{nuc}). The contribution from the nucleus to the magnetocaloric effect can be neglected, since it is only important at very low temperature. Thus, as a good approximation, the total entropy of a solid can be written as:

$$S(T, B, P) = S_{el}(T, B, P) + S_{mag}(T, B, P) + S_{lat}(T, B, P). \tag{1}$$

In the general case, the contributions S_{lat}, S_{el}, and S_{mag} are supposed to depend on temperature, magnetic field and pressure. However, for the sake of simplicity, we suppose in this section, that the crystalline lattice and the electronic entropy do not depend on the applied magnetic field and pressure. It is well known that for a given magnetic field, the total entropy of a usual ferromagnet increases with increasing temperature. On the other hand, for a given temperature, the total entropy of a usual ferromagnet decreases with increasing applied magnetic field. In Fig. 1 is schematically plotted the total entropy (S) of a usual ferromagnet, as a function of temperature, for two values of the applied magnetic field B_1 and B_2 under the condition $B_2 > B_1$. In this figure are also represented the magnetocaloric potentials ΔS_{iso} and ΔT_{ad}.

In order to qualitatively discuss the behavior of the magnetocaloric potentials ΔS_{iso} and ΔT_{ad}, we consider the entropy versus temperature diagram shown in Fig. 1. The magnetocaloric potential ΔS_{iso} is obtained by taking the difference between the entropy in the final and initial states of any isothermal process. For instance, in the isothermal process represented by the path AB in the diagram of Fig. 1, the entropy change is $\Delta S_{iso} = S_B - S_A < 0$ since $S_B < S_A$. The sign of ΔS_{iso} is opposite,

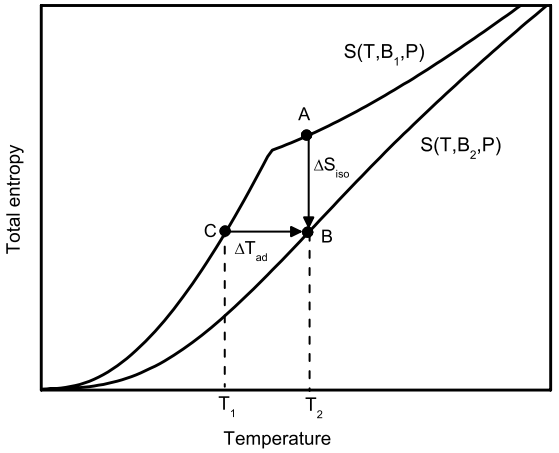

Fig. 1. Entropy versus temperature diagram for two values of applied magnetic field.

i.e., $\Delta S_{iso} > 0$ if the magnetic field is isothermally removed from the initial state B to final state A. According to the entropy versus temperature diagram shown in Fig. 1, the isothermal entropy change ΔS_{iso} upon magnetic field variation from B_1 to B_2 is determined by:

$$\Delta S_{iso}(T, B_2 - B_1, P) = S(T, B_2, P) - S(T, B_1, P). \tag{2}$$

The magnetocaloric potential ΔT_{ad} is obtained by taking the difference between the temperature of the final and initial states in any adiabatic process. For instance, when the magnetic field is adiabatically applied in the process represented by the path *CB* in Fig. 1, the temperature change is positive, ($\Delta T_{ad} > 0$) and the material heats up. When the magnetic field is adiabatically removed in the process represented by the path *BC* in Fig. 1, the temperature change is negative, ($\Delta T_{ad} < 0$) and the material cools down. According to the entropy versus temperature diagram shown in Fig. 1, the adiabatic temperature change, upon magnetic field variation from B_1 to B_2 is determined by:

$$\Delta T_{ad}(T, B_2 - B_1, P) = T_2(B_2) - T_1(B_1), \tag{3}$$

under the adiabatic condition $S(T_2, B_2, P) = S(T_1, B_1, P)$.

2.1. Alternative determination of the magnetocaloric potentials

In the previous discussion, the magnetocaloric potentials ΔS_{iso} and ΔT_{ad} were determined on the basis of the total entropy diagram. However, there are analytical expressions for the magnetocaloric potentials in terms of the total entropy and specific heat capacity. In addition, the magnetocaloric potentials ΔS_{iso} and ΔT_{ad} can also be indirectly determined by using magnetization data. In order to show this, we consider for the sake of simplicity that the entropy depends only on temperature and magnetic field, i.e., $S(T, B)$. An increment in temperature (δT) and magnetic field (δB) yields the following change in the entropy:

$$\delta S(T, B) = S(T + \delta T, B + \delta B) - S(T, B). \tag{4}$$

Using the mean value theorem from the fundamental calculus [129], we can rewrite the equation before as:

$$\delta S(T, B) = \left[\frac{\partial S(T_C, B)}{\partial T}\right]_B \delta T + \left[\frac{\partial S(T, B_C)}{\partial B}\right]_T \delta B. \tag{5}$$

The partial derivative $\partial S(T_C, B)/\partial T$ can be written as [129]:

$$\left[\frac{\partial S(T_C, B)}{\partial T}\right]_B = \left[\frac{\partial S(T, B)}{\partial T}\right]_B + \left[\frac{\delta S(T_C, B)}{\delta T}\right]_B, \tag{6}$$

where $[\delta S(T_C, B)/\delta T]_B$ is the difference between the derivatives at the points T_C and T. A similar relation holds for $[\delta S(T, B_C)/\delta B]_T$. Thus, in the infinitesimal limit, we can rewrite Eq. (5) in the form:

$$\mathrm{d}S(T, B) = \left\{\left[\frac{\partial S(T, B)}{\partial T}\right]_B + \left[\frac{\delta S(T_C, B)}{\delta T}\right]_B\right\} \mathrm{d}T + \left\{\left[\frac{\partial S(T, B)}{\partial B}\right]_T + \left[\frac{\delta S(T, B_C)}{\delta B}\right]_T\right\} \mathrm{d}B. \tag{7}$$

For compounds undergoing a second order phase transition, the entropy is a continuous function of temperature and magnetic field. In this case, the terms $[\delta S(T_C, B)/\delta T]_B$ and $[\delta S(T, B_C)/\delta B]_T$ go to zero, so that the total differential of the entropy is then given by:

$$\mathrm{d}S(T, B) = \left[\frac{\partial S(T, B)}{\partial T}\right]_B \mathrm{d}T + \left[\frac{\partial S(T, B)}{\partial B}\right]_T \mathrm{d}B. \tag{8}$$

In an isothermal process, the entropy change upon magnetic field variation from B_1 to B_2 in compounds undergoing a second order phase transition, is calculated by integrating Eq. (8) from B_1 to B_2 i.e.,

$$\Delta S_{iso}(T, \Delta B) = \int_{B_1}^{B_2} \left[\frac{\partial S(T, B)}{\partial B}\right]_T \mathrm{d}B, \tag{9}$$

where $\Delta S_{iso}(T, \Delta B) = S(T, B_2) - S(T, B_1)$. For an adiabatic process, Eq. (8) turns out to be:

$$\left[\frac{\partial S(T, B)}{\partial T}\right]_B \mathrm{d}T + \left[\frac{\partial S(T, B)}{\partial B}\right]_T \mathrm{d}B = 0. \tag{10}$$

From this equation, we can obtain:

$$\Delta T_{ad}(T, \Delta B) = -\int_{B_1}^{B_2} \frac{T}{C_B(T, B)} \left[\frac{\partial S(T, B)}{\partial B}\right]_T \mathrm{d}B, \tag{11}$$

where $\Delta T_{ad}(T, \Delta B) = [T(B_2) - T(B_1)]$ and $C_B(T, B) = T[\partial S(T, B)/\partial T]_B$ is the heat capacity at constant magnetic field.

For compounds undergoing a first order phase transition, the terms $[\delta S(T_C, B)/\delta T]_B$ and $[\delta S(T, B_C)/\delta B]_T$ should be kept in Eq. (7), so that the total differential of the entropy should be written considering whether the temperature and the magnetic field are inside or outside the region of the phase transition. For the range of temperatures and magnetic fields away from the first order phase transition, the terms $[\delta S(T_C, B)/\delta T]_B$ and $[\delta S(T, B_C)/\delta B]_T$ also go to zero, so that the total differential of the entropy is given by a relation similar to Eq. (8), i.e.:

$$\mathrm{d}S^{fo}_{out}(T, B) = \left[\frac{\partial S(T, B)}{\partial T}\right]_B \mathrm{d}T + \left[\frac{\partial S(T, B)}{\partial B}\right]_T \mathrm{d}B. \tag{12}$$

Here, we use the notation S^{fo}_{out} to characterize the entropy outside the region of the first order phase transition, where the entropy is a continuous function of temperature and magnetic field. Therefore, the entropy change in an isothermal process, far from the temperature region of the first order phase transition, is calculated by integrating Eq. (12) from B_1 to B_2 i.e.:

$$[\Delta S^{fo}_{iso}]_{out}(T, \Delta B) = \left\{\int_{B_1}^{B_2} \left[\frac{\partial S(T, B)}{\partial B}\right]_T \mathrm{d}B\right\}_{out}. \tag{13}$$

On the other hand, inside the temperature range of the first order phase transition, the isothermal entropy change upon magnetic field variation from B_1 to B_2, calculated from Eq. (7) is given by:

$$\int_{B_1}^{B_2} \mathrm{d}S^{fo}_{in}(T, B) = \int_{B_1}^{B_2} \left\{\left[\frac{\partial S(T, B)}{\partial B}\right]_T + \left[\frac{\delta S(T, B_C)}{\delta B}\right]_T\right\} \mathrm{d}B. \tag{14}$$

Here, we use the notation S^{fo}_{in} to characterize the entropy inside the region of the first order phase transition. The first term involving the partial derivative $[\partial S(T, B)/\partial B]_T$ is only defined in the magnetic field intervals $[B_1, B_C]$ and $[B_C + \delta B, B_2]$. Here B_C is the critical magnetic field, where the first order phase transition takes place. On the other hand, the second term is only defined in the magnetic field interval $[B_C, B_C + \delta B]$ with $\delta B \longrightarrow 0$. Thus, using this consideration the above expression may be explicitly written as:

$$[\Delta S^{fo}_{iso}]_{in}(T, \Delta B) = \int_{B_1}^{B_C} \left[\frac{\partial S(T, B)}{\partial B}\right]_T \mathrm{d}B + \int_{B_C+\delta B}^{B_2} \left[\frac{\partial S(T, B)}{\partial B}\right]_T \mathrm{d}B + [\delta S(T, B_C)]_T. \tag{15}$$

Note that, if there is no first order phase transition, the last term vanishes, so that the isothermal entropy change is reduced to Eq. (9). *However, it should be emphasized that inside the temperature region of the first order phase transition, the determination of* ΔS_{iso} *using* Eq. (9) *is not valid.*

Now we discuss the evaluation of ΔS_{iso} around the first order phase transition using magnetization data. In order to do this, we consider for the sake of simplicity, the Gibbs free energy as a function of temperature and magnetic field, i.e., $G(T, B)$. The change in the free energy as the temperature goes from T to $T + \delta T$ and the magnetic field goes from B to $B + \delta B$ is given by: $\delta G(T, B) = G(T + \delta T, B + \delta B) - G(T, B)$. Following the same procedure used before, we can write in the infinitesimal limit that:

$$\mathrm{d}G(T, B) = \left\{\left[\frac{\partial G(T, B)}{\partial T}\right]_B + \left[\frac{\delta G(T_C, B)}{\delta T}\right]_B\right\} \mathrm{d}T + \left\{\left[\frac{\partial G(T, B)}{\partial B}\right]_T + \left[\frac{\delta G(T, B_C)}{\delta B}\right]_T\right\} \mathrm{d}B. \tag{16}$$

For compounds undergoing a second order phase transition the terms $[\delta G(T_C, B)/\delta T]_B$ and $[\delta G(T, B_C)/\delta B]_T$ go to zero, so that the differential "dG" becomes:

$$\mathrm{d}G(T, B) = \left[\frac{\partial G(T, B)}{\partial T}\right]_B \mathrm{d}T + \left[\frac{\partial G(T, B)}{\partial B}\right]_T \mathrm{d}B. \tag{17}$$

Using the thermodynamic relations $S = -[\partial G(T, B)/\partial T]_B$ and $M = -[\partial G(T, B)/\partial B]_T$ we can write: $\mathrm{d}G(T, B) = -S(T, B)\mathrm{d}T - M(T, B)\mathrm{d}B$. Since the free energy $G(T, B)$ is an exact differential, we can write the following Maxwell relation $[\partial S(T, B)/\partial B]_T = [\partial M(T, B)/\partial T]_B$. Using this Maxwell relation, we can replace in Eq. (9) the derivative $[\partial S(T, B)/\partial B]_T$ by $[\partial M(T, B)/\partial T]_B$, so that the isothermal entropy change for compounds undergoing a second order phase transition can be written as:

$$\Delta S_{iso}(T, \Delta B) = \int_{B_1}^{B_2} \left[\frac{\partial M(T, B)}{\partial T}\right]_B \mathrm{d}B. \tag{18}$$

This equation enables us to determine the magnetocaloric potential ΔS_{iso} by using $M \times T$ curves. In addition, this equation shows that the isothermal entropy change is expected to be maximum around the magnetic ordering temperature, since $(\partial M/\partial T)$ is maximum there. For practical purpose, the previous equation can be written in the form:

$$\Delta S_{iso}(T, \Delta B) = \frac{1}{\delta T} \int_{B_1}^{B_2} [M(T + \delta T, B) - M(T, B)\mathrm{d}B]. \tag{19}$$

This equation shows that ΔS_{iso} can also be obtained by using $M \times B$ curves. It should be mentioned that the Eq. (18) [or Eq. (19)], has been widely used by many authors to determine the isothermal entropy change around a first order phase transition. However, as it will be shown below, these equations should not be used to determine the isothermal entropy change around first order phase transition, where the order parameter (magnetization) becomes discontinuous. This is a controversial issue, which has been discussed in the literature [130–135].

Using the Maxwell relation $(\partial S/\partial B)_T = (\partial M/\partial T)_B$, the adiabatic temperature change given in Eq. (11) turns out to be:

$$\Delta T_{ad}(T, \Delta B) = -\int_{B_1}^{B_2} \frac{T}{C_B(T, B)} \left[\frac{\partial M(T, B)}{\partial T}\right]_B \mathrm{d}B. \tag{20}$$

Eq. (20) enable us to analyze the temperature variation of the magnetic material in an adiabatic process. For usual ferromagnets, the derivative of the magnetization curve $(\partial M/\partial T)$ is always negative, so that the adiabatic temperature change has the same sign of the magnetic field variation, i.e., $\Delta T_{ad} > 0$ for $\mathrm{d}B > 0$ and $\Delta T_{ad} < 0$ for $\mathrm{d}B < 0$.

For compounds undergoing a first order phase transition we have to handle Eq. (16) very carefully. Let us separate the discussion into two distinct regions namely: the range of temperatures and magnetic fields outside and inside the region of the first order phase transition. Outside the temperature and magnetic field range of the first order phase transition $[\delta G(T_C, B)/\delta T]_B = [\delta G(T, B_C)/\delta B]_T = 0$, so that we can rewrite Eq. (16) in the form:

$$\mathrm{d}G^{fo}_{out}(T, B) = \left\{\left[\frac{\partial G(T, B)}{\partial T}\right]_B \mathrm{d}T + \left[\frac{\partial G(T, B)}{\partial B}\right]_T \mathrm{d}B\right\}_{out}. \tag{21}$$

Notice that this equation is similar to Eq. (17) for compounds with second order phase transition. Since the free energy G^{fo}_{out} is also an exact differential, the Maxwell relation $[\partial S(T, B)/\partial B]_T = [\partial M(T, B)/\partial T]_B$ holds for compounds undergoing a first order phase transition in a range of temperatures away from phase transition, where the magnetization is a continuous function of temperature and magnetic field. Therefore, we may write Eq. (13) in the form:

$$[\Delta S^{fo}_{iso}]_{out}(T, \Delta B) = \left\{\int_{B_1}^{B_2} \left[\frac{\partial M(T, B)}{\partial T}\right]_B \mathrm{d}B\right\}_{out}. \tag{22}$$

In the range of temperatures and magnetic fields inside the region of the first order phase transition, we may write Eq. (16) as:

$$\mathrm{d}G^{fo}_{in}(T, B) = \left\{\left[\frac{\delta G(T_C, B)}{\delta T}\right]_B\right\}_{in} \mathrm{d}T + \left\{\left[\frac{\delta G(T, B_C)}{\delta B}\right]_T\right\}_{in} \mathrm{d}B. \tag{23}$$

According to thermodynamics, the Gibbs free energy, at the first order phase transition, should fulfill the condition $(G_P - G_F) = W_m$, where W_m is the work done under the variation of the magnetic field to take the system from the paramagnetic state to the ferromagnetic one [136]. From Eq. (23) the differential of the free energy at the paramagnetic and ferromagnetic phases, around the first order phase transition, should be:

$$\mathrm{d}G_P(T, B) = \frac{\delta G_P(T_C, B)}{\delta T}\mathrm{d}T_C + \frac{\delta G_P(T, B_C)}{\delta B}\mathrm{d}B_C \tag{24}$$

$$\mathrm{d}G_F(T, B) = \frac{\delta G_F(T_C, B)}{\delta T}\mathrm{d}T_C + \frac{\delta G_F(T, B_C)}{\delta B}\mathrm{d}B_C. \tag{25}$$

Thus, using Eqs. (24) and (25), and the condition $dG_P = dG_F + dW_m$ we can write:

$$(S_F - S_P)dT_C = -(M_F - M_P)\,dB_C + dW_m, \tag{26}$$

where $S_F = -\frac{\delta G_F(T_C,B)}{\delta T}$ and $S_P = -\frac{\delta G_P(T_C,B)}{\delta T}$ represent the entropy at the ferromagnetic and paramagnetic phases respectively. In the same way $M_F = -\frac{\delta G_F(T,B_C)}{\delta B}$ and $M_P = -\frac{\delta G_P(T,B_C)}{\delta B}$ represent the magnetization at the ferromagnetic and paramagnetic phases respectively. From the previous equation we can write:

$$\delta S(T,B) = -\delta M(T,B)\left(\frac{dB_C}{dT_C}\right) + \frac{dW_m}{dT_C}, \tag{27}$$

where $\delta S = (S_F - S_P)$ and $\delta M = (M_F - M_P)$. Let us discuss the last term, which is associated with the work necessary to magnetize a given material. To this end, we suppose that the magnetic material is made up of a great number of small pieces with a given magnetic moment [137]. Let us suppose that we can build the magnetic body by bringing each one of the small pieces from the infinity into the body. To bring the first magnetic piece from the infinity into the magnetic body it is not necessary to do magnetic work. The work needed to bring the second magnetic piece into the body in the presence of the first one, is equal to the magnetic energy interaction between the two magnetic pieces. The magnetic energy interaction between these two pieces is then given by:

$$U_m = -m_1 B_2, \tag{28}$$

where m_1 is the magnetic moment of the first piece and B_2 is the magnetic field of the second magnetic piece. Repeating this procedure until all the pieces are brought into the magnetic body, the magnetic energy will be:

$$U_m = -\left(m_1B_2 + m_1B_3 + m_1B_4 + \cdots m_1B_j + m_2B_3 + m_2B_4 + \cdots m_iB_j\right). \tag{29}$$

This expression can be written in a more compact form as:

$$U_m = -\sum_{i,j>i} m_iB_j = -\frac{1}{2}\sum_{i,j} m_iB_j. \tag{30}$$

The factor 1/2 appears to avoid the double counting in the summation. Its physical meaning is related to the magnetic interactions into the magnetic body. Using the definition of magnetization $M = (1/V)\sum_i m_i$ and taking $B = \sum_j B_j$ as the magnetic field inside the magnetic body, the magnetic energy per volume can be written as $U_m = -(1/2)M.B$. The magnetic work necessary to bring the system from the paramagnetic phase to the ferromagnetic one is equal to the difference between the magnetic energy of these two states, i.e.,

$$W_m = -(U_m^F - U_m^P) = \frac{1}{2}\left(M_FB_F - M_PB_C\right), \tag{31}$$

where $U_m^F = -M_F.B_F/2$ is the energy of the ferromagnetic phase and $U_m^P = -M_P.B_C/2$ is the energy of the paramagnetic phase. Supposing $B_F = B_C + \delta B$, we can write the magnetic work as:

$$W_m = \frac{1}{2}B_C\delta M + \frac{1}{2}M_F\delta B, \tag{32}$$

where $\delta M = (M_F - M_P)$. In the limit where $\delta B \to 0$, we get that the derivative dW_m/dT_C can be approximately written as:

$$\frac{dW_m}{dT_C} \cong \frac{1}{2}\delta M(T,B_C)\frac{dB_C}{dT_C}. \tag{33}$$

Putting (33) into (27), we can write a magnetic version of the Clausius–Clapeyron equation for the entropy change as:

$$\delta S(T,B_c) \cong -\frac{1}{2}\delta M(T,B_C)\left(\frac{dB_C}{dT_C}\right). \tag{34}$$

Using the Maxwell relation $[\partial S(T,B)/\partial B]_T = [\partial M(T,B)/\partial T]_B$ and putting $\delta S(T,B_c)$ given before into Eq. (15), the isothermal entropy change in the range of temperatures inside the region of the first order phase transition should be determined using magnetization data as:

$$[\Delta S_{iso}^{fo}]_{in}(T,\Delta B) \cong \int_{B_1}^{B_C}\left[\frac{\partial M(T,B)}{\partial T}\right]_B dB + \int_{B_C+\delta B}^{B_2}\left[\frac{\partial M(T,B)}{\partial T}\right]_B dB - \frac{1}{2}\left(\frac{dB_C}{dT_C}\right)\delta M(T,B_C). \tag{35}$$

This equation shows that the determination of ΔS_{iso} via magnetization data, in the temperature range inside the region of the first order phase transition, involves three terms. The first and the second terms with the integration of the derivative of the magnetization, are valid only in the magnetic field intervals $[B_1, B_C]$ and $[B_C + \delta B, B_2]$. The third term involving the magnetization change (δM) around T_C, should be used to calculate the contribution in the magnetic field interval between B_C and $B_C + \delta B$. It should be mentioned that all discussion made so far, consider the discontinuity in the order parameter as the

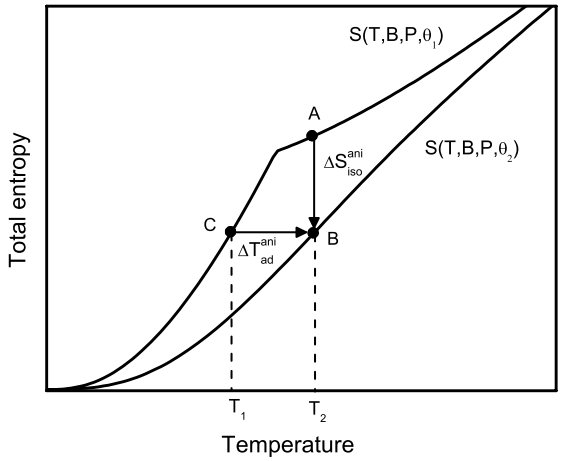

Fig. 2. Entropy versus temperature diagram for constant magnetic field applied along two different directions. The anisotropic magnetocaloric potentials ΔS_{iso}^{ani} and ΔT_{ad}^{ani} are also shown.

only signature of the first order phase transition. The present discussion does not consider the hysteresis effect, which is also a signature of the first order phase transition. A discussion of the determination of the isothermal entropy change including the hysteresis effect has been made in References [138–141], by using phenomenological models based in the expansion of the free energy around the magnetic ordering temperature. A microscopical description of the hysteresis effect on the magnetocaloric properties is still lacking. It is also worth mentioning here that an alternative way to get the isothermal entropy change using magnetization data without the use of the Maxwell relation was suggested in the References [142,143].

2.2. Alternative processes for entropy change

There are physical mechanisms other than magnetic field variation to change the entropy of a solid. For instance, the entropy of anisotropic magnetic materials, in which the magnetization depends on the direction of the applied magnetic field can be changed by rotating the sample into a constant magnetic field [144,145]. A similar process can be obtained by keeping the sample fixed and changing the direction of the applied magnetic field. The mechanism of cooling/heating through this process, is called the anisotropic magnetocaloric effect. The anisotropic magnetocaloric effect is measured by the isothermal entropy change ΔS_{iso}^{ani} and by the adiabatic temperature change ΔT_{ad}^{ani} under the variation of the direction of the applied magnetic field. Here the label "ani" is used as superscript to distinguish the anisotropic magnetocaloric potentials ΔS_{iso}^{ani} and ΔT_{ad}^{ani} from the conventional magnetocaloric ones ΔS_{iso} and ΔT_{ad}. In Fig. 2, are schematically plotted the entropy versus temperature curves for constant magnetic field applied along two different directions represented by the angles θ_1 and θ_2. The anisotropic isothermal entropy change upon variation of the applied magnetic field direction from θ_1 to θ_2 is given by:

$$\Delta S_{iso}^{ani}(T, B, P, \theta_2 - \theta_1) = S(T, B, P, \theta_2) - S(T, B, P, \theta_1). \tag{36}$$

The adiabatic temperature change upon variation of the applied magnetic field direction from θ_1 to θ_2 is determined by:

$$\Delta T_{ad}^{ani}(T, B, P, \theta_2 - \theta_1) = T_2(\theta_2) - T_1(\theta_1), \tag{37}$$

under the adiabatic condition $S(T, B, P, \theta_2) = S(T, B, P, \theta_1)$.

The entropy of a solid can also be changed by applying external pressure. In this case, the mechanism of heating and/or cooling is called the barocaloric effect [146–152]. The barocaloric effect is characterized by the isothermal entropy change ΔS_{iso}^{bar} and by the adiabatic temperature change ΔT_{ad}^{bar} under the variation of the applied pressure. The label "bar" is used as a superscript to distinguish the barocaloric potentials ΔS_{iso}^{bar} and ΔT_{ad}^{bar} from their magnetocaloric counterparts ΔS_{iso} and ΔT_{ad}. In order to illustrate the barocaloric effect, we consider the case of magnetic materials, in which the applied pressure contributes to the appearance of the magnetic order. In this particular case, the applied pressure increases the magnetic order, so that the magnetic entropy at a given temperature is reduced. In Fig. 3, is schematically shown the total entropy as a function of temperature for two values of the applied pressure. According to the entropy versus temperature diagram shown in Fig. 3, the isothermal entropy change ΔS_{iso}^{bar} upon pressure variation from P_1 to P_2 is determined by:

$$\Delta S_{iso}^{bar}(T, B, P_2 - P_1) = S(T, B, P_2) - S(T, B, P_1). \tag{38}$$

The adiabatic temperature change ΔT_{ad}^{bar} upon pressure variation from P_1 to P_2 is determined by

$$\Delta T_{ad}^{bar}(T, B, P_2 - P_1) = T_2(P_2) - T_1(P_1), \tag{39}$$

under the adiabatic condition $S(T_2, B, P_2) = S(T_1, B, P_1)$.

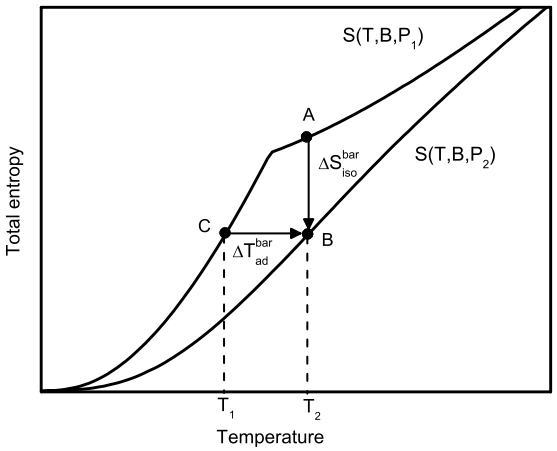

Fig. 3. Entropy versus temperature diagram for two values of applied pressure. ΔS_{iso}^{bar} and ΔT_{ad}^{bar} are the barocaloric potentials.

So far, we have discussed the magnetocaloric effect at constant pressure and the barocaloric effect at constant magnetic field. The magnetocaloric effect can also be studied in the general situation, where both magnetic field and pressure are changed. In this case, the isothermal entropy change upon magnetic field variation from B_1 to B_2 and pressure variation from P_1 to P_2 can be determined by:

$$\Delta S_{iso}(T, B_2 - B_1, P_2 - P_1) = S(T, B_2, P_2) - S(T, B_1, P_1). \tag{40}$$

The adiabatic temperature change upon magnetic field variation from B_1 to B_2 and pressure variation from P_1 to P_2 can be determined by:

$$\Delta T_{ad}(T, B_2 - B_1, P_2 - P_1) = T_2(B_2, P_2) - T_1(B_1, P_1), \tag{41}$$

under the adiabatic condition $S(T_2, B_2, P_2) = S(T_1, B_1, P_1)$.

Applied electric field [153–158] can also be used for changing the entropy of solid materials. In this case, the applied electric field changes the polarization of the material and consequently their entropy. As a result, the temperature of ferroelectric materials can be reduced/increased by changing the applied electric field. This type of cooling mechanism, known as electrocaloric effect, is not so effective because the temperature change is small. For instance, the usual values of the temperature variation (ΔT) obtained via the electrocaloric effect is around 2.5 K. However, it has been recently reported [156] that thin films of $Pb(Zr, Ti)O_3$ exhibit a giant electrocaloric effect, in which ΔT is around 12 K for an electric field variation of 480 kV cm^{-1}. This discovery reopens the discussion about the application of the electrocaloric effect as an efficient cooling mechanism. It is worth mentioning that the electric field could also be used to modify the entropy of magnetic materials. In principle, this process would be more effective in magnetic systems in which the electric field is able to yield changes in the electronic structure large enough to modify their magnetization and consequently their magnetic entropy. This may be the case for magnetic semiconductors [159,160], multiferroic materials with the coexistence of piezoelectricity and magnetism [161] and magnetic nanosystems [162].

There is also a cooling mechanism, known as the Pomeranchuk effect [163,164], used to reduce the temperature of melting ^{3}He via the application of an external pressure. Although, this cooling process is not so efficient as adiabatic demagnetization, it is worth mentioning it here. The Pomeranchuk effect is based on that fact that the coexistence between liquid and solid phases along the melting line of ^{3}He occurs in such a way that the entropy of the liquid phase is smaller than the entropy of the solid one. Thus, an applied pressure induces a transition from the liquid phase to the solid one, so that the temperature of ^{3}He is reduced. Recently, the idea of the Pomeranchuk effect was extended to the solid material $YbInCu_4$ [165–167], which exhibits a first order iso-structural phase transition around 42 K. In the phase transition of $YbInCu_4$, there is a coexistence between the Fermi liquid and local moments phases, in such a way that the entropy of the Fermi liquid phase is smaller than the entropy of the local moments phase. Thus, in the solid state version of the Pomeranchuk effect, the temperature reduction in the Kondo lattice system $YbInCu_4$ occurs due to the transition between the Fermi liquid phase and local moments one, induced by applied pressure. Independently of the possible technological applications, all of these alternative processes for entropy change discussed in this subsection, are worth investigating, because the complete understanding of these phenomena can reveal important aspects of the fundamental physics involved in the process of cooling and heating of the materials.

3. Magnetic refrigeration

In this section, we briefly discuss the application of the magnetocaloric effect on magnetic refrigeration. It is not our intention to provide in this report technical details of magnetic refrigeration. For more information about magnetic

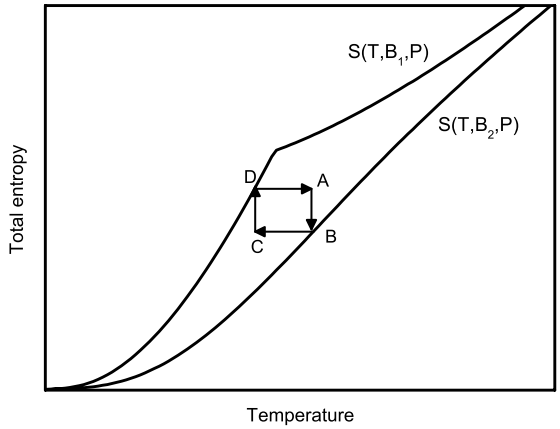

Fig. 4. Carnot cycle: two isothermal (*AB* and *CD*) and two adiabatic (*DA* and *BC*) processes.

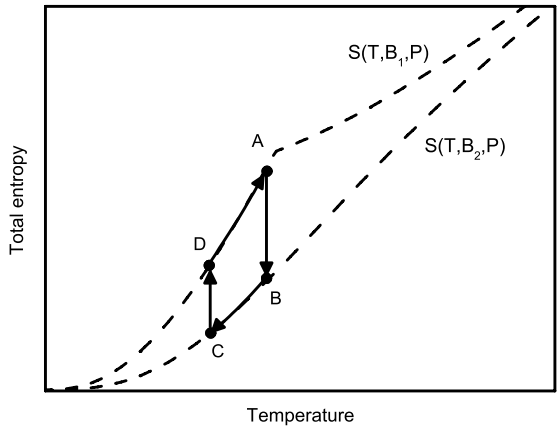

Fig. 5. Ericsson cycle: two isothermal (*AB* and *CD*) and two isofield (*BC* and *DA*) processes.

refrigeration, the readers are recommended to see References [168–173]. In a conventional vapor cycle refrigerator, the refrigeration process occurs due to the compression/decompression of a fluid working in a given thermodynamic cycle. The fluids commonly used in this type of refrigerator are dangerous to the environment and cause the depletion of the ozone layer. In a magnetic refrigerator, the refrigeration process occurs due to the application/removal of a magnetic field in a magnetic material, called the magnetic refrigerant. In magnetic refrigerators, water or fluids not harmful to the environment are used as heat exchangers. In order to extract heat from a cold reservoir and release it to a hot sink, the magnetic refrigerant should work in a given thermodynamic cycle. The main thermodynamic cycles suitable to implement magnetic refrigeration are the: Carnot cycle, Ericsson cycle and Brayton cycle. The Carnot cycle, which is made up of two isothermal and two adiabatic processes, is shown in Fig. 4. In this cycle, the magnetic material absorbs heat in the isothermal process *CD*, while it releases heat in the isothermal process *AB*.

The Ericsson cycle is composed of two isothermal and two isofield processes. A sketch of this cycle is shown in Fig. 5. In the isofield process *BC* at constant magnetic field B_2, the magnetic refrigerant releases heat, while in the isofield process *DA* at constant magnetic field B_1, the magnetic refrigerant absorbs heat. The Ericsson cycle exhibits optimal performance when the entropy curve of the magnetic refrigerant in the isofield process *BC* is parallel to the entropy curve in the isofield process *DA*. A more detailed discussion about the Ericsson cycle can be found in References [174–176]. The Brayton cycle, formed by two adiabatic and two isofield processes, is schematically shown in Fig. 6. A similar discussion about the isofield processes discussed in the Ericsson cycle holds also for the Brayton cycle.

In order to illustrate the principle of magnetic refrigeration, we consider the scheme shown in Fig. 7, which contains a magnetic material used as the magnetic refrigerant, a coil to provide the magnetic field and two thermal switches to connect and disconnect the magnetic refrigerant with the cold reservoir (volume to be refrigerated) and the hot sink. Here, we suppose for the sake of convenience, a magnetic refrigerator operating in the Carnot cycle shown in Fig. 4.

In the first step of the process, the thermal switch 1 is turned on to connect the magnetic material with the hot sink and the magnetic field is isothermally applied. In this isothermal process, which can be represented by the path *AB* in Fig. 4, the entropy of the magnetic material is reduced, so that the entropy change is less than 0, i.e., $dS < 0$. Thus, according to the thermodynamic relation $dQ = T dS$ we get $dQ < 0$, so that an amount of heat is released from the magnetic material

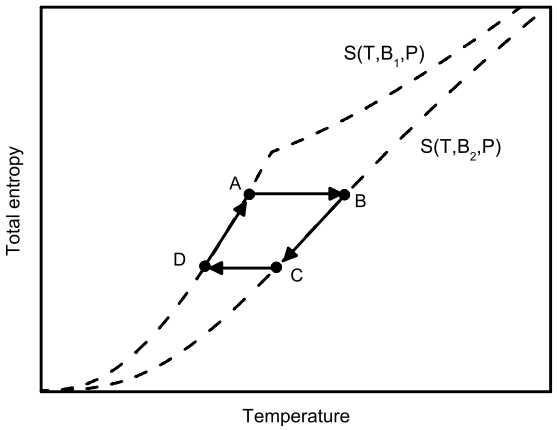

Fig. 6. Brayton cycle: two isofield (*BC* and *DA*) and two adiabatic (*AB* and *CD*) processes.

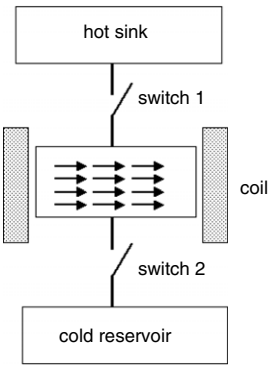

Fig. 7. Scheme to illustrate magnetic refrigeration.

to the hot sink. In the second step, the thermal switch 1 is turned off to disconnect the magnetic material from the hot sink and the magnetic field is adiabatically reduced. In this adiabatic process, which can be represented by the path *BC* in Fig. 4, the temperature of the magnetic material decreases. In the third step, the thermal switch 2 is turned on to connect the magnetic material with the cold reservoir and the magnetic field is isothermally reduced. In this isothermal process, which can be represented by the path *CD* in Fig. 4, the entropy of the magnetic material is increased so that the entropy change is greater than 0, i.e., $dS > 0$. Thus, according to the thermodynamic relation $dQ = TdS$ we get $dQ > 0$, so that an amount of heat is absorbed by the magnetic material from the cold reservoir. As a consequence, the temperature of the cold reservoir decreases. In the fourth process, the thermal switch 2 is turned off to disconnect the magnetic material from the cold reservoir and the magnetic field is adiabatically increased. In this adiabatic process, represented by the path *DA* in Fig. 4, the temperature of the magnetic material increases and the thermodynamic cycle is completed. It should be emphasized that this qualitative discussion about magnetic refrigeration, is just illustrative and does not constitute a real prototype of magnetic refrigerator operating in the Carnot Cycle.

4. Magnetocaloric effect in rare earth compounds

In rare earth metals, the magnetization comes mainly from the 4f electrons, which have a localized character, although a small contribution comes from the 5d electrons. Rare earth elements combine with many other elements from the Periodic Table to form a great deal of rare earth based compounds, which can be put into two main classes namely: (i) rare earth based compounds with non magnetic elements, such as RAl_2, RNi_2, RNi_5, RZn, RCd, and $R_5(Si_{1-x}Ge_x)_4$, where the magnetism comes entirely from the rare earth ions. (ii) Rare earth compounds with transition elements such as RFe_2 and RCo_2, where the magnetism comes from both rare earth ions and transition elements. In this section, we only discuss the magnetocaloric effect in rare earth based compounds without magnetic transition ions. The magnetocaloric effect in rare earth based compounds with transition elements is discussed in Section 6.

4.1. Theoretical formulation

In order to discuss the magnetocaloric effect in rare earth compounds, it is necessary to describe the effect of temperature, magnetic field and pressure on the localized moments of rare earth ions. In addition, it is also necessary to describe the

conduction electrons and the crystalline lattice. The outmost electrons in rare earth ions lose their atomic localization and are transferred to the conduction electron band. The role of the conduction electrons in rare earth compounds is very important for the establishment of different types of magnetic order, such as ferromagnetic, antiferromagnetic and ferrimagnetic. The conduction electrons will be scattered by the localized magnetic moments from the j-th site to the i-th site and the information of the orientation of the magnetic moment of the j-th site will be transmitted to the i-th site. In this way, an indirect exchange interaction between rare earth magnetic ions, occurs via the conduction electrons. This type of interaction, known as Ruderman–Kittel–Kasuya–Yosida (RKKY) interaction [177,178], is described by the term $\sum_{ij} \mathcal{J}_{ij}\vec{J}_i.\vec{J}_j$, where $\mathcal{J}_{ij}$ is an exchange interaction parameter and J is the total angular momentum of the rare earth ions. Besides the exchange interaction, the magnetic moments interact with the applied magnetic field via the Zeeman interaction. The energy associated with the Zeeman interaction is given by: $-\vec{\mu}.\vec{B}$, where $\vec{\mu} = g\mu_B\vec{J}$ is the effective dipolar magnetic moment operator of the i-th magnetic ion, g is the Landé factor and μ_B is the Bohr magneton. Apart from the Zeeman and exchange interactions between magnetic moments, the effect of the crystalline electrical field should be included to describe the magnetic properties associated with 4f-electrons. In fact, the electrostatic field due to the surrounding ions, modifies the free-ion wave functions and the energy levels. As a result, it is expected that the crystalline electrical field removes partly the $(2J + 1)$ degeneracy of each 4f-multiplet. Therefore, the model Hamiltonian suitable to describe the magnetization in rare earth compounds should include the interaction between magnetic moments, their coupling with the applied magnetic field and the crystalline electrical field. Thus, the magnetic Hamiltonian should be:

$$\mathcal{H}_{mag}^{4f} = -\sum_{i,j} \mathcal{J}_{ij}(r)\vec{J}_i.\vec{J}_j - \sum_i g\mu_B\vec{B}.\vec{J}_i + \sum_i \mathcal{H}_i^{CF}, \tag{42}$$

where the indices "i" and "j" in the sum run over all magnetic sites. The total Hamiltonian including the magnetic ions, the conduction electrons and the crystalline lattice is:

$$\mathcal{H} = \mathcal{H}_{el}^{spd} + \mathcal{H}_{mag}^{4f} + \mathcal{H}_{lat}, \tag{43}$$

where $\mathcal{H}_{mag}^{4f}$ is the magnetic Hamiltonian, given in Eq. (42). The Hamiltonian $\mathcal{H}_{el}^{spd}$ given by:

$$\mathcal{H}_{el}^{spd} = \sum_k \varepsilon_k c_k^+ c_k, \tag{44}$$

describes the "spd" conduction electrons. The Hamiltonian $\mathcal{H}_{lat}$ given by:

$$\mathcal{H}_{lat} = \sum_q \hbar\omega_q a_q^+ a_q \tag{45}$$

describes the vibrations of the ions into the crystalline lattice.

The contribution from the conduction electrons to the total magnetization can be neglected. Details about this statement are given in Section 5, where the magnetism of itinerant electrons is discussed. On the other hand, the electronic heat capacity and entropy associated with the conduction electron Hamiltonian are respectively given by [179]:

$$C_{el}^{spd}(T) = \gamma T \tag{46}$$

and

$$S_{el}^{spd}(T) = \gamma T. \tag{47}$$

Here $\gamma = \pi^2 k_B^2 \rho(\varepsilon_f)/3$, is the Sommerfeld coefficient, where $\rho(\varepsilon_f)$ is the density of electronic states at the Fermi energy level.

4.1.1. Magnetic Hamiltonian

In this subsection is discussed in more detail the magnetic part of the Hamiltonian. Let us start our discussion with the term accounting for the crystalline electrical field. The simplest approach to describe the crystalline electrical field is the so-called point-charge model, whose detailed calculation can be found in Hutchings'paper [180]. In the point-charge model, the charge distribution on the ions surrounding the central atom (in our case the rare-earth ion, see Fig. 8), is considered as a point charge. In other words, the finite extent of the charges on the ions are neglected. On the assumption of the point-charge model, the crystalline electrical field perturbed Hamiltonian can be written as:

$$\mathcal{H}^{CF} = \sum_{ij} \frac{q_i q_j}{\left|\vec{R}_j - \vec{r}_i\right|}, \tag{48}$$

where $\vec{R}_j$ and $\vec{r}_i$ are the position vectors of the j-th point charge and the i-th 4f electron, respectively. Here the sum in the label "i" extends over all 4f electrons and the sum in "j" extends over the nearest neighbors. The above representation for the crystalline electrical field Hamiltonian, uses Cartesian expressions for the operators, which is not appropriate to handle

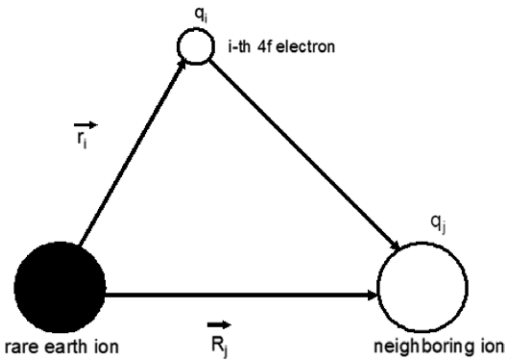

Fig. 8. Scheme to illustrate the point-charge model.

on the total angular momentum representation of the unperturbed 4f quantum states, in which the Zeeman and exchange interaction terms of the magnetic Hamiltonian are represented.

In order to represent in the same space, the three parts of the magnetic Hamiltonian given in Eq. (42), we should write the crystalline electrical field term in the angular momentum representation. This procedure uses the Wigner–Eckart theorem and detailed calculations can be found in Stevens'paper [181]. The rules for determining the so-called equivalent operator are exemplified below:

$$\sum_i (3z_i - r^2) \equiv \theta_2 \langle r^2 \rangle \left[3J_z^2 - J(J+1)\right] = \theta_2 \langle r^2 \rangle O_2^0, \tag{49}$$

$$\sum_i (x_i^4 - 6x_i^2 y_i^2 + x_i^4 r) \equiv \theta_4 \langle r^4 \rangle \frac{1}{2}\left[J_+^4 + J_-^4\right] = \theta_4 \langle r^4 \rangle O_4^4, \tag{50}$$

where $\langle r^n \rangle$ is the mean value of the radial operator; θ_2 and θ_4 are numerical factors, that have been determined for all rare earth elements, in Hutchings' paper [180]. The O_n^m are called equivalent operators, due to the fact that the matrix elements of the Cartesian operators, e.g., $\sum_i (3z_i - r^2)$ are equivalent to those of O_n^m, when sandwiched in the angular part of the coupled wave function, $|J, m\rangle$.

The equivalent operators, were discussed for all total angular momentum of the rare-earth elements in reference [180]. Here, we show some Stevens's operators, which will be used into the crystalline electrical field Hamiltonian for the cubic and hexagonal symmetry. Note that the Stevens's operators are written in terms of the z-component of the total angular momentum, J_z, and the ladders operators $J_\pm = J_x \pm \mathrm{i}J_y$.

$$O_2^0 = \left[3J_z^2 - J(J+1)\right], \tag{51}$$

$$O_4^0 = \left[35J_z^4 - 30J(J+1)J_z^2 + 25J_z^2 - 6J(J+1) + 3J^2(J+1)^2\right], \tag{52}$$

$$O_4^4 = \frac{1}{2}\left[\left(J_+^4 + J_-^4\right)\right], \tag{53}$$

$$\begin{aligned} O_6^0 = {} & 231J_z^6 - 315J(J+1)J_z^4 + 735J_z^4 + 105J^2(J+1)^2 J_z^2 - 525J(J+1)J_z^2 \\ & + 294J_z^2 - 5J^3(J+1)^3 + 40J^2(J+1)^2 - 60J(J+1), \end{aligned} \tag{54}$$

$$O_6^4 = \frac{1}{4}\left[\left(11J_z^2 - J(J+1) - 38\right)\left(J_+^4 + J_-^4\right) + \left(J_+^4 + J_-^4\right)\left(11J_z^2 - J(J+1) - 38\right)\right], \tag{55}$$

$$O_6^6 = \frac{1}{2}\left[\left(J_+^6 + J_-^6\right)\right]. \tag{56}$$

The crystalline electrical field term per ion, can be written as a linear combination of the equivalent operators in the form [182]:

$$\mathcal{H}^{CF} = \sum_{nm} B_n^m O_n^m. \tag{57}$$

Here B_n^m are the crystalline electrical field parameters, which are usually adjusted by using experimental data, such as inelastic neutron scattering, heat capacity, and magnetic susceptibility. The number of parameters in Eq. (57) depends on the point symmetry group. In rare earth compounds, the maximum value for "n" and "m" is six, which is associated with the rules that restrict the number of non-zero matrix elements. It is also possible to obtain the crystalline electrical field parameters from theoretical calculations considering the crystalline lattice, see for example the calculation performed by

Andres and coworkers [183] for $PrNi_5$ with hexagonal symmetry. For the cubic symmetry, we have only two crystalline electrical field parameters, so that the crystalline electrical field Hamiltonian is given by [182]:

$$\mathcal{H}^{CF}_{cub} = B_4(O^0_4 + 5O^4_4) + B_6(O^0_6 - 21O^4_6). \tag{58}$$

This Hamiltonian can be written in the Lea–Leask–Wolf (LLW) notation [184] as:

$$\mathcal{H}^{CF}_{cub} = W\left[\frac{x}{F_4}\left(O^0_4 + 5O^4_4\right) + \frac{(1-x)}{F_6}\left(O^0_6 - 21O^4_6\right)\right], \tag{59}$$

where $B_4F_4 = Wx$ and $B_6F_6 = W(1-x)$ with F_4 and F_6 being constants common to all matrix elements. The parameter W gives the energy scale and x gives the relative importance of the fourth and sixth order terms. For hexagonal symmetry the crystalline electrical field Hamiltonian has four parameters and is given by:

$$\mathcal{H}^{CF}_{hex} = B^2_2O^0_2 + B^0_4O^0_4 + B^0_6O^0_6 + B^6_6O^6_6. \tag{60}$$

Using the general form of the crystalline electrical field Hamiltonian given in Eq. (57), the magnetic Hamiltonian $\mathcal{H}^{4f}_{mag}$ can be written in the form:

$$\mathcal{H}^{4f}_{mag} = -\sum_{ij}\mathcal{J}_{ij}(r)\vec{J}_i.\vec{J}_j - \sum_i g\mu_B\vec{J}_i.\vec{B} + \sum_{inm}B^m_nO^m_n(i). \tag{61}$$

The exchange interaction integral $\mathcal{J}_{il}(r)$ in the previous magnetic Hamiltonian, depends on the variation of the distance between neighboring sites in the crystalline lattice as a function of temperature. This exchange interaction integral can be written as [185] $\mathcal{J}(r) = \alpha^{4f}_0\mathcal{J}_0(r_0) + \alpha^{4f}_1\mathcal{J}_1(r_0)J_i.J_j$, where $\mathcal{J}_0$ and $\mathcal{J}_1$ are parameters. On the one hand $\mathcal{J}_0$ is the bare value of the exchange interaction integral, which depends on the fixed position (r_0) of the ions in the crystalline lattice. On the other hand $\mathcal{J}_1(r_0) = \kappa[(d\mathcal{J}(r)/dr)^2]_{r=r_0}$, where κ is a proportionality constant, depends on the vibration of the ions. The parameters α^{4f}_0 and α^{4f}_1 were introduced to simulate the effect of external pressure. Using $\mathcal{J} = \alpha^{4f}_0\mathcal{J}_0 + \alpha^{4f}_1\mathcal{J}_1J_i.J_j$, the magnetic Hamiltonian $\mathcal{H}_{mag}$ turns out to be:

$$\mathcal{H}^{4f}_{mag} = -\sum_{ij}\hat{\mathcal{J}}_0\vec{J}_i.\vec{J}_j - \sum_{ij}\hat{\mathcal{J}}_1(\vec{J}_i.\vec{J}_j)(\vec{J}_i.\vec{J}_j) - \sum_i g\mu_B\vec{J}_i.\vec{B} + \sum_{inm}B^m_nO^m_n(i), \tag{62}$$

where we have defined the new parameters $\hat{\mathcal{J}}_0 = \alpha^{4f}_0\mathcal{J}_0$ and $\hat{\mathcal{J}}_1 = \alpha^{4f}_1\mathcal{J}_1$. It is worth mentioning that the ratio between the parameters $\hat{\mathcal{J}}_1/\hat{\mathcal{J}}_0$ controls the nature of the phase transition. For $\hat{\mathcal{J}}_1 = 0$ the phase transition is of second order. For $\hat{\mathcal{J}}_1/\hat{\mathcal{J}}_0$ greater than a given critical value, the phase transition is of first order. The great difficult in calculating the energy eigenvalues of this magnetic Hamiltonian is related to the two-body interaction represented by the first and second terms. This two-body interaction term can be treated either in the molecular field approximation or in a Monte Carlo simulation [186–193]. In this report, we only discuss the molecular field theory, which consists in replacing all the spin operators, except that of the j-th site, by their average value. Using the relation $\Delta\vec{J}_i = \vec{J}_i - \langle\vec{J}_i\rangle$, where $\langle\vec{J}_i\rangle$ is the thermal average of the operator, we can write the two-body term $\sum_{ij}\hat{\mathcal{J}}_0\vec{J}_i.\vec{J}_j$, in the form:

$$\sum_{ij}\hat{\mathcal{J}}_0\vec{J}_i.\vec{J}_j = \sum_{ij}\hat{\mathcal{J}}_0\left[\Delta\vec{J}_i.\Delta\vec{J}_j + \Delta\vec{J}_i.\langle\vec{J}_j\rangle + \langle\vec{J}_i\rangle.\Delta\vec{J}_j + \langle\vec{J}_i\rangle.\langle\vec{J}_j\rangle\right]. \tag{63}$$

The term $\langle\vec{J}_i\rangle.\langle\vec{J}_j\rangle$ may be abandoned, since it is not an operator and represents only a shift in the energy eigenvalue spectrum. The average value $\langle\vec{J}_j\rangle$ can be considered as site independent, i.e., $\langle\vec{J}_i\rangle = \langle\vec{J}_j\rangle$ which is associated with the magnetic lattice translation symmetry. In the mean field approximation, the product $\Delta\vec{J}_i.\Delta\vec{J}_j$ is neglected. This is a weak point of the approximation, because the information of magnetic fluctuations, associated with the short-range order interactions, is lost. Thus, in the mean field approximation, the two-body interaction term can be written as:

$$\sum_{ij}\hat{\mathcal{J}}_0\vec{J}_i.\vec{J}_j \approx g\mu_B\sum_i\frac{2\hat{\mathcal{J}}_0}{g\mu_B}\left[\sum_j\langle\vec{J}_j\rangle\right].\vec{J}_i. \tag{64}$$

Similarly, we can write the term $\sum_{ij}\hat{\mathcal{J}}_1\left(\vec{J}_i.\vec{J}_j\right)^2$ in the mean field approximation as:

$$\sum_{ij}\hat{\mathcal{J}}_1\left(\vec{J}_i.\vec{J}_j\right)^2 \approx g\mu_B\sum_i\frac{4\hat{\mathcal{J}}_1}{g\mu_B}\left[\sum_j\langle\vec{J}_j\rangle^3\right].\vec{J}_i. \tag{65}$$

Defining the mean value $\sum_j\langle\vec{J}_j\rangle = Z_n\langle\vec{J}\rangle$, where Z_n is the number of first nearest neighbors, we can rewrite Eqs. (64) and (65) as:

$$\sum_{ij}\hat{\mathcal{J}}_0\vec{J}_i.\vec{J}_j \approx g\mu_B\sum_i\frac{2Z_n\hat{\mathcal{J}}_0}{g\mu_B}\langle\vec{J}\rangle.\vec{J}_i \tag{66}$$

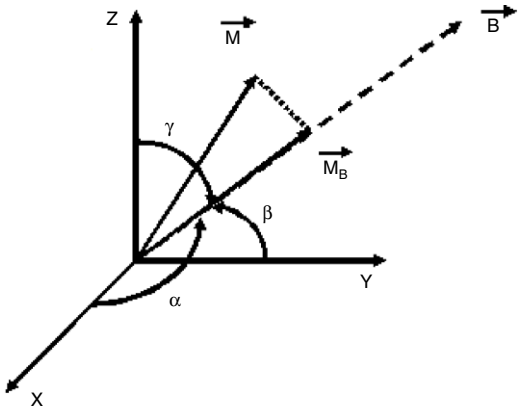

Fig. 9. Applied magnetic field and the magnetization vectors.

and

$$\sum_{ij} \hat{\mathcal{J}}_1 \left(\vec{J}_i.\vec{J}_j\right) . \left(\vec{J}_i.\vec{J}_j\right) \approx g\mu_B \sum_i \frac{4Z_n\hat{\mathcal{J}}_1}{g\mu_B} \langle\vec{J}\rangle^3 .\vec{J}_i. \tag{67}$$

Putting (66) and (67) into (62) and defining the renormalized parameters $\tilde{\mathcal{J}}_0$ and $\tilde{\mathcal{J}}_1$ as $\tilde{\mathcal{J}}_0 = 2Z_n\hat{\mathcal{J}}_0$ and $\tilde{\mathcal{J}}_1 = 4Z_n\hat{\mathcal{J}}_1$ we get:

$$\mathcal{H}^{4f}_{mag} = -\sum_i g\mu_B\vec{J}_i.\vec{B}_{eff} + \sum_{inm} B^m_n O^m_n(i). \tag{68}$$

Here $\vec{B}_{eff} = \vec{B} + (\tilde{\mathcal{J}}_0\langle\vec{J}\rangle + \tilde{\mathcal{J}}_1\langle\vec{J}\rangle^3)/g\mu_B$ is the effective magnetic field that acts on the magnetic ion. This effective magnetic field can also be written as: $\vec{B}_{eff} = \vec{B} + \tilde{\lambda}_0 M + \tilde{\lambda}_1 M^3$, where $\tilde{\lambda}_0 = \tilde{\mathcal{J}}_0/(g^2\mu_B^2)$ and $\tilde{\lambda}_1 = \tilde{\mathcal{J}}_1/(g^4\mu_B^4)$. It is worth noticing that, due to the crystalline electrical field anisotropy, represented by the second term in the magnetic Hamiltonian in Eq. (68), the easy magnetization direction is also an input parameter. Therefore, two cases should be analyzed, namely: (i) the case where the external magnetic field is applied along the easy magnetization direction, and (ii) the case where the magnetic field is applied along an arbitrary direction.

In Fig. 9, is shown a scenario where the magnetic field is applied along an arbitrary direction making the angles α, β and γ with the crystallographic axes x, y and z. In this figure, $\vec{M}$ is the magnetization and $\vec{M}_B$ is the component of the magnetization vector along the applied magnetic field direction. Note that $\vec{M}_B = \vec{M}$, only when the magnetic field is applied along the easy magnetization direction. Including the information about the applied magnetic field direction in the model Hamiltonian in Eq. (68), we can write:

$$\begin{aligned}\mathcal{H}^{4f}_{mag} = &\sum_{inm} B^m_n O^m_n(i) - \sum_i g\mu_B \left[\left(B\cos\alpha + \frac{\tilde{\mathcal{J}}^{eff}_x\langle J_x\rangle}{g\mu_B}\right)J_x\right.\\ &\left. + \left(B\cos\beta + \frac{\tilde{\mathcal{J}}^{eff}_y\langle J_y\rangle}{g\mu_B}\right)J_y + \left(B\cos\gamma + \frac{\tilde{\mathcal{J}}^{eff}_z\langle J_z\rangle}{g\mu_B}\right)J_z\right],\end{aligned} \tag{69}$$

where $\tilde{\mathcal{J}}^{eff}_k = \tilde{\mathcal{J}}_0 + \tilde{\mathcal{J}}_1\langle J_k\rangle^2$ with $k = x, y, z$. The magnetization components M_k, $(k = x, y, z)$ are calculated by:

$$M_k(T, B, P) = g\mu_B\langle J_k\rangle, \tag{70}$$

where the averages $\langle J_k\rangle$ $(k = x, y, z)$ are given by:

$$\langle J_k\rangle = \frac{\sum_m \langle\psi_m|J_k|\psi_m\rangle\, e^{-\beta\varepsilon_m}}{\sum_m e^{-\beta\varepsilon_m}}, \tag{71}$$

where $\beta = 1/k_B T$, with k_B being the Boltzmann constant. Here $|\psi_m\rangle$ and ε_m are respectively, the eigenfunctions and energy eigenvalues of the Hamiltonian given in Eq. (69). The total magnetization is given by $\vec{M} = M_x\hat{x} + M_y\hat{y} + M_z\hat{z}$, where M_x, M_y and M_z are calculated in Eq. (70). The magnitude of the total magnetization is given by $M = (M_x^2 + M_y^2 + M_z^2)^{1/2}$. The magnitude of the magnetization component along the applied magnetic field direction is calculated by $M_B = \vec{M}.\hat{u}$, where $\hat{u} = \hat{x}\cos(\alpha) + \hat{y}\cos(\beta) + \hat{z}\cos(\gamma)$ is the unit vector along the direction of the applied magnetic field. It should be noted that the energy eigenvalues and eigenfunctions of the Hamiltonian in Eq. (69) can only be calculated if the averages

$\langle J_k \rangle (k = x, y, z)$, are known. On the other hand, to calculate the averages $\langle J_k \rangle$ using Eq. (71), it is necessary to know the energy eigenvalues and eigenfunctions of the magnetic Hamiltonian given in Eq. (69). Therefore, a numerical procedure should be used in order to calculate the energy eigenvalues and the averages $\langle J_k \rangle$. It should be mentioned that for a fixed value of the magnetic field, a set of eigenfunctions and energy eigenvalues of the Hamiltonian given in Eq. (69) emerges self consistently for each value of temperature. Using these proper energy eigenvalues, the magnetic partition function per ion reads $Z_{mag}^{4f} = \sum_m \exp(-\beta\varepsilon_m)$. Thus, the magnetic free energy per mol is given by:

$$F_{mag}^{4f}(T, B, P) = -N_A k_B T \ln \left[\sum_m \exp(-\beta\varepsilon_m) \right], \tag{72}$$

where N_A is Avogadro's number. The magnetic entropy for a mol of the sample, calculated from the thermodynamic relation $S_{mag}^{4f} = -(\partial F_{mag}^{4f}/\partial T)_{B^{eff}}$, is given by:

$$S_{mag}^{4f}(T, B, P) = N_m \Re \left[\sum_m \exp(-\beta\varepsilon_m) + \frac{1}{k_B T} \frac{\sum_m \varepsilon_m \exp(-\beta\varepsilon_m)}{\sum_m \exp(-\beta\varepsilon_m)} \right], \tag{73}$$

where $\Re = N_A k_B$ is the gas constant, whose value in the international system of units is 8.314 (J/mol K). Here N_m represents the number of magnetic ions per unit formula. For instance, in $GdAl_2$, $N_m = 1$ and in the compound $Gd_5Si_2Ge_2$, $N_m = 5$. The magnetic heat capacity at constant magnetic field can be calculated from the thermodynamic relation $C_{mag}^{4f} = T(\partial S_{mag}^{4f}/\partial T)_{B^{eff}}$.

4.1.2. Crystalline lattice Hamiltonian

The magnetic moments and the conduction electrons somehow influence the lattice vibrations. A rigorous treatment of this effect is somewhat difficult and is beyond the scope of this report. Here we suppose, for the sake of simplicity, that the magnetic and electronic channels change the phonon frequency from ω to $\tilde{\omega}$. With this assumption, the lattice Hamiltonian in Eq. (45) can be written as:

$$\mathcal{H}_{lat} = \sum_q \hbar\tilde{\omega}_q a_q^+ a_q, \tag{74}$$

where $\tilde{\omega}_q = \alpha^{ph}\xi^{ph}\omega_q$ is a renormalized phonon frequency, where ξ^{ph} is a model parameter representing the interaction between magnetic moments and phonons. The parameter α^{ph} was introduced to simulate the effect of the applied pressure. For the sake of convenience, the parameter ξ^{ph} may be written in terms of the volume change as $\xi^{ph} = (1 - \xi_0^{ph}\Delta V/V_0)$. The energy eigenvalues of the lattice Hamiltonian describing phonons in the crystalline lattice, with the renormalized phonon frequency $\tilde{\omega}_q$, is given by: $\tilde{\varepsilon}_q = \left(n_q + \frac{1}{2}\right)\hbar\tilde{\omega}_q$. The partition function associated with the lattice Hamiltonian in Eq. (74) is given by:

$$Z_{lat}(T, B, P) = \sum_{n_q = n_1, n_2 \ldots} \mathrm{e}^{-\beta \sum_q (n_q + \frac{1}{2})\hbar\tilde{\omega}_q}. \tag{75}$$

After some algebra, the crystalline lattice partition function reads:

$$Z_{lat}(T, B, P) = \prod_q \frac{1}{(1 - \mathrm{e}^{-\beta\hbar\tilde{\omega}_q})}. \tag{76}$$

The lattice free energy per mol of the sample, calculated by $F_{lat} = (-1/\beta)\ln Z_{lat}$, is given by:

$$F_{lat}(T, B, P) = 3N_A k_B T \sum_q \ln\left(1 - \mathrm{e}^{-\beta\hbar\tilde{\omega}_q}\right), \tag{77}$$

where N_A is Avogadro's number and the factor 3 takes into account the three crystallographic axes. Transforming the sum in q into an integral over frequency, the lattice free energy turns out to be:

$$F_{lat}(T, B, P) = \Re T \int \ln\left(1 - \mathrm{e}^{-\beta\hbar\tilde{\omega}}\right) \rho^{ph}(\tilde{\omega}) \mathrm{d}\tilde{\omega}, \tag{78}$$

where $\Re = N_A k_B$ is the gas constant and $\rho^{ph}(\tilde{\omega})$ is a renormalized density of phonon frequencies, which should fulfill the following condition $\int \rho^{ph}(\tilde{\omega})\mathrm{d}\tilde{\omega} = 3N_A$. The crystalline lattice entropy calculated by $S_{lat} = (-\partial F_{lat}/\partial T)$ is given by:

$$S_{lat}(T, B, P) = N_i \Re \left[-\int \ln\left(1 - \mathrm{e}^{-\beta\hbar\tilde{\omega}}\right) \rho^{ph}(\tilde{\omega})\mathrm{d}\tilde{\omega} + \frac{1}{k_B T} \int \frac{\hbar\tilde{\omega}}{\left(\mathrm{e}^{\beta\hbar\tilde{\omega}} - 1\right)} \rho^{ph}(\tilde{\omega})\mathrm{d}\tilde{\omega} \right], \tag{79}$$

where N_i is the total number of ions per unit formula. The lattice heat capacity can be calculated from the thermodynamic relation $C_{lat} = T(\partial S_{lat}/\partial T)$. Taking the derivative of Eq. (79) we get:

$$C_{lat}(T,B,P) = N_i\Re\int \frac{(\hbar\tilde{\omega})^2\,\rho^{ph}(\tilde{\omega})\mathrm{e}^{\beta\hbar\tilde{\omega}}}{k_B T^2\left(\mathrm{e}^{\beta\hbar\tilde{\omega}}-1\right)^2}\mathrm{d}\tilde{\omega}. \tag{80}$$

Notice that the lattice entropy and heat capacity depend on the magnetic field and pressure through the renormalized frequency $\tilde{\omega}$. Using the assumption made in this report that the normalized phonon frequency is given by $\tilde{\omega}_q = \alpha^{ph}\xi^{ph}\omega_q$ we may write that $\mathrm{d}\tilde{\omega}_q = \alpha^{ph}\xi^{ph}\mathrm{d}\omega_q$ and $\rho^{ph}(\tilde{\omega}) = \rho^{ph}(\omega)/\alpha^{ph}\xi^{ph}$. In this case, the crystalline lattice entropy and specific heat capacity can be written in terms of the bare phonon frequency as:

$$S_{lat}(T,B,P) = N_i\Re\left[-\int \ln\left(1-\mathrm{e}^{-\beta\hbar\alpha^{ph}\xi^{ph}\omega}\right)\rho^{ph}(\omega)\mathrm{d}\omega + \frac{1}{k_B T}\int \frac{\hbar\alpha^{ph}\xi^{ph}\omega}{\left(\mathrm{e}^{\beta\hbar\alpha^{ph}\xi^{ph}\omega}-1\right)}\rho^{ph}(\omega)\mathrm{d}\omega\right] \tag{81}$$

$$C_{lat}(T,B,P) = N_i\Re\int \frac{\left(\hbar\alpha^{ph}\xi^{ph}\omega\right)^2\rho^{ph}(\omega)\mathrm{e}^{\beta\hbar\alpha^{ph}\xi^{ph}\omega}}{k_B T^2\left(\mathrm{e}^{\beta\hbar\alpha^{ph}\xi^{ph}\omega}-1\right)^2}\mathrm{d}\omega. \tag{82}$$

In order to discuss the magnetic field and pressure dependence of the lattice entropy, let us take a closer look at the density of phonon frequencies. Using the Green's function technique, the density of phonon frequencies given by $\rho^{ph}(\omega) = \sum_q(1/(z-\tilde{\omega}_q))$, where $z = \omega + \mathrm{i}0$, can be written in the form:

$$\rho^{ph}(\omega) = -\frac{1}{\pi}Im\int \frac{\rho_0^{ph}(\omega')\mathrm{d}\omega'}{z-\alpha^{ph}(1-\xi_0^{ph}\Delta V/V_0)\omega'}, \tag{83}$$

where ρ_0^{ph} is an unperturbed density of phonon frequencies. Assuming that the volume change can be taken proportional to the magnetization square, i.e., $\Delta V/V_0 \approx M^2$ we get:

$$\rho^{ph}(\omega) = -\frac{1}{\pi}Im\int \frac{\rho_0^{ph}(\omega')\mathrm{d}\omega'}{z-\alpha^{ph}(1-\xi_0^{ph}M^2)\omega'}. \tag{84}$$

A realistic density of phonon frequencies is not easily determined. In order to simplify the numerical calculations of the lattice heat capacity and entropy, we use the Debye approximation, in which the density of phonon frequencies is given by the parabolic function:

$$\rho^{ph}(\tilde{\omega}) = \frac{3V\tilde{\omega}^2}{2\pi^2 v^3}. \tag{85}$$

Putting (85) into (79), and considering the Debye cutoff frequency given by $\tilde{\omega}_D = (6\pi^2 v^3 N_A/V)^{1/3}$, the lattice entropy in the Debye approximation is given by:

$$S_{lat}(T,B,P) = N_i\left[-3\Re\ln\left(1-\mathrm{e}^{-\frac{\tilde{\Theta}_D}{T}}\right) + 12\Re\left(\frac{T}{\tilde{\Theta}_D}\right)^3\int_0^{\tilde{\Theta}_D/T}\frac{x^3}{\mathrm{e}^x-1}\mathrm{d}x\right], \tag{86}$$

where $\tilde{\Theta}_D = \hbar\tilde{\omega}_D/k_B$ is the renormalized Debye temperature. Using $V = V_0 + \Delta V$ in the Debye cutoff frequency and taking the volume change ΔV proportional to the square of the magnetization, the renormalized Debye temperature can be written as $\tilde{\Theta}_D = \Theta_0\alpha^{ph}(1-\xi_0^{ph}M^2)$, where Θ_0 is the bare value of the Debye temperature. The crystalline lattice heat capacity in the Debye approximation, calculated by $C_{lat} = T(\partial S_{lat}/\partial T)$ is given by:

$$C_{lat}(T,B,P) = N_i\Re\left[36\left(\frac{T}{\tilde{\Theta}_D}\right)^3\int_0^{\tilde{\Theta}_D/T}\frac{x^3}{(\mathrm{e}^x-1)}\mathrm{d}x - 9\left(\frac{\tilde{\Theta}_D}{T}\right)\frac{1}{\left(\mathrm{e}^{\tilde{\Theta}_D/T}-1\right)}\right]. \tag{87}$$

Notice that the crystalline lattice entropy and heat capacity depend on the applied magnetic field and pressure through the renormalized Debye temperature $\tilde{\Theta}_D$. If the magnetoelastic coupling is neglected, i.e., $\xi_0^{ph} = 0$, the Debye temperature and consequently the crystalline lattice entropy and heat capacity become magnetic field independent. The total heat capacity is given by: $C(T,B,P) = C_{el}^{spd}(T) + C_{mag}^{4f}(T,B,P) + C_{lat}(T,B,P)$, where $C_{el}^{spd}(T) = \gamma T$ is the electronic heat capacity, $C_{mag}^{4f}(T,B,P)$ is the magnetic heat capacity and $C_{lat}(T,B,P)$ is the crystalline lattice heat capacity given in Eq. (87). The total entropy is $S(T,B,P) = S_{el}^{spd}(T) + S_{mag}^{4f}(T,B,P) + S_{lat}(T,B,P)$, where $S_{el}^{spd}(T) = \gamma T$ is the electronic entropy, $S_{mag}^{4f}(T,B,P)$ is the magnetic entropy given in Eq. (73) and $S_{lat}(T,B,P)$ is crystalline lattice entropy given in Eq. (86). Once the total entropy is known, the isothermal entropy change (ΔS_{iso}) and the adiabatic temperature change (ΔT_{ad}) upon magnetic field variation are calculated by Eqs. (2) and (3), respectively.

4.1.3. Calculations without crystalline electrical field

The discussion made so far, is quite general and can be suitable for many rare earth based compounds, with or without the crystalline electrical field interaction. However, if the crystalline electrical field interaction can be neglected, a very useful discussion with analytical expressions for the magnetic and thermodynamic quantities can be obtained. In the absence of the crystalline electrical field and supposing that the magnetic field is applied along the z direction, the magnetic Hamiltonian given in Eq. (68) reduces to:

$$\mathcal{H}_{mag}^{4f} = -\sum_i g\mu_B B^{eff} J_i^z \tag{88}$$

where $\vec{B}_{eff} = \vec{B} + (\tilde{\mathcal{J}}_0\langle\vec{J}\rangle + \tilde{\mathcal{J}}_1\langle\vec{J}\rangle^3)/g\mu_B$. Using $J^z\,|J, m\rangle = m\,|J, m\rangle$, the energy eigenvalues of this Hamiltonian per ion, are given by:

$$\varepsilon_m = -g\mu_B m B^{eff}, \tag{89}$$

where m can assume $(2J + 1)$ values in the interval $-J \le m \le J$. Using these energy eigenvalues, we can write the partition function for the magnetic Hamiltonian as a function of temperature, magnetic field and pressure as: [194]

$$Z_{mag}^{4f}(T, B, P) = \sum_{m=-J}^{J} \exp\left(\beta g\mu_B m B^{eff}\right). \tag{90}$$

The temperature and magnetic field dependence of the partition function is directly included through β and B^{eff}. The pressure dependence is indirectly included through the renormalization of the exchange interaction parameters $\tilde{\mathcal{J}}_0$ and $\tilde{\mathcal{J}}_1$. Defining the auxiliary variable

$$y = \frac{g\mu_B B^{eff}}{k_B T} = \beta g\mu_B\left(B + \frac{\tilde{\mathcal{J}}_0\langle J\rangle + \tilde{\mathcal{J}}_1\langle J\rangle^3}{g\mu_B}\right), \tag{91}$$

and after a simple algebra, the magnetic partition function per ion reads:

$$Z_{mag}^{4f}(T, B, P) = \frac{\sinh\left[\left(J + \frac{1}{2}\right)y\right]}{\sinh\left(\frac{y}{2}\right)}. \tag{92}$$

The magnetic free energy per ion, calculated from $F_{mag}^{4f} = -(1/\beta)\ln Z_{mag}^{4f}$ is given by:

$$F_{mag}^{4f}(T, B, P) = -\frac{1}{\beta}\left[\ln\frac{\sinh\left[\left(J + \frac{1}{2}\right)y\right]}{\sinh\left(\frac{y}{2}\right)}\right]. \tag{93}$$

The magnetization, calculated from $M = -(\partial F/\partial B^{eff})_T$, is given by:

$$M(T, B, P) = g\mu_B J B_J(y), \tag{94}$$

where $B_J(y)$ is the Brillouin function given by:

$$B_J(y) = \frac{1}{J}\left[\left(\frac{2J+1}{2}\right)\coth gh\left[\left(J + \frac{1}{2}\right)y\right] - \frac{1}{2}\coth gh\left(\frac{y}{2}\right)\right]. \tag{95}$$

Using the relation $JB_J(y) = \langle J\rangle$, the magnetization can be written as $M = g\mu_B\langle J\rangle$. Notice that Eq. (94) enable us to calculate the effects of temperature, magnetic field and pressure on the magnetization.

The magnetic part of the entropy is calculated by taking the derivative of the magnetic free energy with respect to temperature with constant effective magnetic field, i.e., $S_{mag}^{4f} = -(\partial F_{mag}^{4f}/\partial T)_{B^{eff}}$. Thus, taking the temperature derivative of Eq. (93), the magnetic entropy per mol is:

$$S_{mag}^{4f}(T, B, P) = N_m\Re\left\{\ln\left[\frac{\sinh\left[\left(J + \frac{1}{2}\right)y\right]}{\sinh\left(\frac{y}{2}\right)}\right] - \frac{g\mu_B B^{eff}}{k_B T}\left[\left(J + \frac{1}{2}\right)\frac{\cosh\left[\left(J + \frac{1}{2}\right)y\right]}{\sinh\left[\left(J + \frac{1}{2}\right)y\right]} - \frac{1}{2}\frac{\cosh\left(\frac{y}{2}\right)}{\sinh\left(\frac{y}{2}\right)}\right]\right\}, \tag{96}$$

where $\Re = N_A k_B$ is the gas constant and N_m represents the number of magnetic ions per unit formula. In the limit of high temperatures, the second term in the magnetic entropy given before, goes to zero. Moreover, at high temperatures the auxiliary variable y, given in Eq. (91), goes to zero, so that the function $\sinh(y)$ goes to y. Therefore, at high temperatures the magnetic entropy gets the value:

$$S_{mag}^{4f}(T, B, P) = N_m\Re\ln\left[\frac{\left(J + \frac{1}{2}\right)y}{\left(\frac{y}{2}\right)}\right] = N_m\Re\ln(2J + 1). \tag{97}$$

This upper limit of the magnetic entropy has been experimentally observed. Using the partition function given in Eq. (92) and the Brillouin function given in Eq. (95), we can rewrite the magnetic entropy given in Eq. (96) as:

$$S_{mag}^{4f}(T,B,P) = N_m \Re \left[\ln Z - yJB_J(y)\right]. \tag{98}$$

The magnetic heat capacity at constant magnetic field, calculated from the relation $C_{mag}^{4f} = T(\partial S_{mag}^{4f}/\partial T)_{B^{eff}}$ is given by:

$$C_{mag}^{4f}(T,B,P) = \frac{N_m \Re \left(g\mu_B B^{eff}\right)^2 J}{k_B T\left[k_B T - \mathcal{J}_{eff} J \frac{\partial B_J(y)}{\partial y}\right]}\left[\frac{\partial B_J(y)}{\partial y}\right], \tag{99}$$

where $\tilde{\mathcal{J}}_{eff} = \tilde{\mathcal{J}}_0 + \tilde{\mathcal{J}}_1\langle J\rangle^2$ and $\partial B_J(y)/\partial y$ is the derivative of the Brillouin function, given by:

$$\frac{\partial B_J(y)}{\partial y} = \frac{1}{J}\left[-\left(J+\frac{1}{2}\right)^2 \cos\sec h^2\left[\left(J+\frac{1}{2}\right)y\right] + \left(\frac{1}{2}\right)^2 \cos\sec h^2\left(\frac{y}{2}\right)\right]. \tag{100}$$

The total heat capacity is $C(T,B,P) = C_{el}^{spd}(T) + C_{lat}(T,B,P) + C_{mag}^{4f}(T,B,P)$ where $C_{el}^{spd}(T) = \gamma T$ is the electronic heat capacity, $C_{lat}(T,B,P)$ is the crystalline lattice heat capacity given in Eq. (87) and $C_{mag}^{4f}(T,B,P)$ is the magnetic heat capacity given in Eq. (99). Thus the total heat capacity is:

$$\begin{aligned} C(T,B,P) = {} & \gamma T + N_i \Re\left[36\left(\frac{T}{\tilde{\Theta}_D}\right)^3 \int_0^{\tilde{\Theta}_D/T} \frac{x^3}{(e^x-1)}dx - 9\left(\frac{\tilde{\Theta}_D}{T}\right)\frac{1}{\left(e^{\tilde{\Theta}_D/T}-1\right)}\right] \\ & + \frac{N_m \Re\left(g\mu_B B^{eff}\right)^2 J}{k_B T\left[k_B T - \mathcal{J}_{eff} J \frac{\partial B_J(y)}{\partial y}\right]}\left[\frac{\partial B_J(y)}{\partial y}\right]. \end{aligned} \tag{101}$$

The total entropy is $S(T,B,P) = S_{el}^{spd}(T) + S_{lat}(T,B,P) + S_{mag}^{4f}(T,B,P)$ where $S_{el}^{spd}(T) = \gamma T$ is the electronic entropy, $S_{lat}(T,B,P)$ is the crystalline lattice entropy given in Eq. (86) and $S_{mag}^{4f}(T,B,P)$ is the magnetic entropy given in Eq. (98). Thus the total entropy is

$$S(T,B,P) = \gamma T + N_i\left[-3\Re \ln\left(1 - e^{-\frac{\tilde{\Theta}_D}{T}}\right) + 12\Re\left(\frac{T}{\tilde{\Theta}_D}\right)^3 \int_0^{\tilde{\Theta}_D/T} \frac{x^3}{e^x-1}dx\right] + N_m \Re\left[\ln Z - yJB_J(y)\right]. \tag{102}$$

4.2. *Application to* Gd *based compounds*

In Gadolinium based compounds, the effect of the crystalline electrical field can be neglected, so that the magnetocaloric properties can be calculated using the formalism of the Section 4.1.3. In order to calculate the magnetocaloric effect in gadolinium metal, we take $J = 7/2$ and $g = 2$. The exchange interaction parameter was taken as $\tilde{\mathcal{J}}_0 = 4.6$ meV in order to reproduce the experimental value of the Curie temperature around 292 K. The magnetoelastic coupling parameter $\tilde{\mathcal{J}}_1$ was taken as zero, since Gd undergoes a second order phase transition. The Debye temperature and the Sommerfeld coefficient were taken as $\Theta_D = 154$ K and $\gamma = 5.4$ mJ/(mol K^2) respectively [195].

The magnetic and total specific heat capacity for Gd, calculated for $B = 0$ (solid line) and $B = 5$ T (dashed line) are shown in Fig. 10. From this figure, an overall agreement can be observed between theoretical calculations and the available experimental data [196]. However, around the magnetic ordering temperature, there is some deviation between calculations and experimental data for $B = 0$. This discrepancy comes mainly from the magnetic part of the specific heat capacity, which exhibits an abrupt drop around the magnetic ordering temperature. This is an artifact of the mean field theory, since short range interactions are not taken into account. The isothermal entropy change ΔS_{iso} and the adiabatic temperature change ΔT_{ad}, calculated from the entropy curves upon magnetic field variation from 0 to 5 T are shown in Figs. 11 and 12 respectively.

We also calculate the magnetocaloric effect in the compounds GdZn, GdPd and Gd_5Si_4. Due to the fact that the magnetism in these compounds comes mainly from Gd ions, we can consider them as an effective gadolinium. With this assumption, we use the same formalism of the Section 4.1.3 to calculate the magnetocaloric properties in these compounds. To this end is necessary to determine effective exchange interaction parameters to fit the corresponding experimental data of their magnetic ordering temperatures. The Debye temperature for Gd_5Si_4 was taken as $\Theta_D = 350$ K. The remaining parameters are the same used in the case of metallic gadolinium. The magnetocaloric potentials ΔS_{iso} and ΔT_{ad} calculated for GdZn, GdPd and Gd_5Si_4 are also shown in Figs. 11 and 12 respectively. From these figures, a good agreement can be observed between theoretical calculations and the available experimental data [19,172,196–199]. It is worth mentioning that the model developed in Section 4.1.3 can be applied to calculate the magnetocaloric effect in many other Gd based compounds with non magnetic ions.

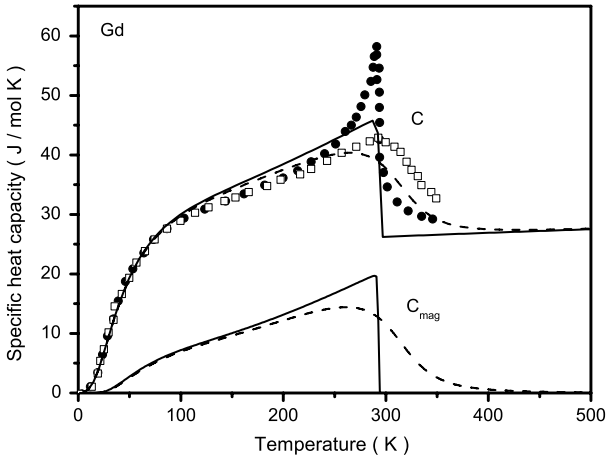

Fig. 10. Magnetic and total specific heat capacity (C_{mag} and C) in gadolinium metal. Solid and dashed lines are theoretical calculations for $B = 0$ and 5 T, respectively. Solid circles and open squares are experimental data [196] for $B = 0$ and 5 T.

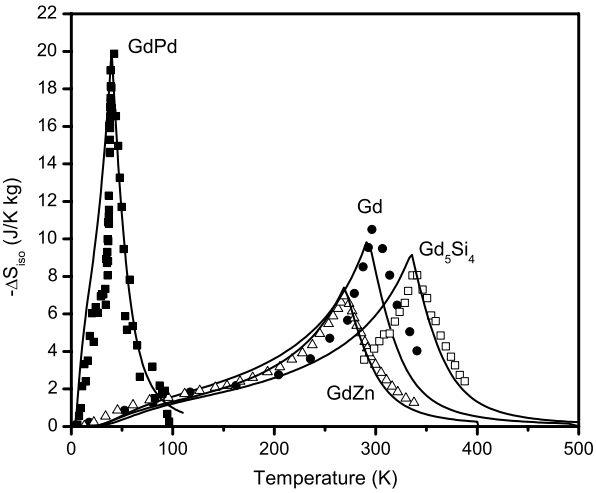

Fig. 11. Isothermal entropy changes upon magnetic field variation from 0 to 5 T for Gd, GdPd, GdZn and Gd_5Si_4. Solid lines are theoretical calculations and symbols represent experimental data.

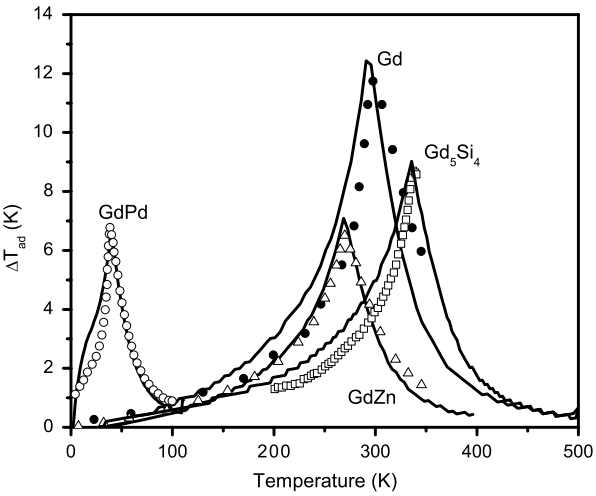

Fig. 12. Adiabatic temperature changes upon magnetic field variation from 0 to 5 T for Gd, GdPd, GdZn, and Gd_5Si_4. Solid lines are theoretical calculations and symbols represent experimental data.

Table 1
Crystalline electrical field parameters, exchange interaction parameter ($\tilde{\lambda}_0$) and the easy magnetization direction for $R\mathrm{Al}_2$ compounds.

Compounds	x	W (meV)	$\tilde{\lambda}_0$ (T^2/meV)	Easy direction	Refs.
PrAl_2	0.74	−0.330	256.0	⟨100⟩	[182,106,200]
NdAl_2	−0.37	0.160	417.6	⟨100⟩	[182,106,201]
TbAl_2	0.90	0.020	81.6	⟨111⟩	[182,106,200]
DyAl_2	0.30	−0.011	44.0	⟨100⟩/ ⟨111⟩	[182,100,202]
HoAl_2	−0.34	0.015	18.2	⟨100⟩	[182,106]
ErAl_2	−0.26	−0.025	13.5	⟨111⟩	[182,100,203]
TmAl_2	0.5	0.04	9.9	⟨111⟩	[182,106]

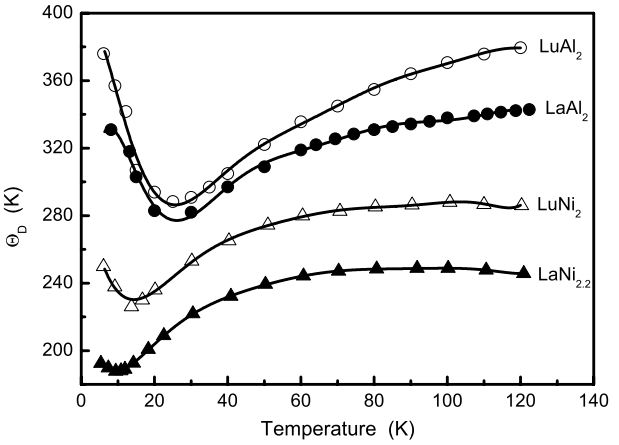

Fig. 13. Temperature dependence of the Debye temperature in LaAl_2, LuAl_2, $\mathrm{LaNi}_{2.2}$ and LuNi_2.

4.3. Application to $R\mathrm{Al}_2$ compounds

The magnetism in the compounds $R\mathrm{Al}_2$ comes from the rare earth ions, since Al is non magnetic. For rare earth ions other than Gd, the crystalline electrical field interaction plays a key role in the establishment of the magnetic order. Therefore, the formalism described in Section 4.1.3 should not be used to calculate the magnetocaloric effect in this type of compound. In this case, the magnetic and magnetocaloric properties should be calculated through the general formalism of Section 4.1, where the crystalline electric field is taken into account. The compounds $R\mathrm{Al}_2$ exhibit cubic symmetry, so that the crystalline electrical field can be described by the model given in Eq. (59). The crystalline electrical field parameters, the exchange interaction parameter and the easy magnetization direction for some $R\mathrm{Al}_2$ compounds [100,106,182,200–203] are shown in Table 1. The magnetoelastic parameter $\tilde{\lambda}_1 = \tilde{\mathcal{J}}_1/(g^4\mu_B^4)$ was taken as zero, since all compounds of the $R\mathrm{Al}_2$ series undergo a second order phase transition. The electronic heat capacity coefficient was taken as $\gamma = 5.4$ mJ/(mol K^2).

The lattice entropy for each compound of the $R\mathrm{Al}_2$ series was determined assuming that it varies linearly in the series, when the rare earth component changes from the non-magnetic La to the non-magnetic Lu. On this assumption, the expression for the lattice entropy can be determined by the following average expression [100]:

$$S_{lat}^{R}(T) = \frac{(14-n)S_{lat}^{La}(T) + nS_{lat}^{Lu}(T)}{14}, \tag{103}$$

where $1 \leq n \leq 14$ gives the relative position of the rare earth element in the rare earth series. Here S_{lat}^{La} and S_{lat}^{Lu} are the lattice entropy for LaAl_2 and LuAl_2 obtained in the Debye approximation by using the experimental data [204,205] of the Debye temperature shown Fig. 13.

In Fig. 14, we plot the isothermal entropy change upon magnetic field variation from 0 to 5 T for the $R\mathrm{Al}_2$ series. In this figure, the solid lines represent the theoretical calculations, obtained using the model parameters shown in Table 1, and the symbols represent the available experimental data for ErAl_2 and DyAl_2.

Now, we discuss the magnetocaloric effect in DyAl_2 considering the magnetic field applied along the three main crystallographic directions. Experimental data show that at 4.2 K, when the magnetic field is applied along the ⟨111⟩ direction, the initial magnetization vector, which is along the ⟨100⟩ direction, rotates in the ⟨100⟩–⟨111⟩ plane. This rotation is almost linear with the magnetic field intensity until a critical field $B_C \approx 5.8$ T is achieved. After that, a jump occurs in the magnetization vector so that it becomes parallel to the direction of the applied magnetic field.

The rotation of the magnetization can be described by an angle between the magnetization vector and the easy magnetization direction. This angle, which we call Θ, depends on the temperature and the magnitude of the applied magnetic field. A sketch of this angle is shown in the inset of the Fig. 15. The temperature and magnetic field dependence of

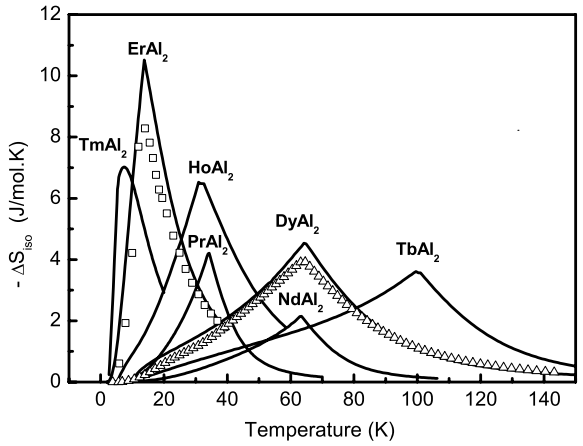

Fig. 14. Isothermal entropy change in RAl_2 upon magnetic field variation from 0 to 5 T. Solid lines are calculations and symbols are experimental data for $ErAl_2$ and $DyAl_2$.

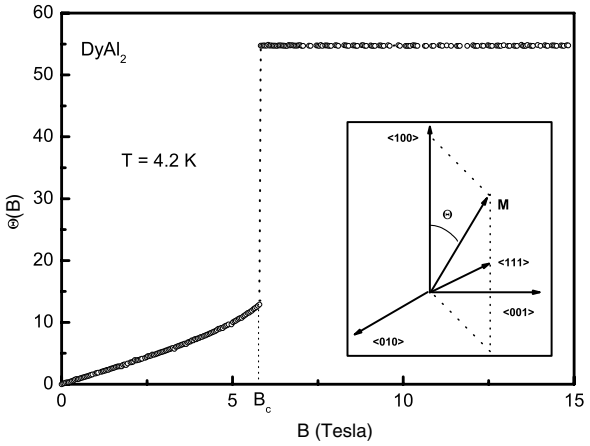

Fig. 15. Magnetic field dependence of the angle Θ between the easy magnetization direction $\langle 100\rangle$ and the magnetization vector in $DyAl_2$. Inset shows the angle Θ.

the angle Θ can be calculated by the following relation:

$$\tan\Theta = \frac{\sqrt{M_y^2 + M_z^2}}{M_x}, \tag{104}$$

where the magnetization components M_x, M_y and M_z are given by Eq. (70). Fig. 15 shows the magnetic field dependence of the angle Θ between the easy magnetization direction $\langle 100\rangle$ and the magnetization vector in $DyAl_2$, when the magnetic field is applied along the $\langle 111\rangle$ direction. Fig. 16 shows at $T = 4.2$ K, the magnetization component along the crystallographic directions $\langle 100\rangle$, $\langle 110\rangle$ and $\langle 111\rangle$.

The temperature dependence of the magnetic entropy, was theoretically calculated considering the magnetic field applied along the directions $\langle 100\rangle$, $\langle 110\rangle$ and $\langle 111\rangle$. When the magnetic field is applied along the directions $\langle 100\rangle$ and $\langle 110\rangle$ the usual behavior of the magnetic entropy was observed [107], i.e., the entropy increases smoothly with increasing temperature and decreases when the magnetic field is increased. These entropy curves are not shown in this report. However, when the magnetic field is applied along the $\langle 111\rangle$ direction, an anomalous behavior of the magnetic entropy appears at low temperature, i.e., the magnetic entropy increases with increasing magnetic field, as can be seen in Fig. 17. In this figure, the open squares show the temperatures where the crossing occurs between the entropy curves for $B = 0$ and $B \neq 0$. From Fig. 17, it can be observed that the temperature region where the anomaly appears becomes narrower when the magnetic field is increased. It should also be mentioned that the set of entropy curves for $B \neq 0$ (full lines) has the normal behavior.

Fig. 18 shows the isothermal entropy change upon magnetic field variation from 0 to 1 T (curve A), from 0 to 2 T (curve B) and from 0 to 5 T (curve C) applied along the $\langle 111\rangle$ crystallographic direction. In this figure, open squares indicate the temperature where ΔS_{iso} changes sign. From Fig. 18, the inverse magnetocaloric effect (i.e., negative values for $-\Delta S_{iso}$) can

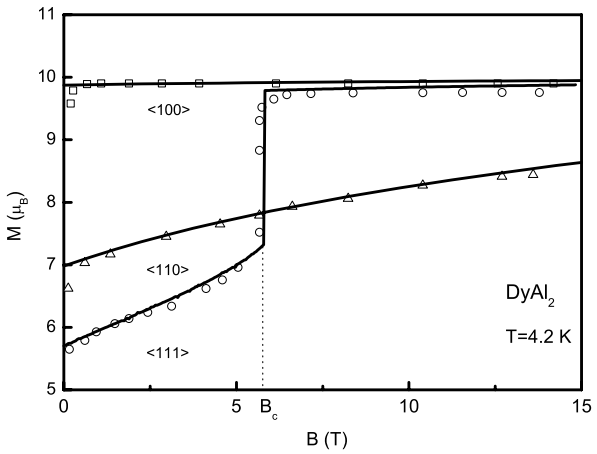

Fig. 16. Magnetization component at 4.2 K in $DyAl_2$. Solid lines are theoretical calculations and symbols are experimental data [182].

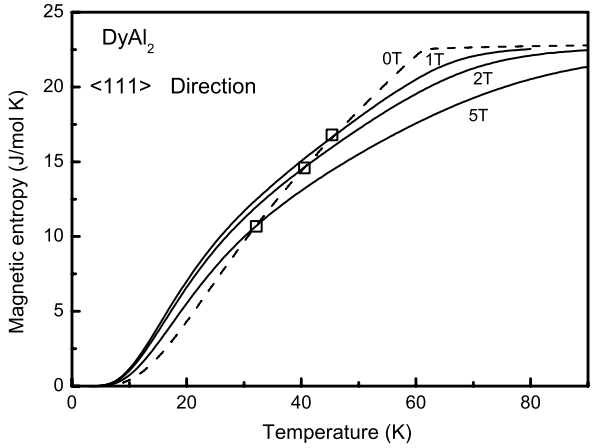

Fig. 17. Magnetic entropy in $DyAl_2$ in the absence of magnetic field and for magnetic field of 1, 2 and 5 T applied along ⟨111⟩ direction.

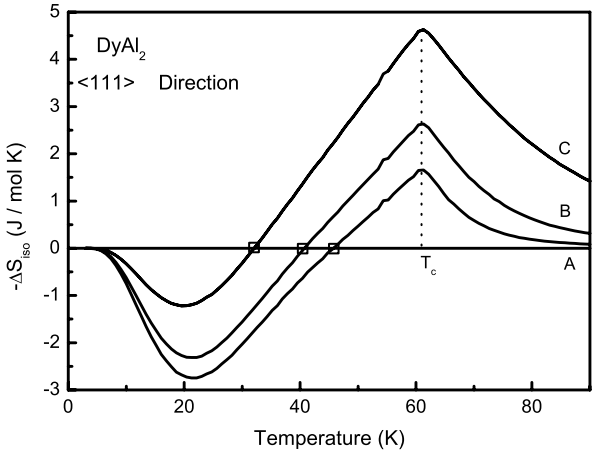

Fig. 18. Isothermal entropy change in $DyAl_2$ upon magnetic field variation from 0 to 1 T (curve A), from 0 to 2 T (curve B) and from 0 to 5 T (curve C) applied along the ⟨111⟩ direction.

be observed at low temperatures. Also, it can be observed that the inverse magnetocaloric effect is reduced with increasing magnetic field variation. Such a behavior has been experimentally [206] observed in $DyAl_2$ single crystal.

Table 2
Crystalline electrical field and exchange interaction parameters, Curie temperatures and the easy magnetization direction for RNi_2.

Comp.	x	W (meV)	$\tilde{\lambda}_0$ (T^2/meV)	T_C (K)	Easy direction	Refs.
$GdNi_2$	0	0	93.5	77.8	⟨001⟩	[207,208]
$PrNi_2$	−0.64	−0.23	115.7	–	⟨001⟩	[209]
$NdNi_2$	0.89	0.28	119	11	⟨001⟩	[210]
$TbNi_2$	0.73	−0.066	32	37.5	⟨111⟩	[210,211]
$DyNi_2$	−0.1	−0.019	15.5	20.6	⟨001⟩	[100]
$HoNi_2$	−0.44	0.021	11.3	15	⟨001⟩	[210]
$ErNi_2$	−0.54	−0.034	10	7	⟨001⟩	[212]

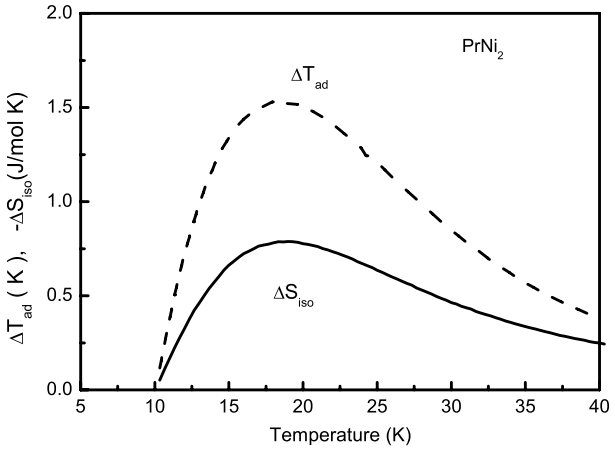

Fig. 19. ΔS_{iso} and ΔT_{ad} in $PrNi_2$ upon magnetic field variation from 0 to 5 T.

4.4. Application to RNi_2 compounds

The compounds RNi_2 have also cubic symmetry, so that the crystalline electrical field can be described by the model in Eq. (59). The crystalline electrical field and exchange interaction parameters (see References [100,207–212]) used to calculate the magnetocaloric effect in this series of compounds are shown in Table 2. The magnetoelastic parameter $\tilde{\lambda}_1 = \tilde{\mathcal{J}}_1/(g^4\mu_B^4)$ was taken as zero, since all compounds of the RNi_2 series undergo a second order phase transition. The crystalline lattice entropy in the RNi_2 series was also determined using relation (103), where the lattice entropy for $LaNi_2$ and $LuNi_2$ was determined in the Debye approximation, using the Debye temperature for $LaNi_{2.2}$ and $LuNi_2$ shown in Fig. 13. It should be mentioned that the data for the Debye temperature in the compound $LaNi_{2.2}$ can be considered as a good approximation for the compound $LaNi_2$ [213]. The electronic heat capacity coefficient $\gamma = 5.4(\text{mJ/mol K}^2)$ was used for all RNi_2 compounds.

The magnetocaloric potentials ΔS_{iso} and ΔT_{ad} upon magnetic field variation from 0 to 5 T, for the paramagnetic compound $PrNi_2$ are shown in Fig. 19. The corresponding magnetocaloric potentials for the remaining compounds of the RNi_2 series are plotted in Figs. 20 and 21 respectively. From Figs. 20 and 21, an anomalous second peak can be observed at low temperature ($T \approx 1.5$ K) in the ΔS_{iso} and ΔT_{ad} curves of the compound $HoNi_2$. The existence of this second peak was ascribed to the high density of crystalline electrical field states in $HoNi_2$ at low temperature, for the crystalline electrical field parameter $x = -0.44$.

Fig. 22 shows the temperature dependence of the refrigerant capacity $\Delta S_{iso}\Delta T_{ad}$ in RNi_2 series. From this figure, a good agreement can be observed between theoretical calculations and the available experimental data for $ErNi_2$ and $DyNi_2$. It can also be observed that the compounds $ErNi_2$, $DyNi_2$ and $TbNi_2$ exhibit approximately the same value of the refrigerant capacity at T_C. These almost constant peak values can be important to design composite materials [214–217] with the table-like behavior (i.e., a constant refrigerant capacity as a function of temperature). This feature is very important for magnetic refrigerators working in the Ericsson cycle. A composite material was simulated formed by samples of $ErNi_2$, $DyNi_2$ and $TbNi_2$. The best molar ratios for the composite material $[ErNi_2]_{y_1}[DyNi_2]_{y_2}[TbNi_2]_{y_3}$ were determined to be $y_1 = 0.3437$; $y_2 = 0.3108$ and $y_3 = 0.3456$. The refrigerant capacity $\Delta S_{iso}\Delta T_{ad}$, for this composite material is shown by the solid line in Fig. 23. For the sake of comparison, also plotted in this figure is the refrigerant capacity for each component of the composite material.

4.5. Application to RNi_5 compounds

The compounds of the RNi_5 series, crystallize in the hexagonal $CaCu_5$ — type structure [218] and their magnetism is mainly due to the R^{3+} ions. Their magnetic properties can be calculated by using the magnetic Hamiltonian, with the crystalline electrical field term in the hexagonal symmetry as given in Eq. (60).

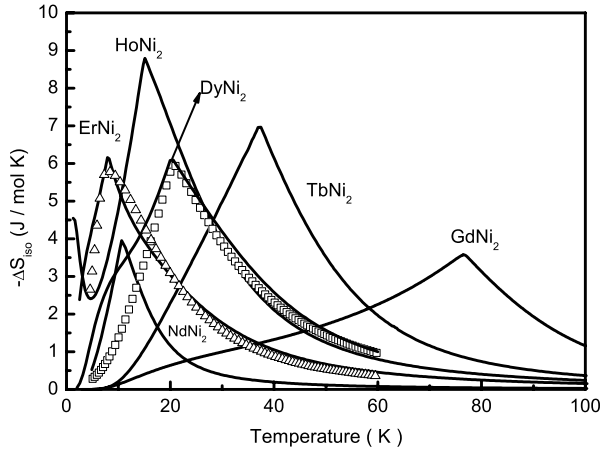

Fig. 20. Isothermal entropy change in RNi_2 upon magnetic field variation from 0 to 5 T. Solid lines are calculations and symbols represent the available experimental data.

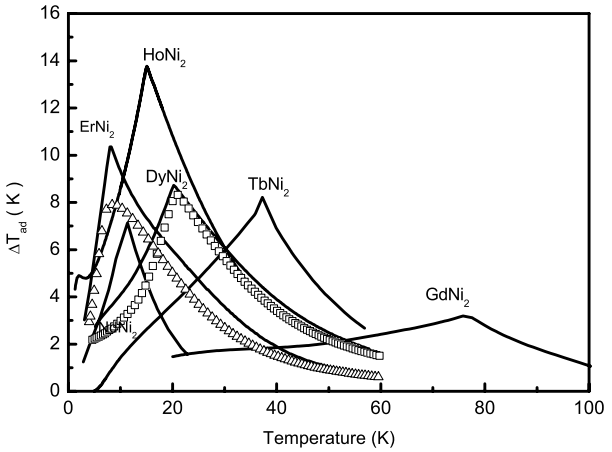

Fig. 21. Adiabatic temperature change in RNi_2 upon magnetic field variation from 0 to 5 T. Solid lines are calculations and symbols represent the available experimental data.

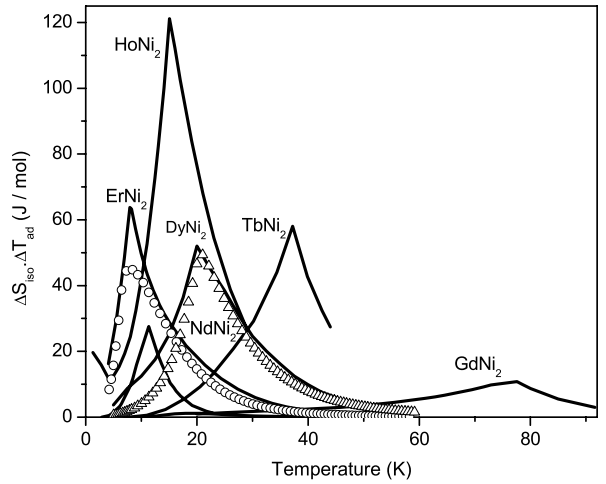

Fig. 22. Refrigerant capacity for the series RNi_2 upon magnetic field variation from 0 to 5 T. The solid lines are the theoretical calculations, while open circles and triangles represent experimental data for $ErNi_2$ and $DyNi_2$ respectively.

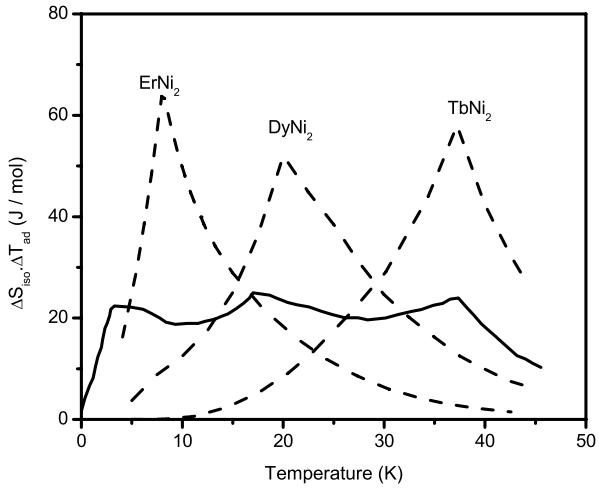

Fig. 23. Calculated refrigerant capacity for the composite material $[ErNi_2]_{0.3437}[DyNi_2]_{0.3108}[TbNi_2]_{0.3456}$ (solid line). Dashed lines represent the refrigerant capacity for $ErNi_2$, $DyNi_2$ and $TbNi_2$.

Table 3
Model parameters for RNi_5 series. The crystalline electrical field parameters B_2^0, B_4^0, B_6^0 and B_6^6 are in meV. The exchange interaction parameter $\tilde{\lambda}_0$ is in (T^2/meV).

Comp.	B_2^0	$B_4^0 \times 10^2$	$B_6^0 \times 10^4$	$B_6^6 \times 10^2$	$\tilde{\lambda}_0$	T_C (K)	Easy dir.	Refs.
$GdNi_5$	–	–	–	–	–	32	–	[219]
$DyNi_5$	0.198	0.0190	0.0095	0.0024	–	11.6	b	[220]
$HoNi_5$	0.0991	0.0164	−0.0017	−0.0026	3.09	5	a	[221]
$NdNi_5$	0.289	0.125	−0.302	−0.116	63.8	8	a	[222]
$TbNi_5$	0.331	−0.0034	−0.0345	−0.0034	13.9	23	a	[220]
$ErNi_5$	−0.073	−0.0092	0.00124	0.0028	–	9	c	[223]
$PrNi_5$	0.61	0.496	1.01	0.27	29.9	–	a	[224]

The crystalline electrical field and the exchange interaction parameters for RNi_5, collected from References [219–224], are shown in Table 3. The magnetoelastic parameter $\tilde{\lambda}_1 = \tilde{\mathcal{J}}_1/(g^4\mu_B^4)$ was taken as zero, since all compounds of the RNi_5 series undergo a second order phase transition. The Sommerfeld coefficient used to calculate the electronic entropy was $\gamma = 36$ mJ/mol K^2, taken from the non-magnetic compound $LaNi_5$ [225]. The lattice entropy was considered in the Debye approximation, where the Debye temperature was adjusted to fit the experimental data of heat capacity [219].

In Figs. 24 and 25 are plotted the isothermal entropy change and the adiabatic temperature change upon magnetic field variation from 0 to 5 T in the compounds $GdNi_5$ and $PrNi_5$ respectively. From these figures, it can be observed that the theoretical calculations reproduce very well the available experimental data [111]. In addition, it can also be observed from Fig. 25, that $PrNi_5$ exhibits at low temperature, the inverse magnetocaloric effect, i.e., $(-\Delta S_{iso} < 0)$ for positive magnetic field change $(\Delta B > 0)$. The inverse magnetocaloric effect in $PrNi_5$ was attributed to the crossing of the quantum energy levels due to the crystalline electrical field [90].

4.6. *Anisotropic magnetocaloric effect: Application to* $DyAl_2$

The entropy of anisotropic materials can be varied by changing the direction of the applied magnetic field. In this case, the magnetic entropy given in Eq. (73) can be rewritten as:

$$S_{mag}(T, B, P, \theta_x, \theta_y, \theta_z) = N_m \Re \left[\sum_m \exp(-\beta\varepsilon_m) + \frac{1}{k_B T} \frac{\sum_m \varepsilon_m \exp(-\beta\varepsilon_m)}{\sum_m \exp(-\beta\varepsilon_m)} \right], \tag{105}$$

where the angles θ_x, θ_y and θ_z represent the direction of the applied magnetic field. However, it should be emphasized that now the energies ε_m and consequently the magnetic entropy depend on the direction of the applied magnetic field. The total entropy is $S = S_{el} + S_{lat} + S_{mag}$, where $S_{el} = \gamma T$ is the electronic entropy, S_{lat} is the lattice entropy given in Eq. (86) and S_{mag} is the magnetic entropy given in Eq. (105). The anisotropic magnetocaloric potentials ΔS_{iso}^{ani} and ΔT_{ad}^{ani} are calculated from Eqs. (36) and (37).

When the magnetic field is applied along a direction different from the easy one, the magnetization vector and its component along the direction of the applied magnetic field are not parallel. In this scenario, two interesting processes

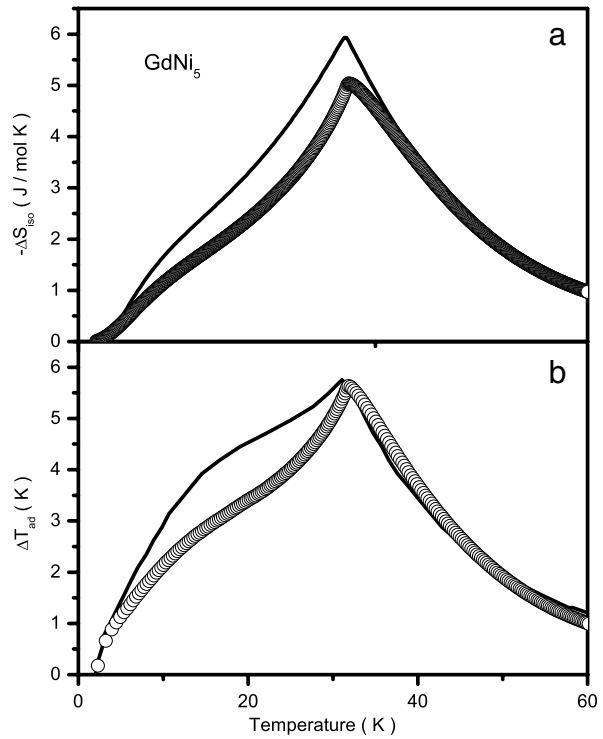

Fig. 24. Isothermal entropy change (a) and adiabatic temperature change (b) in $GdNi_5$ upon magnetic field variation from 0 to 5 T. Solid lines are calculations and symbols are experimental data [111].

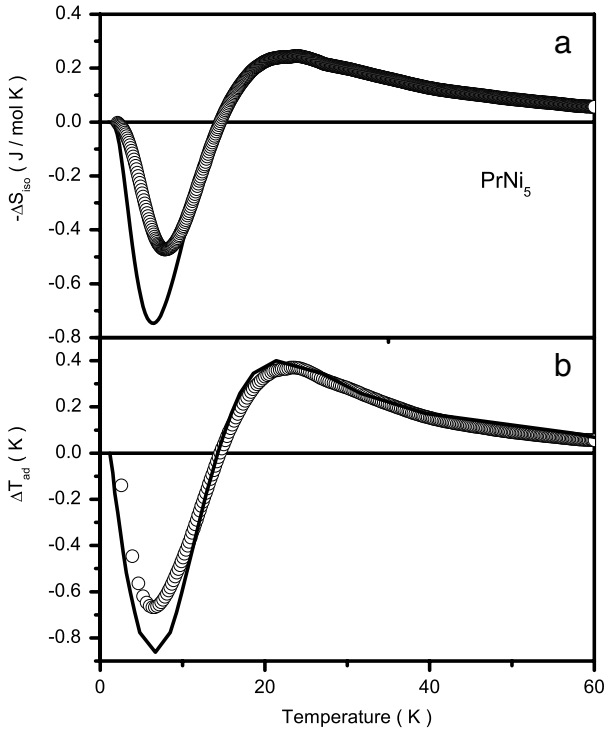

Fig. 25. Isothermal entropy change (a) and adiabatic temperature change (b) in $PrNi_5$ upon magnetic field variation from 0 to 5 T. Solid lines are calculations and symbols are experimental data [111].

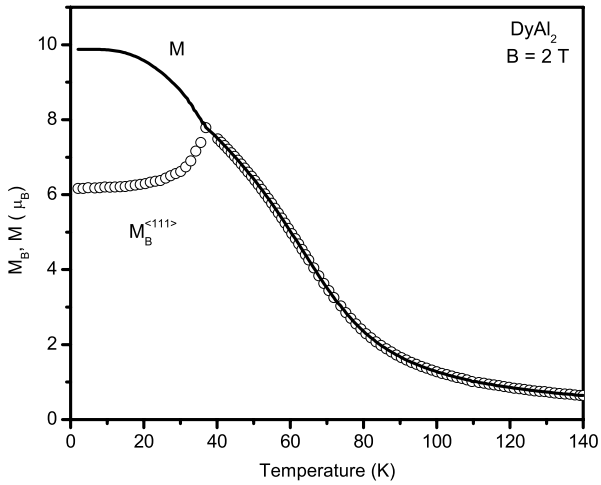

Fig. 26. Magnetization M (solid line) and its component M_B (open circles) in $DyAl_2$ for a magnetic field of 2 T applied along the ⟨111⟩ direction.

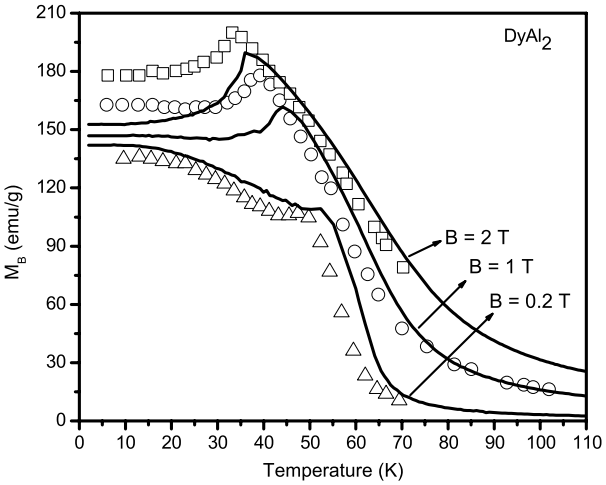

Fig. 27. Magnetization component M_B in $DyAl_2$ for magnetic fields of 0.2, 1 and 2 T applied along the ⟨111⟩ direction. Solid lines are calculations while symbols are experimental data [206].

should be analyzed. In the first one, the magnetic field is kept constant and the temperature increases. In this case, the magnetization rotates from its initial direction towards the direction of the applied magnetic field. At a given critical temperature, called the spin reorientation temperature T_R, the magnetization vector becomes parallel to the applied magnetic field. In a second process, the temperature is kept fixed and the magnetic field is increased. In this case, as the magnetic field increases, the magnetization starts to rotate from the easy magnetization direction towards the direction of the applied magnetic field. At a given critical magnetic field, called the spin reorientation magnetic field B_R, the magnetization becomes parallel to the applied magnetic field direction.

With this discussion in mind, we calculate the magnetization in $DyAl_2$ by applying the magnetic field along a direction different from the easy one, which is ⟨100⟩. In Fig. 26, is shown the temperature dependence of the magnetization M (solid line) and its components M_B (open circles) along the direction of a magnetic field of 2 T applied along the ⟨111⟩ direction [144]. From this figure it can be observed that, while the magnetization M decreases with increasing temperature, the magnetization component along the direction of the applied magnetic field increases until the temperature $T_R \approx 36$ K. Above this temperature, both M and M_B curves are coincident. Therefore, $T_R \approx 36$ K is the spin reorientation temperature for $DyAl_2$ at an applied magnetic field of 2 T.

We calculate the magnetization M and its component M_B for different values of the magnetic field applied along ⟨111⟩ direction. In Fig. 27 is shown the temperature dependence of the magnetization component $M_B^{\langle 111\rangle}$ for magnetic fields of 0.2, 1 and 2 T applied along the ⟨111⟩ direction. The solid lines represent theoretical results and the symbols represent experimental data [206] obtained for monocrystalline sample. The spin reorientation temperatures are at the peaks in the $M_B^{\langle 111\rangle}$ curves, shown in Fig. 27. Thus, the spin reorientation temperatures are $T_R \approx 52.6$, 44 and 36 K, for magnetic fields of 0.2, 1 and 2 T respectively. It is worth noticing that, the higher the magnetic field intensity the smaller the spin reorientation

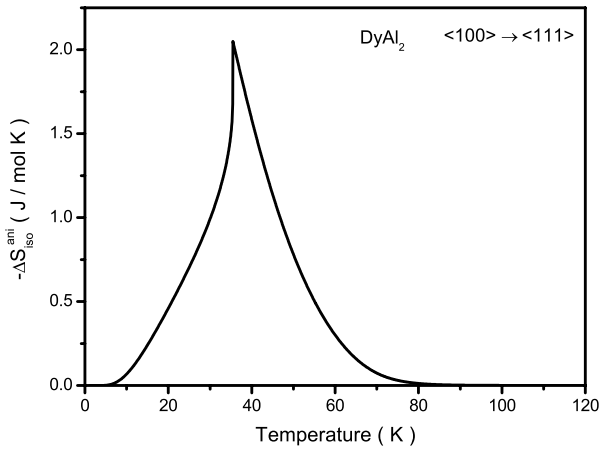

Fig. 28. Anisotropic isothermal entropy change in $DyAl_2$ for an applied magnetic field of 2 T rotating from ⟨100⟩ to ⟨111⟩ direction.

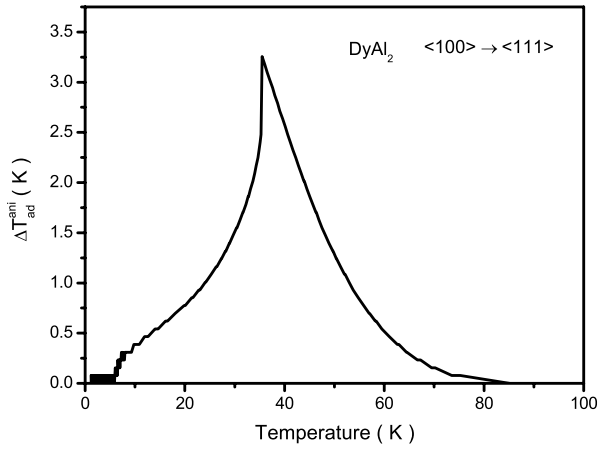

Fig. 29. Anisotropic adiabatic temperature change in $DyAl_2$ for an applied magnetic field of 2 T rotating from ⟨100⟩ to ⟨111⟩ direction.

temperature. This result is physically expected, since the increase of the magnetic field intensity along the ⟨111⟩ direction reduces the anisotropy energy, so that a smaller amount of thermal energy is necessary to rotate the magnetization towards the direction of the applied magnetic field.

We calculate the anisotropic magnetocaloric effect in the Laves phase compound $DyAl_2$, which has ⟨100⟩ as the easy magnetization direction. Fig. 28 shows the temperature dependence of the anisotropic isothermal entropy change in $DyAl_2$ for a fixed magnetic field of 2 T, whose direction changes from the easy magnetization direction ⟨100⟩ to the ⟨111⟩ direction. The corresponding anisotropic adiabatic temperature change is shown in Fig. 29. Notice that the change of the constant magnetic field from the easy magnetization direction ⟨100⟩ to ⟨111⟩ yields peaks in the magnetocaloric potentials around 2 J/mol K for ΔS_{iso}^{ani} and 3.2 K for ΔT_{ad}^{ani}, which occur at the reorientation temperature $T_R = 36$ K. These peaks in the anisotropic magnetocaloric potentials ΔS_{iso}^{ani} and ΔT_{ad}^{ani} are somewhat smaller than the peaks in the usual magnetocaloric potentials ΔS_{iso} and ΔT_{ad} obtained upon magnetic field variation from 0 to 2 T applied along the easy magnetic direction ⟨100⟩.

We also calculate the anisotropic magnetocaloric effect in $DyAl_2$ by rotating the applied magnetic field from arbitrary directions. In Figs. 30 and 31 are plotted the anisotropic isothermal entropy change and the anisotropic adiabatic temperature change obtained by rotating a constant magnetic field of 3 T from the ⟨011⟩ to ⟨100⟩ direction (solid line). For the sake of comparison, also plotted in these figures are the usual magnetocaloric potentials obtained for a magnetic field variation from 0 to 3 T applied along the easy magnetization direction (dashed line). From these figures, it can be observed that the peaks of the anisotropic magnetocaloric potentials ΔS_{iso}^{ani} and ΔT_{ad}^{ani} at the spin reorientation temperature $T_R = 22$ K, are larger than the peaks of the usual magnetocaloric potentials ΔS_{iso} and ΔT_{ad} at the Curie temperature $T_C = 62$ K. This outstanding result indicates that cooling by adiabatic rotation can be more efficient than cooling by adiabatic demagnetization.

4.7. Magnetocaloric effect in the two energy level model

In this subsection, we use the theoretical formulation of Section 4.1.3 to perform a systematic study of the magnetocaloric effect in the simple case of the two energy level model, without the crystalline electrical field interaction. We use the

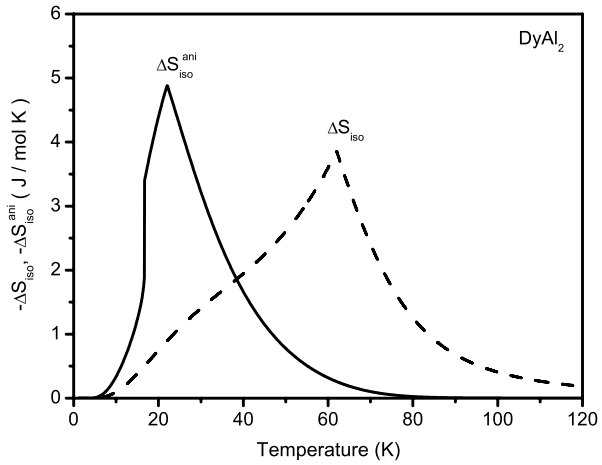

Fig. 30. Anisotropic isothermal entropy change in $DyAl_2$ for a constant magnetic field of 3 T rotating from the ⟨011⟩ to ⟨100⟩ direction (solid line). Dashed line represents the usual isothermal entropy change upon magnetic field variation from 0 to 3 T applied along the easy direction ⟨100⟩.

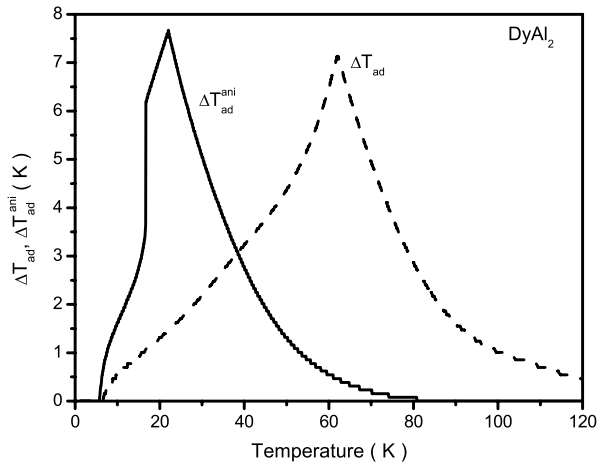

Fig. 31. Anisotropic adiabatic temperature change in $DyAl_2$ for a constant magnetic field of 3 T rotating from the ⟨011⟩ to ⟨100⟩ direction (solid line). Dashed line represents the usual adiabatic temperature change upon magnetic field variation from 0 to 3 T applied along the ⟨100⟩ direction.

following fixed model parameters: $J = 1/2$, $\Theta_D = 150$ K, $\tilde{\mathcal{J}}_0 = 10$ meV, $g = 2$, $\tilde{\mathcal{J}}_1 = 0$, 20, 40 and 60 meV. Here, for the sake of simplicity, we neglect the effect of the magnetoelastic interaction on the lattice Hamiltonian, so that the crystalline lattice entropy does not depend on the magnetic field. In this case, the entropy change in isothermal processes upon magnetic field variation is only the magnetic entropy change. In Fig. 32, we plot the magnetic entropy for $B = 0$ (solid symbols) and $B = 5$ T (open symbols) for $\tilde{\mathcal{J}}_1 = 0$, (triangles) 20 (circles) and 40 meV (squares).

From this figure, it can be observed that for $\tilde{\mathcal{J}}_1 = 0$ the magnetic entropy is a continuous function of temperature, so that the phase transition is of second order around 29 K. For $\tilde{\mathcal{J}}_1 = 20$ meV the system is on the verge of the first order phase transition. For $\tilde{\mathcal{J}}_1 = 40$ meV the magnetic entropy exhibits a discontinuity around 35.2 K, so that the system undergoes a first order phase transition. In Figs. 33 and 34 are respectively plotted for $\tilde{\mathcal{J}}_1 = 40$ meV, the magnetization and the magnetic entropy as a function of the applied magnetic field in the range of temperatures from 31.0 to 40.61 K. From these figures, it can be observed that both the magnetization and entropy curves are discontinuous in the range of temperatures between 35.12 and 38.55 K, (dotted line plus open circles) characterizing the first order phase transition. For temperatures outside this interval, (solid and dashed lines) the magnetization and entropy curves are continuous, so that the phase transition is of second order.

Using the total entropy curves, not shown in this report, we calculate the magnetocaloric potentials ΔS_{iso} and ΔT_{ad} upon magnetic field variation from 0 to 5 T for four different sets of model parameters, namely: (1) [$\tilde{\mathcal{J}}_0 = 10$ meV; $\tilde{\mathcal{J}}_1 = 0$ meV]; (2) [$\tilde{\mathcal{J}}_0 = 10$ meV; $\tilde{\mathcal{J}}_1 = 20$ meV]; (3) [$\tilde{\mathcal{J}}_0 = 10$ meV; $\tilde{\mathcal{J}}_1 = 40$ meV] and (4) [$\tilde{\mathcal{J}}_0 = 10$ meV; $\tilde{\mathcal{J}}_1 = 60$ meV]. The obtained curves for ΔS_{iso} are shown by the solid lines in Fig. 35. The corresponding curves for ΔT_{ad} are plotted in Fig. 36. For the sake of comparison, we also calculate ΔS_{iso} using magnetization data, via Eq. (18), which are represented in Fig. 35 by symbols plus dotted line. The horizontal dashed line in this figure represents the saturation value of the magnetic entropy given by

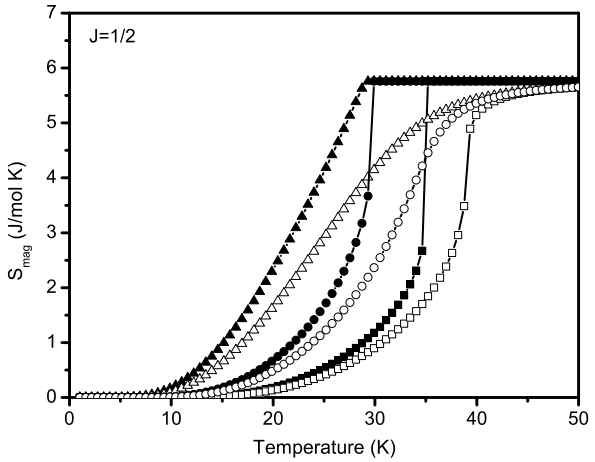

Fig. 32. Magnetic entropy for $B = 0$ (solid symbols) and $B = 5$ T (open symbols) for the two energy level model with $\tilde{\mathcal{J}}_0 = 10$ meV. Triangles, circles and squares represent the calculations for $\tilde{\mathcal{J}}_1 = 0$, 20 and 40 meV respectively.

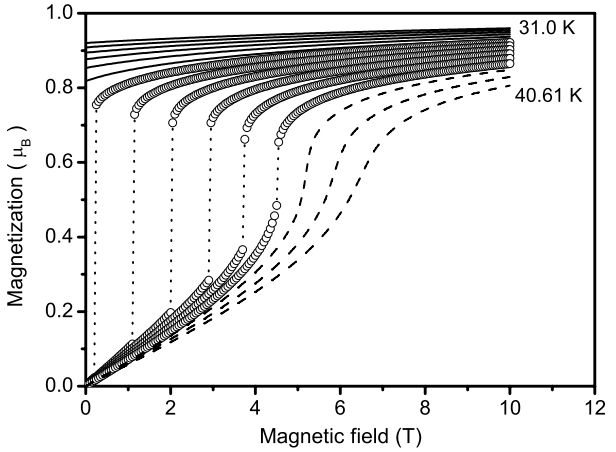

Fig. 33. Magnetization as a function of the applied magnetic field for $\tilde{\mathcal{J}}_0 = 10$ meV and $\tilde{\mathcal{J}}_1 = 40$ meV. Solid lines represent the isotherms from 31.0 K to 34.43 K. Open circles represent the isotherms from 35.12 K to 38.55 K. Dashed lines represent the isotherms from 39.23 K to 40.61 K.

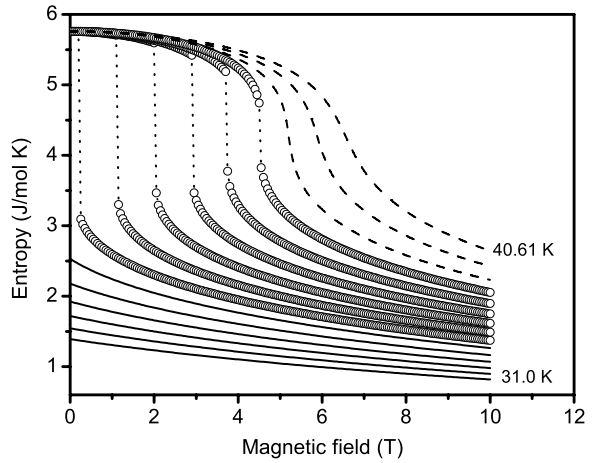

Fig. 34. Magnetic entropy as a function of the applied magnetic field for $\tilde{\mathcal{J}}_0 = 10$ meV and $\tilde{\mathcal{J}}_1 = 40$ meV. Solid lines represent the isotherms from 31.0 K to 34.43 K. Open circles represent the isotherms from 35.12 K to 38.55 K. Dashed lines represent the isotherms from 39.23 K to 40.61 K.

$S_{mag}^{\max} = \Re \ln(2J + 1)$, which in the case of $J = 1/2$ is $S_{mag}^{\max} \approx 5.76$ J/(mol K). For the set of parameters [$\tilde{\mathcal{J}}_0 = 10$ meV; $\tilde{\mathcal{J}}_1 = 0$ meV], where the system undergoes a second order phase transition, the isothermal entropy change calculated

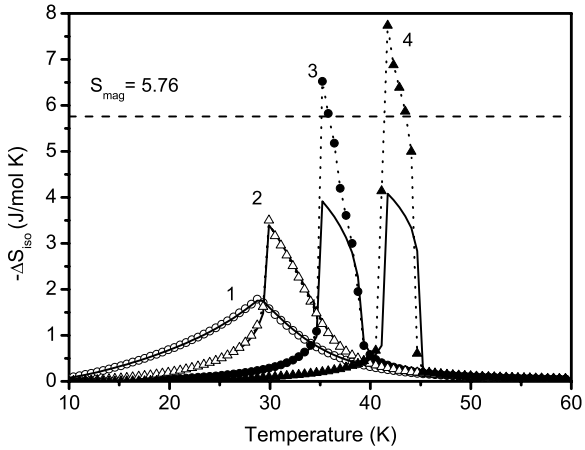

Fig. 35. Isothermal entropy change for magnetic field variation from 0 to 5 T using entropy curves (solid lines) and from Eq. (18) using magnetization data (symbols plus dotted line). The curves 1–4 represent the calculation for $\tilde{\mathcal{J}}_1 = 0$, 20, 40 and 60 meV respectively. For all curves $\tilde{\mathcal{J}}_0 = 10$ meV. The dashed horizontal line represents the saturation value of the magnetic entropy.

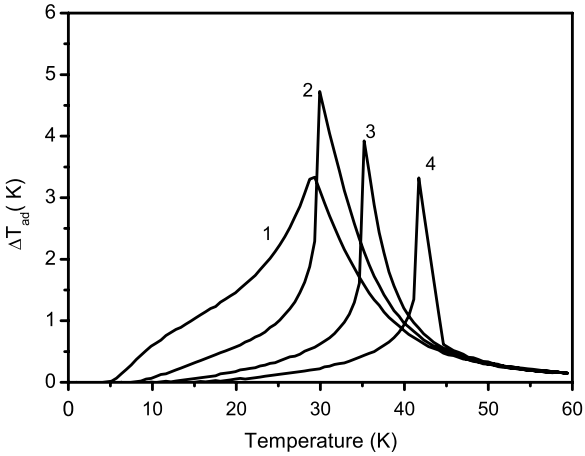

Fig. 36. Adiabatic temperature change for magnetic field variation from 0 to 5 T for $\tilde{\mathcal{J}}_1 = 0$ (curve 1), 20 (curve 2), 40 (curve 3) and 60 meV (curve 4) respectively. For all curves $\tilde{\mathcal{J}}_0 = 10$ meV.

from the entropy curves and the corresponding one obtained via Eq. (18) using magnetization data are coincident, as can be observed from curves 1 (solid line and open circles) shown in Fig. 35. For the set of parameters [$\tilde{\mathcal{J}}_0 = 10$ meV; $\tilde{\mathcal{J}}_1 = 20$ meV], where the system is on the verge of the first order phase transition, the isothermal entropy changes calculated from both methods are still similar to each other, as can be observed from curves 2 (solid line and open triangles) in Fig. 35. However, for the sets of model parameters [$\tilde{\mathcal{J}}_0 = 10$ meV; $\tilde{\mathcal{J}}_1 = 40$ meV] and [$\tilde{\mathcal{J}}_0 = 10$ meV; $\tilde{\mathcal{J}}_1 = 60$ meV], where the system undergoes a first order magnetic phase transition, the isothermal entropy changes calculated from the entropy curves and those ones obtained from Eq. (18), using magnetization data, are coincident only in the temperature range away from the first order phase transition, as can be observed from the curves 3 (solid curve and dotted line plus solid circles) and 4 (solid curve and dotted line plus solid triangles) shown in Fig. 35. However, around the first order phase transition, the calculated values of ΔS_{iso} obtained from Eq. (18) using magnetization data, are larger than the corresponding ones obtained from the entropy curves. Moreover, around the first order phase transition, the values of ΔS_{iso} calculated from Eq. (18), are larger than the expected saturation value of the magnetic entropy, represented by the dashed line in Fig. 35. This result is unphysical because ΔS_{iso}, which in our approximation is only the magnetic entropy change, may not be larger than the upper limit of the magnetic entropy. Therefore, this unphysical result confirms that the calculations of ΔS_{iso} through Eq. (18) using magnetization data, do indeed not apply in the range of temperatures of the first order phase transition.

In order to understand the calculation of ΔS_{iso} using magnetization data via Eq. (18), in which we use the Maxwell relation $(\partial M/\partial T)_B = (\partial S/\partial B)_T$, we consider the magnetization curves plotted in Fig. 33. In the temperature interval below the magnetic ordering temperature from 31.0 to 34.43 K, represented in Fig. 33 by the solid lines, the magnetization curves are monotonic functions of the applied magnetic field. In this case, the partial derivatives $(\partial M/\partial T)_B$ and $(\partial S/\partial B)_T$ exist, so that the Maxwell relation $(\partial M/\partial T)_B = (\partial S/\partial B)_T$ is valid. As a result, the isothermal entropy changes calculated from

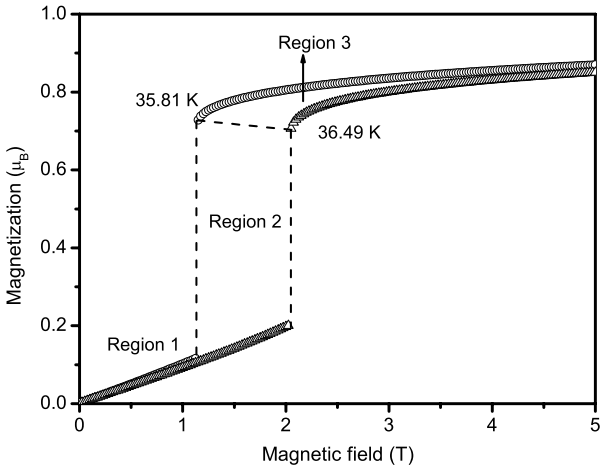

Fig. 37. Magnetization as a function of the applied magnetic field for $\tilde{\mathcal{J}}_0 = 10$ meV and $\tilde{\mathcal{J}}_1 = 40$ meV for the temperatures 35.81 K and 36.49 K. Region 2 delimits the magnetic field interval of the first order phase transition.

Eq. (18), and the ones obtained from the entropy curves, are equal as can be observed in the curves 3 shown in Fig. 35. The same discussion also applies for the temperature range above the magnetic ordering temperature from 39.23 to 40.61 K, represented by the dashed lines in Fig. 33. However, in the temperature range from 35.12 to 38.55 K, where the first order phase transition takes place, the magnetization curves, represented by the open circles in Fig. 33, exhibit jumps at a given critical applied magnetic field. In this range of temperatures, the partial derivatives $(\partial M/\partial T)_B$ and $(\partial S/\partial B)_T$ are not defined, so that the Maxwell relation $(\partial M/\partial T) = (\partial S/\partial B)$ is no longer valid. As a result, the isothermal entropy change may not be calculated via Eq. (18) using magnetization data. Such a calculation, which is basically the difference between the area under the magnetization curves for two consecutive values of temperature per temperature interval, is an artifact of the numerical procedure and does not have any physical meaning.

Inside the temperature range, in which the first order phase transition takes place, the calculations of the isothermal entropy change using magnetization data should be done via Eq. (35). In order to illustrate the process of the calculation of ΔS_{iso} using Eq. (35), we plot in Fig. 37 only two magnetization isotherms, for the consecutive temperatures of 35.81 K and 36.49 K, for the model parameters [$\tilde{\mathcal{J}}_0 = 10$ meV; $\tilde{\mathcal{J}}_1 = 40$ meV]. In the magnetic field range represented in this figure by regions 1 and 3, the entropy change is calculated by the first and the second term in Eq. (35), which represent the difference in the area under the magnetization curves per ΔT. In the magnetic field range, represented by region 2, where the first order phase transition takes place, the entropy change is not the area under the curve. In this magnetic field range, the entropy change must be calculated by the third term in Eq. (35). The total magnetic entropy change is the sum of these three contributions.

In order to determine the contribution from the third term in Eq. (35), we use the magnetization isotherms shown in Fig. 33 to get the temperature dependence of the critical magnetic field (B_C), where the first order phase transition takes place. Then, we plot the curve B_C vs T and determine the derivative dB_C/dT_C. These curves are shown in Fig. 38. In this figure, also plotted is δM obtained directly from Fig. 33. It should be mentioned that to convert δM from (μ_B) to (J/mol T), the magnetization data in Fig. 33 were multiplied by the conversion factor 5.5823. Using δM and dB_C/dT_C plotted in Fig. 38 we calculate the third term of Eq. (35), shown by the solid circles in Fig. 39. For the sake of comparison, also plotted in this figure is ΔS obtained directly from the entropy curves shown in Fig. 34 (open triangles). From this figure, a reasonable agreement can be observed between both ΔS curves.

In Fig. 40, is plotted the isothermal entropy change for the set of model parameters [$\tilde{\mathcal{J}}_0 = 10$ meV; $\tilde{\mathcal{J}}_1 = 40$ meV] calculated via Eq. (18) (dotted lines) and (35) (open symbols) using magnetization data. The calculations of ΔS_{iso} from Eq. (2) using the entropy curves are represented by the solid line. Notice that outside the temperature range of the first order phase transition, ΔS_{iso} calculated from the different methods agree quite well. However, in the temperature range around the first order phase transition only ΔS_{iso} calculated from the entropy curves (solid lines) and the one calculated from Eq. (35) (open symbols) are coincident. The values of ΔS_{iso} calculated from Eq. (18), represented by the dotted line in Fig. 40, are overestimated and do not correspond to the physical reality.

4.8. *Application to* $Gd_5Si_2Ge_2$

In this subsection we use the formalism of the Section 4.1.3 to calculate the magnetocaloric effect in the compound $Gd_5Si_2Ge_2$, which undergoes a first order phase transition. As a matter of fact, $Gd_5Si_2Ge_2$ is a particular compound of the series $Gd_5(Si_cGe_{1-c})_4$, which exhibit a very rich crystallographic and magnetic phase diagram [28]. It has been shown that this series of compounds is formed by orthorhombic and monoclinic crystallographic structures, which depend on the Si–Ge

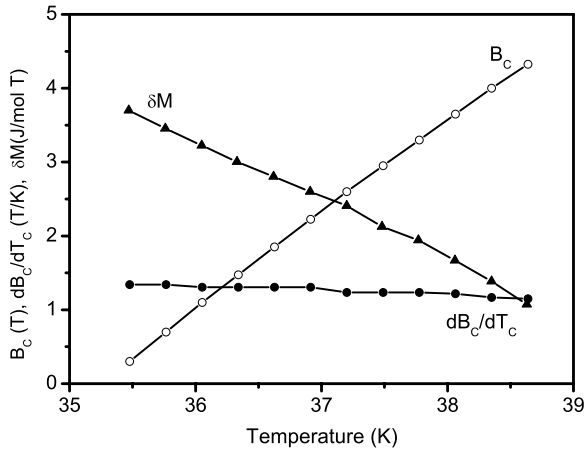

Fig. 38. Critical magnetic field B_C as a function of temperature, for $\tilde{\mathcal{J}}_0 = 10$ meV and $\tilde{\mathcal{J}}_1 = 40$ meV (open circles). Solid circles and triangles represent $\mathrm{d}B_C/\mathrm{d}T$ and δM respectively.

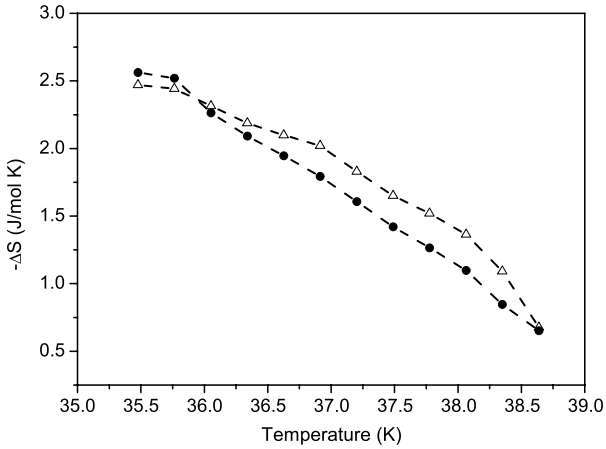

Fig. 39. Entropy change around the first order phase transition for $B = 0$, $\tilde{\mathcal{J}}_0 = 10$ meV and $\tilde{\mathcal{J}}_1 = 40$ meV. Solid circles represent ΔS calculated by $1/2(\mathrm{d}B_C/\mathrm{d}T)\delta M$ and open triangles represent ΔS obtained from Fig. 34.

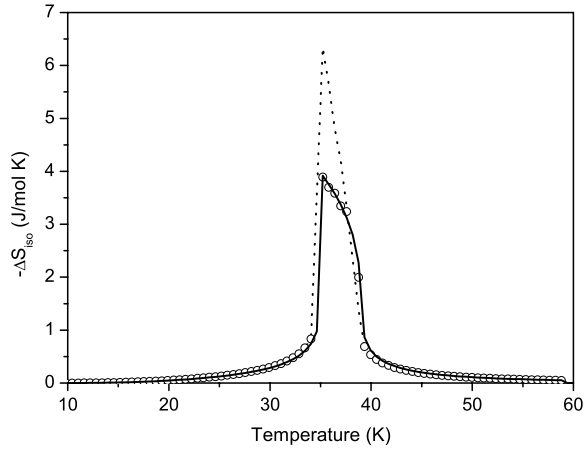

Fig. 40. Isothermal entropy change for $\tilde{\mathcal{J}}_0 = 10$ meV and $\tilde{\mathcal{J}}_1 = 40$ meV upon a magnetic field variation from 0 to 5 T. Open circles represent the calculations obtained via Eq. (35), while solid line represents ΔS_{iso} obtained from the entropy curves. Dotted line represents the calculations using Eq. (18).

concentration. The lattice parameters and the γ-monoclinic angle have been tabulated [18]. It has been shown that the transition from the ferromagnetic phase to the paramagnetic one, in many compounds of the series $Gd_5(Si_cGe_{1-c})_4$, is

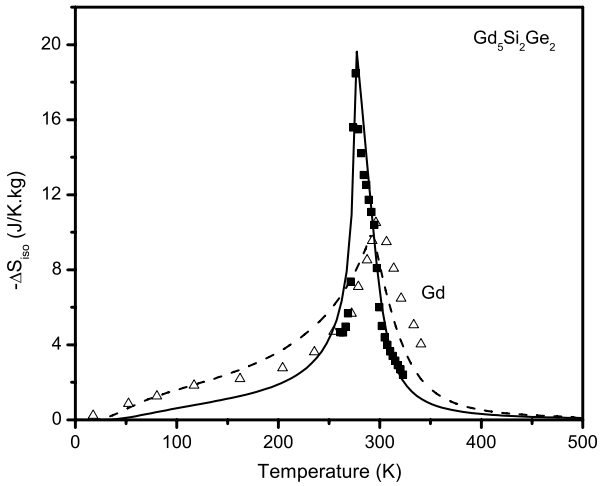

Fig. 41. Calculated isothermal entropy change in $Gd_5Si_2Ge_2$ (solid line) and in Gd (dashed line) upon magnetic field variation from 0 to 5 T. Open triangles and solid squares are experimental data for Gd and $Gd_5Si_2Ge_2$ respectively.

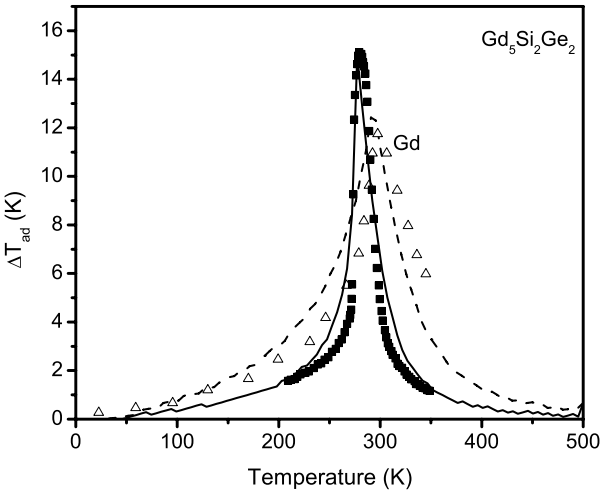

Fig. 42. Calculated adiabatic temperature change in $Gd_5Si_2Ge_2$ (solid line) and in Gd (dashed line) upon magnetic field variation from 0 to 5 T. Open triangles and solid squares are experimental data for Gd and $Gd_5Si_2Ge_2$ respectively.

coupled to the orthorhombic-monoclinic crystallographic phase transformation [30] and has the character of a first order phase transition. The magneto-structural transition can be reversibly induced by magnetic field and occurs with strong magnetoelastic coupling, which leads to a volume deformation $\omega = \Delta V/V_0 = 0.4\%$, indicating that the contribution from the elastic energy term may be an important mechanism for the first order phase transition in this compound. In order to calculate the magnetocaloric effect in the compound $Gd_5Si_2Ge_2$, which undergoes a first order phase transition around 272 K, we use the following model parameters $J = 7/2g = 2$ and $\tilde{\mathcal{J}}_0 = 4.5$ meV; $\tilde{\mathcal{J}}_1 = 0.2$ meV. The Debye temperature and the Sommerfeld coefficient were taken as $\Theta_D = 430$ K and $\gamma = 5.4$ (mJ/mol K^2) respectively. In Figs. 41 and 42 are plotted the isothermal entropy change and the adiabatic temperature change upon magnetic field variation from 0 to 5 T. For the sake of comparison, also plotted in these figures are the corresponding magnetocaloric potentials for Gd metal obtained using the following parameters ($\tilde{\mathcal{J}}_0 = 4.8$ meV; $\tilde{\mathcal{J}}_1 = 0$, $\gamma = 5.4$ (mJ/mol K^2)) and $\Theta_D = 154$ K. From these figures we observe a good agreement between the calculations and experimental data [16]. Moreover, we observe that ΔS_{iso} in $Gd_5Si_2Ge_2$ is much larger than the one in Gd metal. However, we observe from Fig. 42 that ΔT_{ad} in $Gd_5Si_2Ge_2$ is just somewhat larger than the one in Gd metal.

4.9. Alternative description of the magnetoelastic coupling

So far we have discussed the magnetocaloric effect in compounds undergoing a first order transition by using microscopical models, in which the magnetoelastic interaction is included. However, the magnetocaloric effect around a first order phase transition may also be discussed in terms of macroscopic phenomenological models [226,227]. In this section,

we present an alternative description of magnetoelastic coupling, based on an extension of the macroscopic Bean–Rodbell model [228]. The starting point is an extension of the Gibbs free energy, given by:

$$G = -\frac{3}{2}\left(\frac{J}{J+1}\right) Nk_B T_C \sigma^2 - g\mu_B BJN\sigma + \frac{1}{2K}\omega^2 + P\omega - T\left(S_{mag} + S_{lat}\right). \tag{106}$$

Here, the first term represents the exchange interaction in the molecular field approximation, where J is the ion total angular momentum, N is the number of magnetic ions per unit volume, k_B is Boltzmann's constant and σ is the normalized magnetization. The second term is the Zeeman energy, where g is the Landé factor and B is the external magnetic field. The third term represents the elastic energy, where $K = -1/V(\partial V/\partial P)_{T,B}$ is the compressibility. The fourth term represents a correction due to the applied pressure, where ω is the volume change. The last term represents the correction due to the magnetic and lattice entropy of the system. In the Bean–Rodbell model it is supposed that the Curie temperature depends on the volumetric lattice deformation in the form:

$$T_C = T_0\left(1 + \beta_m\omega\right), \tag{107}$$

where $\omega = (V - V_0)/V_0$, T_0 is the bare value of the Curie temperature without the volume deformation and β_m is the slope of the $T_C \times \omega$ curve. It should be mentioned that in some magnetic systems undergoing a first order phase transition there are changes in the lattice parameters without volume deformation (for example, the increase of one lattice parameter can be compensated by the decrease of the others, in such a way that the volume is kept constant). In this case, the Curie temperature can be written in terms of the lattice parameter changes instead of the volume deformation.

In order to obtain the magnetic state equation as a function of temperature, magnetic field and pressure, the variables σ and ω should assume values that minimize the Gibbs free energy. Therefore, fixing σ and assuming that S_{mag} depends only on σ, the Gibbs energy is minimized for the following volume deformation:

$$\omega = \frac{3}{2}\left(\frac{J}{J+1}\right) Nk_B KT_0\beta_m\sigma^2 - PK + KT\frac{\partial S_{lat}}{\partial\omega}. \tag{108}$$

Neglecting the last term and substituting the above equilibrium deformation into Eq. (106), we get a final expression for the Gibbs free energy. Performing the derivative of this Gibbs free energy with respect to σ and considering the relation $\sigma = B_J^{-1}(\sigma) = -\frac{1}{Nk_B}\frac{\partial S_{mag}}{\partial\sigma}$ we get the following magnetic state equation:

$$\sigma = B_J\left\{\frac{1}{T}\left[\left(\frac{T_0 J}{J+1}\right)(3 - 3\beta_m PK)\,\sigma + \frac{g\mu_B J}{k_B}B + \frac{9}{5}\left(\frac{(2J+1)^4 - 1}{[2(J+1)]^4}\right)T_0\eta\sigma^3\right]\right\}, \tag{109}$$

where B_J is the Brillouin function and the parameter η is given by:

$$\eta = \frac{5}{2}\left(\frac{[4J(J+1)]^2}{[(2J+1)^4 - 1]}\right) Nk_B KT_0\beta_m^2. \tag{110}$$

This parameter η controls the nature of the magnetic phase transition in the model. In order to obtain the condition for the first and second order magnetic phase transition, we expand the Gibbs free energy in a power series of the order parameter, (i.e., magnetization M) as follows:

$$\tilde{G} = AM^2 + CM^4 + DM^6, \tag{111}$$

where the coefficients A, C and D are given by:

$$A = \frac{3J\left(T - T_0 + PT_0 K\beta_m\right)}{(J+1)\left(g\mu_B J\right)^2} \tag{112}$$

$$C = \frac{9\left[(2J+1)^4 - 1\right](T - \eta T_0)}{10\left[2\,(J+1)\right]^4\left(g\mu_B J\right)^4} \tag{113}$$

$$D = \frac{T}{(g\mu_B J)^6}\left[\frac{27}{25}\left(\frac{J}{J+1}\right)^3\frac{\left[(2J+1)^4 - 1\right]^2}{[4J\,(J+1)]^4} + \frac{18}{35}\left(\frac{J}{J+1}\right)^6\frac{(2J+1)^6 - 1}{(2J)^6}\right]. \tag{114}$$

For $\beta_m = 0$ we get from Eq. (110) that $\eta = 0$. In this case, the Brillouin function presents only the linear term in σ, so that the magnetic state equation in Eq. (109) reduces to the regular magnetic state equation, where the phase transition is always of second order around $T = T_0 = T_C$. Making $A = 0$ and $C = 0$ we get from relations (112) and (113) that: $T/T_0 = 1 - PK\beta_m$ and $T/T_0 = \eta$ respectively. From the Landau theory of phase transitions, the first order magnetic phase transition occurs under the condition: $C < 0$ and $A > 0$ (note that $D > 0$). Therefore the first order phase transition occurs under the following condition:

$$PK\beta_m > 1 - \eta. \tag{115}$$

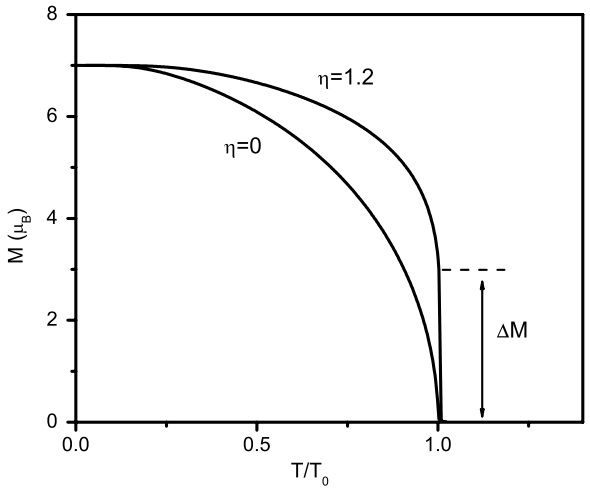

Fig. 43. Temperature dependence of magnetization, for $\eta = 0$ and $\eta = 1.2$.

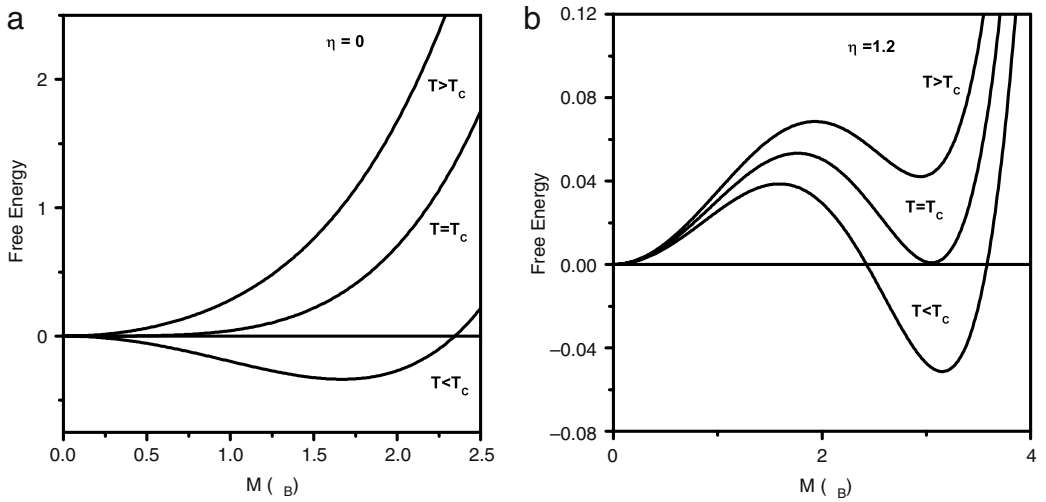

Fig. 44. Landau free energy for $\eta = 0.0$ (a) and $\eta = 1.2$ (b).

The discontinuity in the magnetization that occurs around the first order phase transition is given from Landau theory as:

$$\Delta M = \sqrt{\frac{2A}{|C|}}. \tag{116}$$

In order to illustrate the numerical calculation, we solve the magnetic state equation for the following model parameters $P = 0, B = 0, g = 2, J = 7/2$ and $\eta = 0$ and $\eta = 1.2$. Note from relation (115) that for $P = 0$ the appearance of the first order magnetic phase transition is given by the condition $\eta > 1$. In Fig. 43 is plotted the temperature dependence of the magnetization for $\eta = 0$ and $\eta = 1.2$. For $\eta = 0$, the magnetization curve goes smoothly to zero so that the phase transition is of second order. For $\eta = 1.2$, the system undergoes a first order phase transition, which is associated with the magnetic discontinuity ΔM, also represented in Fig. 43. In Fig. 44 are shown the Landau free energies for $T < T_C$, $T = T_C$ and $T > T_C$, for $\eta = 1.0$ and $\eta = 1.2$. From this figure the different behavior of the free energy for the second and first order magnetic phase transition can be observed. Since the magnetization in the extended Bean–Rodbell model may be written in terms of the Brillouin function, the magnetic entropy can be calculated by Eq. (98), where the auxiliary variable y that contains temperature, magnetic field and pressure is the argument of the Brillouin function given in Eq. (109). The magnetocaloric potentials ΔS_{iso} and ΔT_{ad} can be easily calculated from Eqs. (2) and (3) respectively.

We also apply the extended Bean and Rodbell model to calculate the magnetocaloric effect in the series of compound $Gd_5(Si_cGe_{1-c})_4$ by using the following model parameters $T_0 = 180$ K for $c = 0.43$, and $T_0 = 274.64$ K for $c = 0.5$. In Fig. 45 are plotted the isothermal entropy changes for $Gd_5(Si_{0.43}Ge_{0.57})_4$ and $Gd_5(Si_{0.5}Ge_{0.5})_4$ upon magnetic field variation from 0 to 5 T. From this figure a good agreement can be observed between calculations and experiments. It should be mentioned

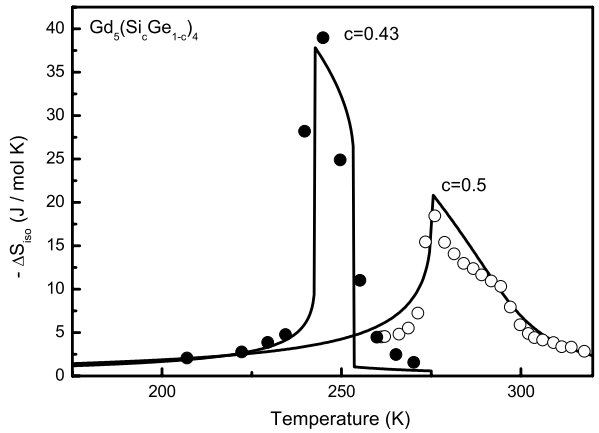

Fig. 45. Isothermal entropy change in $Gd_5(Si_cGe_{1-c})_4$ calculated via the Bean–Rodbell model, upon magnetic field variation from 0 to 5 T (solid lines). Symbols are experimental data.

that a calculation [229] very similar to the one presented in this subsection was applied to study the magnetocaloric effect in the compound $La(Fe_{1-c}Si_c)_{13}$.

5. Magnetocaloric effect in transition metal based compounds

In this section, we discuss the theoretical aspects involved in the magnetocaloric effect of transition metal based compounds, whose magnetism is associated with itinerant electrons. The model of localized moments described previously is more appropriate to discuss the magnetocaloric effect in rare earth based compounds. Nevertheless, it may also be used to calculate the magnetization and the magnetocaloric effect in transition metal based compounds. However, the model of localized moments is not able to correctly calculate the magnetic entropy of transition metals, because their total angular momentum is no longer a good quantum number. As a result, the saturation value of the magnetic entropy, $S_{mag} = \Re ln(2J + 1)$ per magnetic ion, obtained by the model of localized moments does not apply to transition metals. Even though the entropy is miscalculated, the magnetocaloric potentials ΔS_{iso} and ΔT_{ad} obtained with such a model are reasonable. This is because there is a compensation in the calculation process in which differences are taken between the entropy for two values of the magnetic field. Although the localized model may be used to fit the experimental data of the magnetocaloric potentials in transition metals, the physical mechanisms involved in the magnetocaloric effect in these metals are not well described by the model. This is because it does not consider the nature of the itinerant electrons that are responsible for the magnetism in these compounds. Therefore, in order to calculate the magnetocaloric potentials and properly describe the physics involved in the magnetocaloric effect of transition metals based compounds, it is necessary to use a model Hamiltonian in the framework of the band theory, where the role of the itinerant electrons is taken into account [230–238].

5.1. General formulation

In order to describe the magnetocaloric effect in transition metal based compounds, we use the following model Hamiltonian

$$\mathcal{H} = \mathcal{H}_{el}^{sp} + \mathcal{H}_{mag}^{d} + \mathcal{H}_{lat} + \mathcal{H}_{el-lat}, \tag{117}$$

where

$$\mathcal{H}_{el}^{sp} = \sum_{k} \hat{\varepsilon}_k^{sp} c_k^{+} c_k, \tag{118}$$

$$\mathcal{H}_{mag}^{d} = \sum_{i\sigma} \varepsilon_0 d_{i\sigma}^{+} d_{i\sigma} + \sum_{ij\sigma} T_{ij\sigma} d_{i\sigma}^{+} d_{j\sigma} + \sum_{i\sigma} U^d n_{i\uparrow}^d n_{i\downarrow}^d - \sum_{i} g\mu_B B.s_i^d, \tag{119}$$

$$\mathcal{H}_{lat} = \sum_{q} \hbar\omega_q a_q^{+} a_q \tag{120}$$

$$\mathcal{H}_{el-lat} = \sum_{qkk'} M_{kk'} \varepsilon_q \left(a_{-q}^{+} + a_q\right) d_{k\sigma}^{+} d_{k'\sigma}. \tag{121}$$

Here $\mathcal{H}_{el}^{sp}$ describes the sp-conduction electrons, with $\hat{\varepsilon}_k^{sp} = \alpha^{sp}\varepsilon_k^{sp}$, where the parameter α^{sp} simulates the effect of an external pressure. $\mathcal{H}_{lat}$ describes the phonons in the crystalline lattice, where the term a_q^{+} (a_q) is the phonon creation

(annihilation) operator and ω_q is the phonon frequency. $\mathcal{H}^d_{mag}$ is a Hubbard-like Hamiltonian [230] describing the "d"-itinerant electrons in the single band approximation. In the magnetic Hamiltonian $\mathcal{H}^d_{mag}$, the first term describes a local energy, where ε_0 is a reference energy level; $d^+_{i\sigma}$ ($d_{i\sigma}$) is the electron creation (annihilation) operator. The second term describes the electron hopping, where $T_{ij\sigma} = \sum_k \alpha^d \varepsilon^d_{k\sigma} e^{ik(R_i - R_j)}$ is the hopping energy and α^d is a renormalization parameter, which can simulate the effect of an applied pressure. The third term describes the electron–electron interaction, where U^d is the Coulomb interaction parameter and $n^d_i = d^+_{i\sigma} d_{i\sigma}$. The last term is the Zeeman interaction, where B is the applied magnetic field, g is the Landé factor and μ_B is the Bohr magneton. $\mathcal{H}_{el-lat}$ describes the electron–phonon interaction [239]. For the sake of simplicity, considered here is a procedure to decouple the electron–phonon Hamiltonian, in which it is assumed that the electron–phonon interaction renormalizes the electron dispersion relations and the phonon frequencies. A more rigorous treatment of the Hamiltonian $\mathcal{H}_{el-lat}$, in which electrons and phonons are coupled is much complex and is not in the scope of the present text. Thus, with this decoupling procedure, we can write the following effective Hamiltonian:

$$\mathcal{H}^{eff} = \mathcal{H}^{eff\,(sp)}_{el} + \mathcal{H}^{eff\,(d)}_{mag} + \mathcal{H}^{eff}_{lat}, \tag{122}$$

where

$$\mathcal{H}^{eff\,(sp)}_{el} = \sum_k \tilde{\varepsilon}^{sp}_k c^+_k c_k, \tag{123}$$

$$\mathcal{H}^{eff\,(d)}_{mag} = \sum_{i\sigma} \varepsilon_0 d^+_i d_i + \sum_{ij\sigma} \tilde{T_{ij\sigma}} d^+_{i\sigma} d_{j\sigma} + \sum_i U^d n^d_{i\uparrow} n^d_{i\downarrow} - \sum_i g\mu_B B.s^d_i \tag{124}$$

$$\mathcal{H}^{eff}_{lat} = \sum_q \hbar\tilde{\omega}_q a^+_q a_q. \tag{125}$$

$\mathcal{H}^{eff\,(sp)}_{el}$ is an effective Hamiltonian describing sp-conduction electrons, where $\tilde{\varepsilon}^{sp}_k = \alpha^{sp}\xi^{sp}\varepsilon^{sp}_k$ is the dispersion relation renormalized by the electron–phonon interaction and by applied pressure. The effective Hamiltonian $\mathcal{H}^{eff}_{lat}$ describes phonons with the effective phonon frequency $\tilde{\omega}_q = \alpha^{ph}\xi^{ph}\omega_q$ renormalized by the electron–phonon interaction and by applied pressure. $\mathcal{H}^{eff\,(d)}_{mag}$ is an effective Hamiltonian describing itinerant d-electrons, where the term $\tilde{T_{ij\sigma}} = \sum_k \tilde{\varepsilon}^d_{k\sigma} e^{ik(R_i - R_j)}$ represents the electron hopping energy between two different sites, with the renormalized dispersion relation $\tilde{\varepsilon}^d_k = \alpha^d \xi^d \varepsilon^d_k$ taking into account the magnetoelastic interaction and pressure effects. Here, we suppose that the renormalized parameters ξ^{sp}, ξ^{ph} and ξ^d can be written in terms of the volume change in the form: $\xi^{sp} = (1 - \xi^{sp}_0 \Delta V/V_0)$, $\xi^d = (1 - \xi^d_0 \Delta V/V_0)$ and $\xi^{ph} = (1 - \xi^{ph}_0 \Delta V/V_0)$. With this assumption the renormalized electron dispersion relations and phonon frequencies are written as: $\tilde{\varepsilon}^{sp}_k = \alpha^{sp}(1 - \xi^{sp}_0 \Delta V/V_0)\varepsilon^{sp}_k$, $\tilde{\varepsilon}^d_k = \alpha^d(1 - \xi^d_0 \Delta V/V_0)\varepsilon^d_k$ and $\tilde{\omega}_q = \alpha^{ph}(1 - \xi^{ph}_0 \Delta V/V_0)\omega_q$. The electronic entropy associated with the effective Hamiltonian $\mathcal{H}^{eff\,(sp)}_{el}$ is given by $Sel = \gamma T$, where γ is the Sommerfeld coefficient. The lattice entropy associated with the effective Hamiltonian $\mathcal{H}^{eff}_{lat}$ is given in the Debye approximation by Eq. (86).

The appearance of magnetism in itinerant electron systems is determined by the Stoner criterion given by $U\rho(\varepsilon_F) > 1$, where U is the Coulomb interaction parameter and $\rho(\varepsilon_F)$ is the density of states at the Fermi energy level. For a given electron occupation number, the density of states at the Fermi energy level is expected to get larger as the energy bandwidth becomes narrower. In the case of "3d"-electrons, the bandwidth is narrow so that $\rho(\varepsilon_F)$ can be large, depending on the electron occupation number. Thus, the Stoner criterion for the onset of the itinerant magnetization may be fulfilled in some transition metals with an unfilled energy band. This is what happens with Fe, Co and Ni metals, which exhibit non vanishing magnetization. In the case of "sp" conduction electrons, the bandwidth is very wide and $\rho(\varepsilon_F)$ is small, independently of the electron occupation number. As a result, the Stoner criterion is not fulfilled, so that itinerant magnetization does not appear. This is why we can neglect the contribution from the sp conduction electrons to the total magnetization.

The great difficulty in getting the energy eigenvalues of the magnetic Hamiltonian $\mathcal{H}^d_{mag}$ is due to the two-body interaction term $U^d n^d_{i\uparrow} n^d_{i\downarrow}$. This term can be treated in the Hartree–Fock approximation (mean field approximation) or in the functional integral techniques [235,236]. In this report we consider only the mean field approximation, in which the Coulomb interaction term $U^d \sum_i n^d_{i\uparrow} n^d_{i\downarrow}$ may be written as:

$$U^d \sum_i n^d_{i\uparrow} n^d_{i\downarrow} \approx U^d \sum_{i\sigma} \langle n^d_{i-\sigma}\rangle n^d_{i\sigma}. \tag{126}$$

It should be pointed out that short range interactions, which are very important around the magnetic ordering temperature, are not considered in the mean field approximation. Supposing translational invariance, the electron occupation number becomes site independent, i.e., $\langle n^d_{i-\sigma}\rangle = \langle n^d_{-\sigma}\rangle$. Considering $s^d_i = (1/2)(n^d_{i\uparrow} - n^d_{i\downarrow}) = (1/2)\sum_\sigma \sigma n^d_{i\sigma}$ and using $g = 2$, the Zeeman term can be written as: $\sum_i g\mu_B B.s^d_i = \sum_{i\sigma} \sigma\mu_B B d^+_{i\sigma} d_{i\sigma}$. Using the previous considerations, the magnetic Hamiltonian in the mean field approximation turns out to be:

$$\mathcal{H}^{eff\,(d)}_{mag} = \sum_k \left[\tilde{\varepsilon}^d_{k\sigma} + \left(\varepsilon_0 + U^d\langle n^d_{-\sigma}\rangle - \sigma\mu_B B\right)\right] d^+_{k\sigma} d_{k\sigma}. \tag{127}$$

The local Green's function [240] associated with this effective magnetic Hamiltonian is given by:

$$g^d_{00\sigma}(z) = \int \frac{\rho^d_0(\varepsilon')\mathrm{d}\varepsilon'}{z - \alpha^d(1 - \xi^d_0 \Delta V/V_0)\varepsilon' - \varepsilon_0 - U^d\langle n^d_{-\sigma}\rangle + \sigma\mu_B B}, \tag{128}$$

where $z = \varepsilon + \mathrm{i}0$ and $\rho^d_0(\varepsilon')$ is a standard paramagnetic density of states. The volume change can be taken proportional to square of the total magnetization M, i.e., $\Delta V/V_0 \simeq M^2$, (see for instance Eq. (108)) so that the Green's function can be written as:

$$g^d_{00\sigma}(z) = \int \frac{\rho^d_0(\varepsilon')\mathrm{d}\varepsilon'}{z - \alpha^d(1 - \xi^d_0 M^2)\varepsilon' - \varepsilon_0 - U^d\langle n^d_{-\sigma}\rangle + \sigma\mu_B B}. \tag{129}$$

The spin dependent density of states for "d"-electrons, is calculated by $\rho^d_\sigma(\varepsilon) = -\frac{5}{\pi} Im\, g^d_{00\sigma}(z)$, where the factor 5 accounts for the degeneracy of the "d" states. The "d"-electron occupation number per spin direction is given by

$$\langle n^d_\sigma\rangle = \int \rho^d_\sigma(\varepsilon) f(\varepsilon)\mathrm{d}\varepsilon, \tag{130}$$

where $f(\varepsilon)$ is the Fermi distribution function. Eqs. (129) and (130) should be solved self-consistently under the condition that the total electron occupation number $n^d = \langle n^d_\uparrow\rangle + \langle n^d_\downarrow\rangle$ remains constant. This self consistent process is implemented as follows: for an initial values of $\langle n^d_\sigma\rangle$, the local Green's function and consequently the density of states per spin direction is calculated. After that, new values of the electron occupation numbers are determined through Eq. (130). These new values of the electron occupation numbers should be equal to the previous ones within a given numerical precision. Once self consistency is achieved, the itinerant magnetization is calculated by:

$$M^d(T, B, P) = (\langle n^d_\uparrow\rangle - \langle n^d_\downarrow\rangle)\mu_B. \tag{131}$$

It should be mentioned that the parameter ξ^d_o controls the nature of the phase transition. As a matter of fact, it can be observed from Eq. (129) that the width of the electronic density of states, which is controlled by the coefficient $\alpha^d(1-\xi^d_0 M^2)$, changes as a function of temperature due to the magnetoelastic coupling parameter ξ^d_o. For a large value of the magnetoelastic coupling parameter, a substantial change in the width of the electronic density of states may occur around the magnetic ordering temperature. As a result the Stoner criterion is fulfilled yielding a large value of the magnetization at the magnetic ordering temperature, giving rise to a first order phase transition. Conversely, for small values of the parameter ξ^d_0, the width of the electronic density of states is almost temperature independent. As a result it is expected that the magnetization increases smoothly around the magnetic ordering temperature, so that the magnetic phase transition will be of second order.

5.2. Magnetic heat capacity and magnetic entropy

The partition function per ion and per band for the effective Hamiltonian ($\mathcal{H}^{eff(d)}_{mag}$), can be written, in the mean field approximation, as [241]:

$$Z^d_{mag}(T, B, P) = \prod_{k\sigma}\left\{1 + \exp\left[-\beta\left(\tilde{\varepsilon}^d_k - \mu\right)\right]\right\}, \tag{132}$$

where μ is the chemical potential. The magnetic free energy per ion calculated from $F^d_{mag} = -(1/\beta)\ln Z^d_{mag}$ is then:

$$F^d_{mag}(T, B, P) = -\frac{1}{\beta}\sum_{l=1}^{5}\sum_{k\sigma}\ln\left\{1 + \exp\left[-\beta\left(\tilde{\varepsilon}^d_k - \mu\right)\right]\right\}, \tag{133}$$

where the sum $\sum_{l=1}^{5}$ takes into account the degeneracy of the d-states. Transforming the sum over k into an integral in energy, the free energy per mol of the substance is given by:

$$F^d_{mag}(T, B, P) = -N_A k_B T\sum_\sigma\int_{-\infty}^{\infty}\ln\left\{1 + \exp\left[-\beta\left(\varepsilon_\sigma - \mu\right)\right]\right\}\rho^d_\sigma(\varepsilon)\ \mathrm{d}\varepsilon. \tag{134}$$

Here $\rho^d_\sigma(\varepsilon) = -\frac{5}{\pi} Im\, g^d_{00\sigma}(z)$, where $g^d_{00\sigma}(z)$ is the local Green's function given in Eq. (129) and the factor 5 takes into account the degeneracy of the d band. The magnetic entropy per mol of the substance with N_m magnetic ions per unit formula, calculated from $S^d_{mag} = -\left(\partial F^d_{mag}(T, B, P)/\partial T\right)_B$, is given by:

$$S^d_{mag}(T, B, P) = N_m\Re\left\{\sum_\sigma\int_{-\infty}^{\infty}\ln\left\{1 + \exp[-\beta(\varepsilon - \mu)]\right\}\rho^d_\sigma(\varepsilon)\,\mathrm{d}\varepsilon + \frac{1}{k_B T}\sum_\sigma\int_{-\infty}^{\infty}(\varepsilon - \mu)f(\varepsilon)\rho^d_\sigma(\varepsilon)\,\mathrm{d}\varepsilon\right\}, \tag{135}$$

where $\Re = N_A k_B$ is the gas constant. The magnetic entropy of the sample, per magnetic ion, can also be written in the form:

$$S^d_{mag}(T,B,P) = -\Re \sum_{l=1}^{5} \sum_{k\sigma} \{f(k_\sigma)\ln f(k_\sigma) + [1-f(k_\sigma)]\ln[1-f(k_\sigma)]\}, \tag{136}$$

where $f(k_\sigma)$ is the Fermi distribution function. At high temperature the magnetic entropy goes to

$$S^d_{mag}(T,B,P) = -10\Re[p\ln p + (1-p)\ln(1-p)], \tag{137}$$

where the factor 10 takes into account the degeneracy of the d-states, including the two spin directions, and p represents the fraction of the band occupied. Thus, the largest value of the magnetic entropy occurs in the case of a half filled band where $p = 1/2$. In this case the saturation value of the magnetic entropy becomes $S^d_{mag} = 10\Re\ln 2 \approx 57.60\,\mathrm{J/(mol\,K)}$.

The magnetic part of the heat capacity at constant magnetic field can be calculated from $C^d_{mag} = T(\partial S^d_{mag}/\partial T)$. Using the magnetic entropy calculated in Eq. (135), the magnetic heat capacity reads:

$$C^d_{mag}(T,B,P) = \frac{N_m\Re}{k_B^2T^2}\sum_\sigma \int \frac{(\varepsilon-\mu)^2\rho^d_\sigma(\varepsilon)f(\varepsilon)}{\left[e^{-\beta(\varepsilon-\mu)}+1\right]}d\varepsilon. \tag{138}$$

5.3. Total entropy and the magnetocaloric effect

The total entropy is given by $S = S^{sp}_{el} + S^d_{mag} + S_{lat}$, where S^d_{mag} is the magnetic entropy given in Eq. (135), $S^{sp}_{el} = \gamma T$ is the electronic entropy and S_{lat} is the crystalline lattice entropy, which has already been calculated in Eq. (86). Thus, the total entropy is then given by:

$$\begin{aligned} S(T,B,P) = {} & N_i\left[-3\Re\ln\left(1-e^{-\frac{\tilde\Theta_D}{T}}\right) + 12R\left(\frac{T}{\tilde\Theta_D}\right)^3\int_0^{\tilde\Theta_D/T}\frac{x^3}{e^x-1}dx\right] \\ & + N_m\Re\left\{\sum_\sigma\int_{-\infty}^{\infty}\ln\{1+\exp[-\beta(\varepsilon-\mu)]\}\,\tilde\rho_\sigma(\varepsilon)\,d\varepsilon\right. \\ & \left. + \frac{1}{k_BT}\sum_\sigma\int_{-\infty}^{\infty}(\varepsilon-\mu)f(\varepsilon)\rho^{nd}_\sigma(\varepsilon)\,d\varepsilon\right\} + \gamma T, \end{aligned} \tag{139}$$

where N_i is the number of ions per unit formula. Here $\tilde\Theta_D = \Theta_0\alpha^{ph}(1-\xi_0^{ph}M^2)$ is the renormalized Debye temperature, where Θ_0 is the bare value of the Debye temperature, α^{ph} simulates the pressure effect and ξ_0^{ph} is a magnetoelastic coupling parameter. Using the total entropy, the isothermal entropy and the adiabatic temperature changes upon magnetic field variation are calculated by Eqs. (2) and (3) respectively.

5.4. Systematic study

In this subsection, we present a study of the magnetocaloric effect in a system of itinerant electrons as a function of the model parameters. The Sommerfeld coefficient and the Debye temperature were respectively taken as $\gamma = 5.4\,\mathrm{J/mol\,K^2}$ and $\Theta_D = 150$ K. In a first step we neglect the magnetoelastic coupling (i.e., we set $\xi_0^d = \xi_0^{ph} = 0.0$) and study the behavior of the entropy and the magnetocaloric potentials as a function of the electron occupation number and the energy bandwidth.

We calculate the magnetic entropy for $n^d = 5.0$ and $U^d = 0.51$ (in units of the bandwidth) using an electronic density of states of triangular shape, with bandwidth $W = 0.8$ eV and $W = 2.4$ eV. The obtained results are shown by the solid and dashed lines in Fig. 46. For the sake of comparison, we also calculate the magnetic entropy using a constant density of states for the same set of model parameters (open symbols in Fig. 46). It can be observed from this figure that: (i) the magnetic entropy saturates at very high temperatures. (ii) the magnetic entropy curves always saturate at the same value. The first observation is just an artifact of the mean field approximation. The second observation points out that the saturation value of the magnetic entropy does not depend either on the shape of the density of states or on the energy bandwidth. As a matter of fact, the upper limit of the magnetic entropy, depends only on the number of accessible states.

In order to further study the dependence of the saturation value of the magnetic entropy, we adopt the triangular density of states and calculate the magnetic entropy for some values of the electron occupation number. In Fig. 47, is plotted the magnetic entropy for electron occupation number greater than 5. The magnetic entropy for electron occupation number smaller than 5 is plotted in Fig. 48. In these figures the dashed lines represent the saturation value of the magnetic entropy calculated using Eq. (137). Notice that the magnetic entropy, self-consistently calculated by Eq. (135) reproduces very well the saturation value determined by Eq. (137) From these figures, it can be observed that the largest saturation value of the magnetic entropy occurs at the half filled condition, i.e., $n^d = 5$ or $p = 1/2$. As the energy band is filled, the saturation value

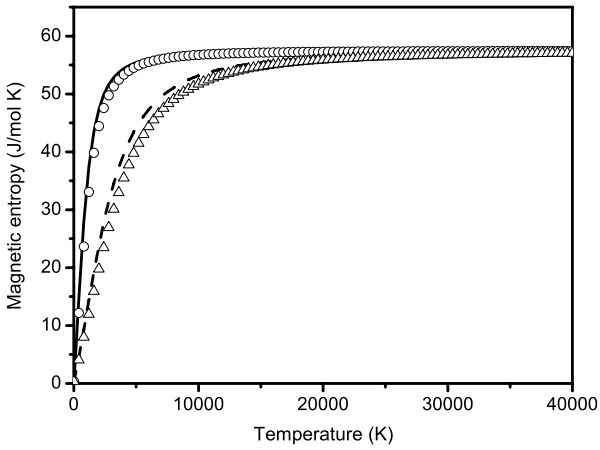

Fig. 46. Magnetic entropy as a function of temperature for a triangular density of states with $n^d = 5.0$, $U^d = 0.51$ and $W = 0.8$ eV (solid line) $W = 2.4$ eV (dashed line). Open circles and triangles represent the corresponding calculations using a constant density of states.

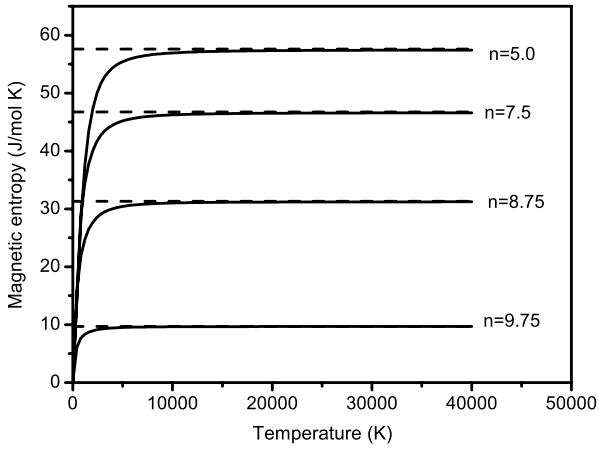

Fig. 47. Magnetic entropy as a function of temperature for $n^d \geq 5.0$. The horizontal dashed lines represent the saturation value determined by Eq. (137).

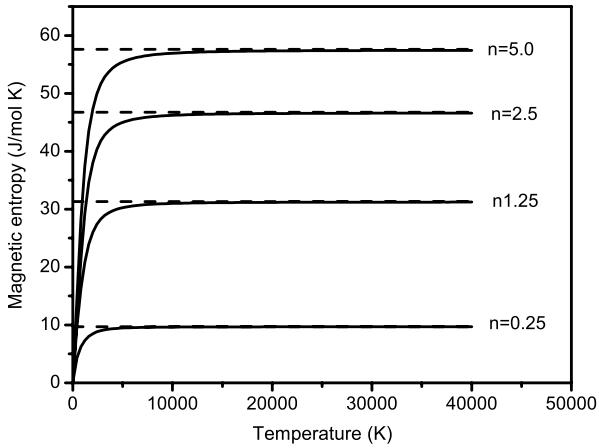

Fig. 48. Magnetic entropy as a function of temperature for $n^d \leq 5.0$. The horizontal dashed lines represent the saturation value determined by Eq. (137).

of the magnetic entropy decreases, and goes to zero as the energy band becomes full, i.e., $n^d = 10$ or $p = 1$. Similarly, as the electron occupation number decreases from the half filled condition, the saturation value of the magnetic entropy also decreases and goes to zero for an empty energy band, i.e., $n^d = 0$ or $p = 0$.

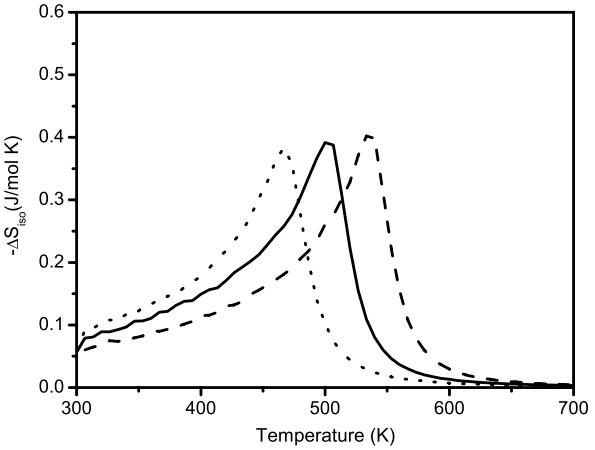

Fig. 49. ΔS_{iso} obtained using ΔB from 0 to 5 T and a triangular density of states with $n^d = 8.0$, $U^d = 0.51$, $\xi_0^d = \xi_0^{ph} = 0$ and $W = 0.8$ eV (solid line) $W = 0.84$ eV (dotted line) $W = 0.76$ eV (dashed line).

In order to calculate the magnetocaloric potentials in the absence of the magnetoelastic coupling ($\xi_0^d = \xi_0^{ph} = 0.0$), we adopt the triangular density of states and take $U^d = 0.51$ (in units of the bandwidth) and $n^d = 8.0$. In Figs. 49 and 50 are plotted the obtained results of the isothermal entropy changes and adiabatic temperature changes upon magnetic field variation from 0 to 5 T for the bandwidth $W = 0.8$ eV (solid lines), $W = 0.84$ eV (dotted lines) and $W = 0.76$ eV (dashed lines). Notice that the magnitudes of the peaks of the magnetocaloric potentials are almost independent of the bandwidth. However, the temperature of the peaks changes as a function of the energy bandwidth. From Figs. 49 and 50 we observe that, the larger the bandwidth the smaller the temperature of the peak. This is an intrinsic characteristic of itinerant electron systems that is related to the Stoner criterion. As matter of fact, the decrease of the energy bandwidth favors the fulfillment of the Stoner criterion and makes the magnetization stronger. As a result, the critical temperature of the magnetic phase transition, from the ordered magnetic state to the disordered one, increases because more thermal energy is necessary to destroy the magnetization.

In order to study the magnetocaloric effect in a system with a first order phase transition, we adopt the triangular density of states and perform numerical calculations using $n^d = 8.0$, $W = 0.8$ eV, $U^d = 0.51$, (in units of bandwidth) $\gamma = 5.4$ J/mol K^2, $\Theta_D = 150$ K and the following magnetoelastic coupling parameters $\xi_0^d = 0$, $\xi_0^d = 1.0$ and $\xi_0^d = 1.86$. For the sake of simplicity we take $\xi_0^{ph} = 0$, so that the crystalline lattice entropy does not depend on the applied magnetic field. Our calculations show that for $\xi_0^d = 0$, the magnetization curve goes to zero very smoothly characterizing the second order phase transition. For $\xi_0^d = 1.0$, the magnetization curve goes to zero less smoothly, but the phase transition is still of second order. For $\xi_0^d = 1.86$, the magnetization curve exhibits a jump around the critical temperature, characterizing a first order phase transition. The continuities or discontinuities around the critical temperature, which are the signatures of the second and first order phase transition are also observed in the entropy curves. In this report, we do not show either the magnetization or the entropy curves. The isothermal entropy changes calculated from the entropy curves, upon magnetic field variation from 0 to 5 T for $\xi_0^d = 0$ (dashed line), $\xi_0^d = 1.0$ (dotted line) and $\xi_0^d = 1.86$ (solid line) are shown in Fig. 51. The corresponding adiabatic temperature changes, for the same model parameters, are plotted in Fig. 52. Notice that the peak of the isothermal entropy change increases as the phase transition becomes first order.

The isothermal entropy changes upon magnetic field variation from 0 to 5 T were also calculated via Eq. (18) using magnetization data, for the same set of model parameters used before. The obtained results for ΔS_{iso} using the magnetoelastic parameters $\xi_0^d = 0$, and $\xi_0^d = 1.86$ are represented respectively by open circles and squares in Fig. 53. For the sake of comparison, also plotted in this figure are the corresponding ΔS_{iso} calculated from the entropy curves (solid lines). Notice that for $\xi_0^d = 0$, where the system undergoes a second order phase transition, ΔS_{iso} calculated both from the entropy curves (solid lines) and from Eq. (18), using magnetization data (circles), are coincident. However, for $\xi_0^d = 1.86$, where the phase transition is of first order, the isothermal entropy changes calculated from both methods are coincident only outside of the temperature range of the first order phase transition. Around the first order phase transition, ΔS_{iso} calculated from Eq. (18) is larger than the one calculated from the entropy curves. This result indicates that Eq. (18) may not be used to obtain ΔS_{iso} around a first order phase transition. This same conclusion has already been drawn before in the model of localized moments (see Fig. 40).

5.5. Application to real compounds

In this subsection we use the present model to calculate the magnetocaloric effect in MnAs. The MnAs compound crystallizes in the NiAs-type structure and undergoes a first order phase transition from the ferromagnetic phase to the

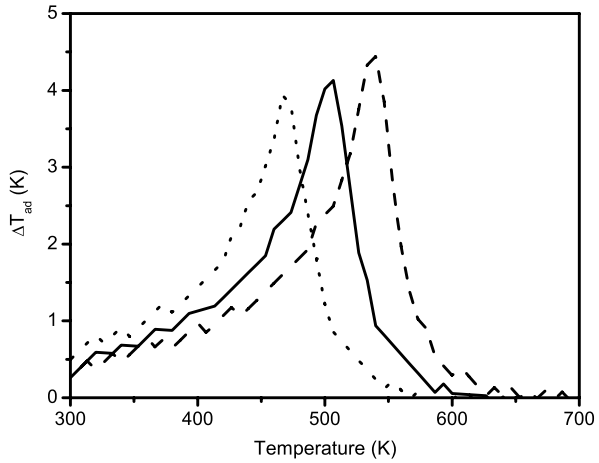

Fig. 50. ΔT_{ad} obtained using ΔB from 0 to 5 T and a triangular density of states with $n^d = 8.0$, $U^d = 0.51$, $\xi_0^d = \xi_0^{ph} = 0$, $\Theta_D = 150$ K and $W = 0.8$ eV (solid line) $W = 0.84$ eV (dotted line) $W = 0.76$ eV (dashed line).

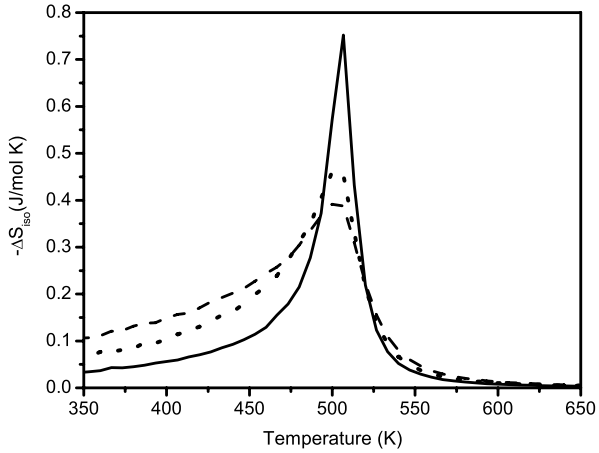

Fig. 51. ΔS_{iso} obtained using ΔB from 0 to 5 T and a triangular density of states with $n^d = 8.0$, $W = 0.8$ eV, $U^d = 0.51$ and $\xi_0^{ph} = 0$. Dashed, dotted and solid lines represent the calculation for $\xi_0^d = 0$, 1.0 and 1.86 respectively.

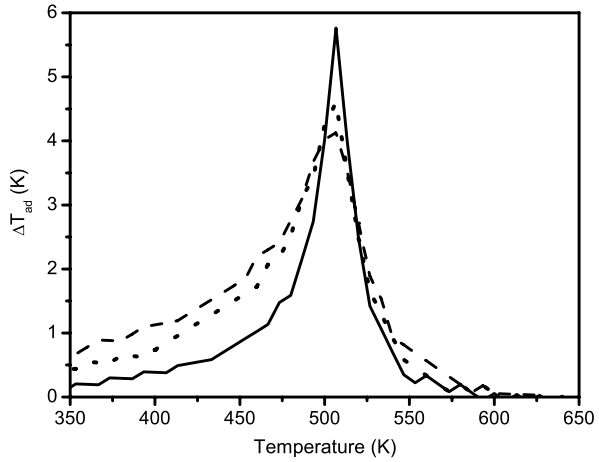

Fig. 52. ΔT_{ad} obtained using ΔB from 0 to 5 T and a triangular density of states with $n^d = 8.0$, $W = 0.8$ eV $U^d = 0.51$, $\xi_0^{ph} = 0$ and $\Theta_D = 150$ K and $\xi_0^{ph} = 0$. Dashed, dotted and solid lines represent the calculation for $\xi_0^d = 0$, 1.0 and 1.86 respectively.

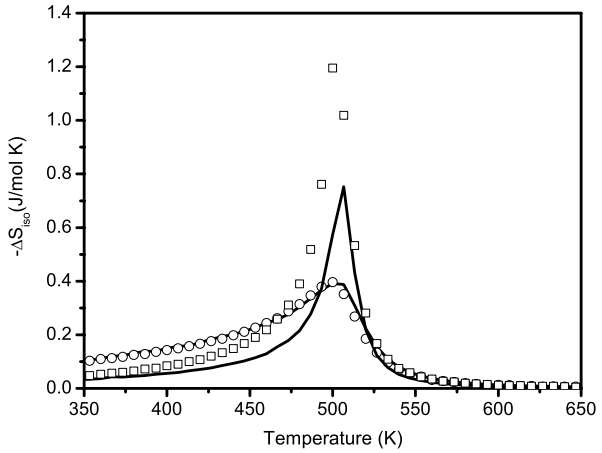

Fig. 53. ΔS_{iso} obtained using ΔB from 0 to 5 T and a triangular density of states with $n^d = 8.0$, $W = 0.8$ eV, $U^d = 0.51$ and $\xi_0^{ph} = 0$. Open circles and squares represent the calculations using magnetization data for $\xi_0^d = 0$ and $\xi_0^d = 1.86$ respectively. Solid lines represent the corresponding quantity obtained from the entropy curves.

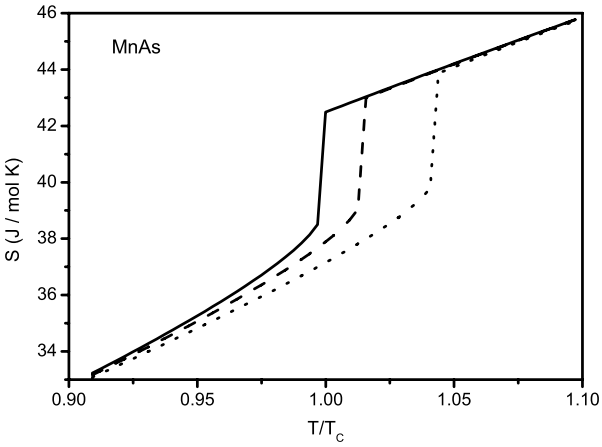

Fig. 54. Total entropy in MnAs calculated for $B = 0$ (solid line) $B = 2$ T (dashed line) and $B = 5$ T (dotted line).

paramagnetic phase, together with a crystallographic phase transformation from the NiAs-type structure to the MnP-type structure, accompanied by a decrease of the volume of the unit cell [242–249]. In order to apply the model of this section to calculate the magnetocaloric effect in MnAs, we consider a density of electronic states, extracted from first principles calculations [245] at $T = 0$ K. The Coulomb interaction parameter was taken as $U^d = 0.477$ in units of bandwidth. Here, we take $\xi_0^{ph} = 0$ and choose the magnetoelastic parameter ξ_0^d in order to reproduce the experimental data [44] of the magnetization around the magnetic ordering temperature.

The bare value of the Debye temperature was taken as $\Theta_D = 400$ K. In order to make a direct comparison between the calculations and experimental data, we made plots using the renormalized temperature T/T_C. This is because the critical temperature calculated using the mean field approximation is larger than the value experimentally observed. In Fig. 54, is plotted the temperature dependence of the total entropy for $B = 0$ (solid line); $B = 2$ T (dashed line) and $B = 5$ T (dotted line). From this figure, we can observe a jump in the total entropy that is pushed to higher temperature as the magnetic field is increased. In Figs. 55 and 56, are respectively plotted the isothermal entropy change and the adiabatic temperature change upon magnetic field variations from 0 to 2 T (solid line) and from 0 to 5 T (dashed line). From these figures, some deviations can be observed between the calculations and experiments, although the theoretical curves show good trends with the experimental data [43,44].

The model discussed in this section can also be applied to calculate the magnetocaloric effect in other transition metal based compounds such as $MnFeP_{1-c}As_c$, $La(Fe_{1-c}Si_c)_{13}$ and Heusler alloys. However, improvements should be made to the model in order to apply it to calculate the magnetocaloric effect in manganites. In addition, in order to provide better values for the magnetic ordering temperature, the model should also be improved to treat the two-body interaction beyond the mean field approximation.

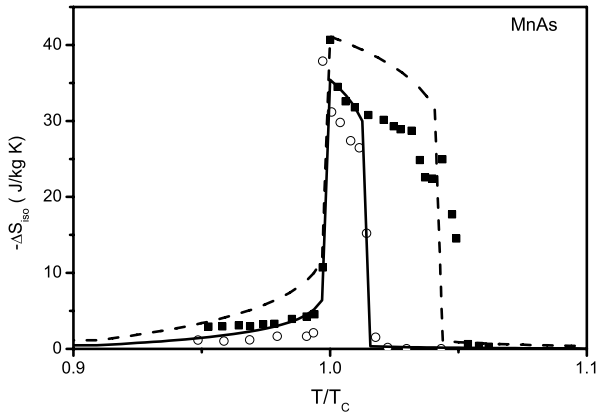

Fig. 55. ΔS_{iso} in MnAs upon magnetic field variations from 0 to 2 T (solid line) and from 0 to 5 T (dashed line). Open circles and solid squares are the corresponding experimental data [44].

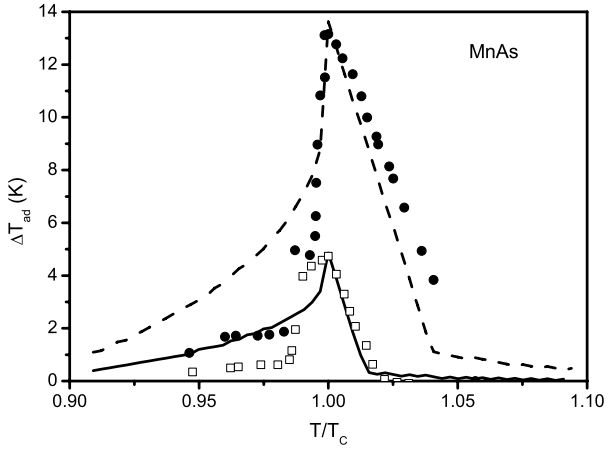

Fig. 56. ΔT_{ad} in MnAs calculated upon magnetic field variation from 0 to 2 T (solid line) and from 0 to 5 T (dashed line). Open squares and solid circles, are the corresponding experimental data [43].

6. Magnetocaloric effect in RCo_2 compounds

In this section, we theoretically discuss the magnetocaloric effect in the rare earth Laves phase intermetallic compounds RCo_2. It has been experimentally shown that the magnetocaloric potentials ΔS_{iso} and ΔT_{ad} in $ErCo_2$, $HoCo_2$ and $DyCo_2$ exhibit a jump around the magnetic ordering temperature, due to the first order magnetic phase transition [250–263]. In the other compounds of the RCo_2 series the phase transition is of second order and the magnetocaloric potentials exhibit the usual behavior. The theoretical description [264–272] of the magnetocaloric effect in RCo_2 is somewhat more complex than the one of rare earth compounds and transition metals made in the previous sections. This is because, in the RCo_2 compounds [273–282] both the localized moments from rare earth ions and the itinerant electrons from Co ions contribute to the magnetization.

6.1. Theoretical formulation

The theoretical description of the magnetocaloric effect in the compounds RCo_2 should be done through a model Hamiltonian, in which both itinerant electrons and localized magnetic moments are included. The starting point is the following model Hamiltonian:

$$\mathcal{H} = \mathcal{H}_{el}^{spd} + \mathcal{H}_{mag}^{4f} + \mathcal{H}_{mag}^{3d} + \mathcal{H}_{lat}, \tag{140}$$

where

$$\mathcal{H}_{el}^{spd} = \sum_{k} \tilde{\varepsilon}_{k}^{spd} c_{k}^{+} c_{k}, \tag{141}$$

$$\mathcal{H}^{4f}_{mag} = -\sum_{il} \mathcal{J}_{il}(r)\vec{J}^f_i.\vec{J}^f_l - \sum_i g^f \mu_B \vec{B}.\vec{J}^f_i - \frac{1}{2}\sum_i \mathcal{J}_{df}\vec{J}^f_i.\vec{s}^d_i + \sum_i \mathcal{H}^{CF}_i, \tag{142}$$

$$\mathcal{H}^{3d}_{mag} = \sum_{i\sigma} \varepsilon_{0\sigma} d^+_{i\sigma} d_{i\sigma} + \sum_{il\sigma} T_{il\sigma} d^+_{i\sigma} d_{l\sigma} + U^{3d}\sum_{i\sigma} n^{3d}_{i\uparrow} n^{3d}_{i\downarrow} - \frac{1}{2}\sum_i \mathcal{J}_{df}\vec{J}^f_i.\vec{s}^d_i - \sum_i g^d \mu_B \vec{B}.\vec{s}^d_i, \tag{143}$$

$$\mathcal{H}_{lat} = \sum_q \hbar\tilde{\omega}_q a^+_q a_q. \tag{144}$$

The Hamiltonian $\mathcal{H}^{spd}_{el}$ describes s, p and 5d conduction electrons, where $\tilde{\varepsilon}^{spd}_k = \alpha^{spd}\xi^{spd}\varepsilon^{spd}_k$ is the electron dispersion relation, renormalized by the electron–phonon interaction and applied pressure. The Hamiltonian $\mathcal{H}_{lat}$ describes the ions into the crystalline lattice with the effective phonon frequency $\tilde{\omega}_q = \alpha^{ph}\xi^{ph}\omega_q$, renormalized by the electron–phonon interaction and applied pressure. The Hamiltonians $\mathcal{H}^{spd}_{el}$ and $\mathcal{H}_{lat}$ and their contributions to the magnetocaloric effect have already been discussed before. The magnetic Hamiltonian $\mathcal{H}^{3d}_{mag}$ describes the itinerant 3d-electrons from Co ions, coupled with localized magnetic moments. The 5d electrons from rare earth ions are assumed to be non magnetic and were included in the conduction electrons Hamiltonian $\mathcal{H}^{spd}_{el}$. Notice that the magnetic Hamiltonian $\mathcal{H}^{3d}_{mag}$ is very similar to the one in Eq. (119), used to describe transition metals based compounds, with the additional coupling term $\mathcal{J}_{df}\vec{J}^f_i.\vec{s}^d_i$. The Hamiltonian $\mathcal{H}^{4f}_{mag}$ describes the localized magnetic moments coupled with itinerant electrons and under the action of the crystalline electrical field. Notice that the Hamiltonian $\mathcal{H}^{4f}_{mag}$ is very similar to the one in Eq. (42) used to describe rare earth based compounds with the additional coupling term $\mathcal{J}_{df}\vec{J}^f_i.\vec{s}^d_i$. In the case of RCo_2 compounds, with cubic symmetry, the crystalline electric field can be described by the Hamiltonian in Eq. (59). Following the procedure used in Section 4, the magnetic Hamiltonian $\mathcal{H}^{4f}_{mag}$ in the mean field approximation can be written as:

$$\begin{aligned}\mathcal{H}^{4f}_{mag} = &-\sum_i \left[\tilde{\mathcal{J}}_0\langle J^f_x\rangle + \tilde{\mathcal{J}}_1\langle J^f_x\rangle^3 + 0.5\mathcal{J}_{df}\langle s^d\rangle + g^f\mu_B B\cos\theta_x\right]J^f_{ix}\\ &-\sum_i \left[\tilde{\mathcal{J}}_0\langle J^f_y\rangle + \tilde{\mathcal{J}}_1\langle J^f_y\rangle^3 + 0.5\mathcal{J}_{df}\langle s^d\rangle + g^f\mu_B B\cos\theta_y\right]J^f_{iy}\\ &-\sum_i \left[\tilde{\mathcal{J}}_0\langle J^f_z\rangle + \tilde{\mathcal{J}}_1\langle J^f_z\rangle^3 + 0.5\mathcal{J}_{df}\langle s^d\rangle + g^f\mu_B B\cos\theta_z\right]J^f_{iz} + \sum_i \mathcal{H}^{CF}_i.\end{aligned} \tag{145}$$

Here $\tilde{\mathcal{J}}_0 = \alpha^{4f}_0\mathcal{J}_0 Z_n$ and $\tilde{\mathcal{J}}_1 = \alpha^{4f}_1\mathcal{J}_1 Z_n$, where $\mathcal{J}_0$ and $\mathcal{J}_1$ are the bare values of the exchange interaction parameters, Z_n is the number of nearest neighbors and the parameters α^{4f}_0 and α^{4f}_1 incorporate the pressure effect. In the cases where $\alpha^{4f}_0 < 1$ the exchange interaction parameter $\tilde{\mathcal{J}}_0$ is reduced, so that the magnetic ordering temperature decreases. The opposite effect, i.e., the increase of the magnetic ordering temperature, is simulated by taking $\alpha^{4f}_0 > 1$. The Greek letters θ_x, θ_y and θ_z represent the angles between the applied magnetic field direction and the crystallographic axes x, y and z. The mean value $\langle J^f_k\rangle (k = x, y, z)$ in Eq. (145) is calculated by:

$$\langle J^f_k\rangle = \frac{\sum_m \langle\psi_m|J^f_k|\psi_m\rangle\, e^{-\beta\varepsilon_m}}{\sum_m e^{-\beta\varepsilon_m}}, \tag{146}$$

where ε_m and $|\psi_m\rangle$ are the energy eigenvalues and eigenvectors of the mean field Hamiltonian $\mathcal{H}^{4f}_{mag}$ respectively. The magnetization component M^{4f}_k $(k = x, y, z)$ at the rare earth sites is: $M^{4f}_k(T, B, P) = g^f\mu_B\langle J^f_k\rangle$. The $4f$ magnetization is given by $M^{4f}(T, B, P) = [(M^{4f}_x)^2 + (M^{4f}_y)^2 + (M^{4f}_z)^2]^{1/2}$:

Following the procedure used in Section 5, the magnetic Hamiltonian $\mathcal{H}^{3d}_{mag}$ in the mean field approximation, turns out to be:

$$\mathcal{H}^{3d}_{mag} = \sum_{i\sigma}\left(\varepsilon_0 + U^{3d}\langle n^{3d}_{-\sigma}\rangle - 0.25\sigma\mathcal{J}_{df}\langle J^f\rangle - \sigma\mu_B B\right)d^+_{i\sigma}d_{i\sigma} + \sum_{il\sigma} T_{il\sigma}d^+_{i\sigma}d_{l\sigma}. \tag{147}$$

The local Green's function for the magnetic Hamiltonian $\mathcal{H}^{3d}_{mag}$ is then given by:

$$g^{3d}_{00\sigma}(z) = \int \frac{\rho_0(\varepsilon')\mathrm{d}\varepsilon'}{z - \alpha^{3d}[1 - \xi^{3d}_0(M^{3d})^2]\varepsilon' - \varepsilon_{0\sigma}}, \tag{148}$$

where $\varepsilon_{0\sigma} = \varepsilon_0 + U^{3d}\langle n^{3d}_{-\sigma}\rangle - 0.25\sigma\mathcal{J}_{df}\langle J^f\rangle - \sigma\mu_B B$, $z = \varepsilon + i0$ and $\rho_0(\varepsilon')$ is a standard paramagnetic density of states. The spin dependent density of states for 3d electrons, is calculated by $\rho^{3d}_\sigma(\varepsilon) = -\frac{5}{\pi}Im\, g^{3d}_{00\sigma}(z)$, where the factor 5 accounts for the degeneracy of the 3d states. The magnetization at the Co sublattice is calculated by:

$$M^{3d}(T, B, P) = (\langle n^{3d}_\uparrow\rangle - \langle n^{3d}_\downarrow\rangle)\mu_B. \tag{149}$$

Table 4
Model parameters for $ErCo_2$, $HoCo_2$ and $DyCo_2$.

Compounds	J^f	g^f	$\mathcal{J}_0$ (meV)	$\mathcal{J}_1$ (meV)	x	W (meV)
$ErCo_2$	15/2	1.20	0.0155	0.0013	−0.24	−0.04214
$HoCo_2$	8	1.25	0.0330	0.0025	−0.4687	0.051702
$DyCo_2$	15/2	1.33	0.0580	0.0017	−0.24	−0.04214

Here $\langle n_\sigma^{3d}\rangle = \int \rho_\sigma^{3d}(\varepsilon) f(\varepsilon) \mathrm{d}\varepsilon$ is the electron occupation number per spin direction, where $f(\varepsilon)$ is the Fermi distribution function.

The equations for the magnetization at the rare earth sublattice and the ones for the magnetization at the Co sublattice, are coupled equations, which should be self-consistently solved. Here we use the following procedure: for initial values of $\langle J_x^f\rangle$, $\langle J_y^f\rangle$, $\langle J_z^f\rangle$ and $\langle s^d\rangle$, the energy eigenvalues and eigenvectors $(\varepsilon_m;\ |\psi_m\rangle)$ of the mean field Hamiltonian $\mathcal{H}_{mag}^{4f}$ are calculated and then used in Eq. (146) to obtain new values for $\langle J_k^f\rangle$. Using the mean value $\langle J^f\rangle = [\langle J_x^f\rangle^2 + \langle J_y^f\rangle^2 + \langle J_z^f\rangle^2]^{1/2}$, the magnetization at the Co sublattice (M^{3d}) is calculated from Eq. (149) and the mean value $\langle s^d\rangle$ is obtained through the relation $\langle s^d\rangle = M^{3d}/g^d\mu_B$. This self consistent process is repeated until two consecutive mean values of $\langle J^f\rangle$ and $\langle s^d\rangle$ are obtained within the numerical precision of 0.001. After solving the self-consistency, the total magnetization of the compound RCo_2 is calculated from $M(T, B, P) = M^{4f}(T, B, P) + 2M^{3d}(T, B, P)$.

The total entropy in RCo_2 is given by

$$S(T, B, P) = S_{el}^{spd}(T) + S_{mag}^{4f}(T, B, P) + S_{mag}^{3d}(T, B, P) + S_{lat}(T, B, P), \tag{150}$$

where $S_{el}^{spd}(T) = \gamma T$ is the electronic entropy, $S_{mag}^{4f}(T, B, P)$ is the contribution from the rare earth ions, given by: (see Section 4)

$$S_{mag}^{4f}(T, B, P) = \Re\left[\ln\sum_j \mathrm{e}^{-\beta\varepsilon_m} + \frac{1}{k_B T}\frac{\sum_m \varepsilon_m \mathrm{e}^{-\beta\varepsilon_m}}{\sum_m e^{-\beta\varepsilon_m}}\right]. \tag{151}$$

Notice that the magnetic entropy S_{mag}^{4f} has the influence of the 3d electrons via the energy ε_m. $S_{mag}^{3d}(T, B, P)$ is the contribution from itinerant 3d-electrons given by: (see Section 5)

$$S_{mag}^{3d}(T, B, P) = 2\Re\left[\sum_\sigma \int_{-\infty}^{\mu} \ln\left[1 + \mathrm{e}^{-\beta(\varepsilon-\mu)}\right] \rho_\sigma^{3d}(\varepsilon)\mathrm{d}\varepsilon + \frac{1}{k_B T}\sum_\sigma \int_{-\infty}^{\mu} (\varepsilon - \mu)\, \rho_\sigma^{3d}(\varepsilon) f(\varepsilon)\mathrm{d}\varepsilon\right], \tag{152}$$

where the factor 2 represents the number of Co ions per unit formula. The magnetic entropy S_{mag}^{3d} for 3d electrons depends on the 4f localized moments, via the effective density of states ρ_σ^{3d}. The term $S_{lat}(T, B, P)$ represents the contribution from the crystalline lattice, which is given in the Debye approximation by:

$$S_{lat}(T, B, P) = 3\left[-3\Re\ln\left(1 - \mathrm{e}^{-\frac{\tilde{\Theta}_D}{T}}\right) + 12\Re\left(\frac{T}{\tilde{\Theta}_D}\right)^3 \int_0^{\tilde{\Theta}_D/T} \frac{x^3}{\mathrm{e}^x - 1}\mathrm{d}x\right]. \tag{153}$$

Here the factor 3 represents the number of ions per unit formula and $\tilde{\Theta}_D = \Theta_0\alpha^{ph}(1 - \xi_0^{ph}M^2)$ is the renormalized Debye temperature, where Θ_0 is the bare value of the Debye temperature; M is the total magnetization and ξ_0^{ph} is a magnetoelastic coupling parameter. Using the total entropy, the magnetocaloric potentials ΔS_{iso} and ΔT_{ad} are calculated by Eqs. (2) and (3) respectively. In the same way, the barocaloric potentials ΔS_{iso}^{bar} and ΔT_{ad}^{bar} are calculated by Eqs. (38) and (39) respectively.

6.2. *Application to* $ErCo_2$, $HoCo_2$, *and* $DyCo_2$

In this section, we present the numerical calculations of the magnetocaloric effect in the compounds $ErCo_2$, $HoCo_2$ and $DyCo_2$. The Landé factor and the total angular momentum, were taken from Hund's rule. The number of first nearest neighbors (Z_n) and the coupling parameter $(\mathcal{J}_{df})$ were respectively taken as: $Z_n = 10\mathcal{J}_{df} = 0.1$ meV. As mentioned before, the crystalline electric field in RCo_2, which has cubic symmetry, is described by the Hamiltonian in Eq. (59). The crystalline electric field parameters x and W were taken from References [283,284] and the factors $F_4 = 60$ and $F_6 = 13\,860$ were used for all the compounds [184].

The exchange interaction parameters were chosen to reproduce the experimental data of the magnetic ordering temperature. In Table 4 are shown the main parameters, associated with localized moments, used in the calculation. In order to describe the 3d-electrons at the Co sites, a standard paramagnetic density of states extracted from reference [285] was adopted. The Coulomb interaction parameter was taken as $U^{3d} = 0.2$, in units of the 3d-bandwidth, and the number of electrons at the Co site was taken as $n = 8.0$. The magnetic field was applied along the $\langle 100\rangle$ direction for $HoCo_2$ and

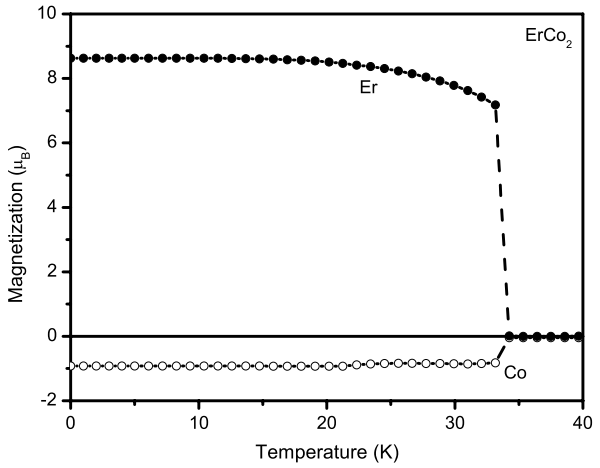

Fig. 57. Magnetization in $ErCo_2$ calculated at ambient pressure for $B = 0$. Solid (open) circles are the magnetization at Er (Co) sites.

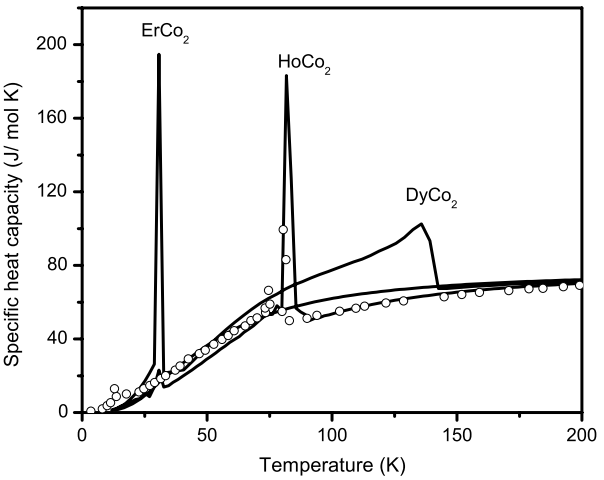

Fig. 58. Specific heat capacity in the absence of magnetic field. Solid lines are theoretical calculations and open circles are experimental data for $HoCo_2$ [274].

along the ⟨111⟩ direction for the compounds $ErCo_2$ and $DyCo_2$. The bare value of the Debye temperature [286] was taken as $\Theta_0 = 230$ K for the compounds $ErCo_2$ and $HoCo_2$ and $\Theta_0 = 200$ K for $DyCo_2$. The magnetoelastic coupling parameters were taken as $\xi_0^{ph} = \xi_0^{3d} = 0.1$ for all the three compounds. First we calculate the magnetocaloric effect at ambient pressure, which means that $\alpha_0^{4f} = \alpha_0^{4f} = 1.0$.

In Fig. 57 is plotted the calculated magnetization in $ErCo_2$ in the absence of an applied magnetic field. From this figure, a jump can be observed in the magnetization curves around the critical temperature of 33 K, characterizing the first order magnetic phase transition. Similar behavior occurs in the magnetization curves of $HoCo_2$ and $DyCo_2$, not shown in this report. In Fig. 58, is plotted the specific heat capacity for $ErCo_2$, $HoCo_2$ and $DyCo_2$ at ambient pressure and for $B = 0$. From this figure, it can be observed that the calculations show the general trend of the available experimental data [274], although there is discrepancy around the magnetic ordering temperature.

In Fig. 59, is plotted the total entropy in the compounds $ErCo_2$ and $HoCo_2$ calculated in the absence of an applied magnetic field (solid symbols) and for an applied magnetic field of 5 T (open symbols). The jump in the total entropy curves of $ErCo_2$ and $HoCo_2$ around the corresponding magnetic ordering temperature, for $B = 0$, is also a signature of the first order phase transition in these compounds.

The isothermal entropy change and the adiabatic temperature change in the compounds $ErCo_2$, $HoCo_2$ and $DyCo_2$, upon magnetic field variation from 0 to 5 T at ambient pressure were calculated from Eqs. (2) and (3) using the total entropy curves. The obtained results are plotted in Figs. 60 and 61 respectively. Notice that the agreement between the theoretical calculations and the available experimental data [253,287] is very good.

In order to simulate the effect of an applied pressure of 1.0 GPa, we take the parameters α_0^{4f} and α_1^{4f} as: $[\alpha_0^{4f} = 0.709, \alpha_1^{4f} = 0.769]$ for $ErCo_2$, $[\alpha_0^{4f} = 0.696, \alpha_1^{4f} = 0.600]$ for $HoCo_2$ and $[\alpha_0^{4f} = 0.912, \alpha_1^{4f} = 0.880]$ for $DyCo_2$. These parameters

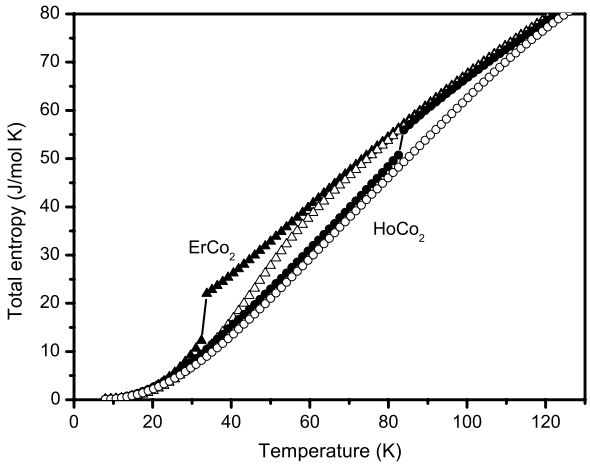

Fig. 59. Total entropy in $ErCo_2$ calculated at ambient pressure, for magnetic field $B = 0$ (solid triangles) and 5 T (open triangles). Solid and open circles are the corresponding calculations for $HoCo_2$.

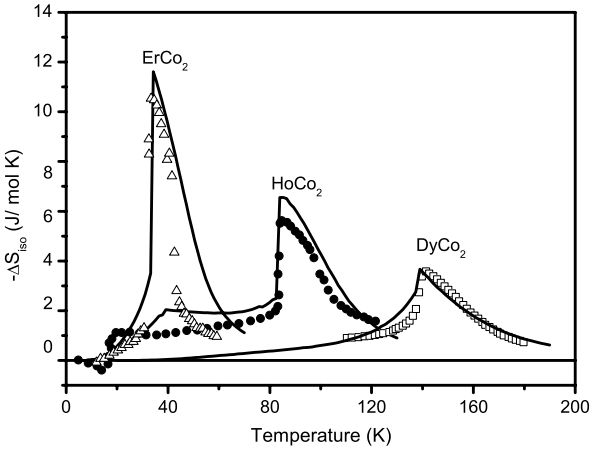

Fig. 60. Isothermal entropy change at ambient pressure upon magnetic field variation from 0 to 5 T. Solid lines are theoretical calculations, while symbols represent the available experimental data [253,287].

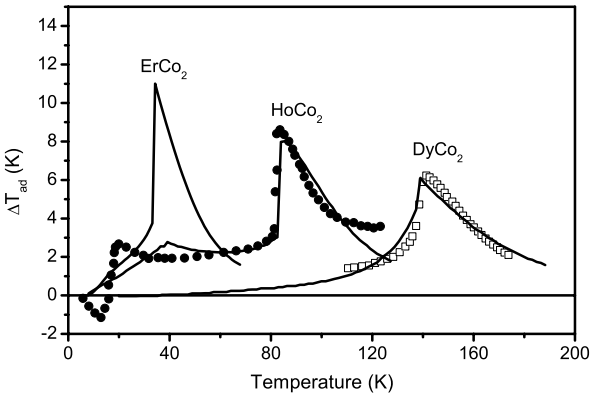

Fig. 61. Adiabatic temperature change at ambient pressure upon magnetic field variation from 0 to 5 T. Solid lines are theoretical calculations while symbols represent the available experimental data [253,287].

were adjusted by using experimental data of T_C as a function of applied pressure [285]. It should be remembered that for ambient pressure these parameters are $\alpha_0^{4f} = \alpha_1^{4f} = 1.0$.

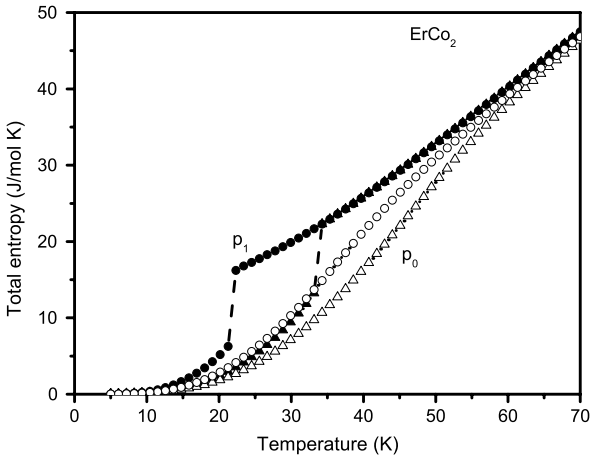

Fig. 62. Calculated total entropy in $ErCo_2$ at ambient pressure for $B = 0$ (solid triangles) and 5 T (open triangles). Solid and open circles represent the calculations at an applied pressure 1.0 GPa and for $B = 0$ and 5 T respectively.

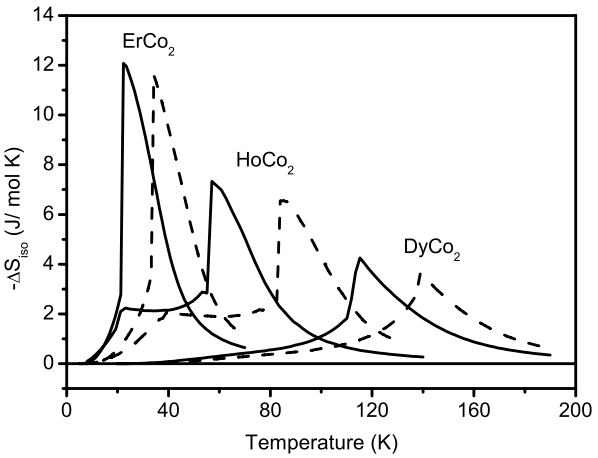

Fig. 63. ΔS_{iso} in RCo_2 (R = Er, Ho, and Dy) calculated at an applied pressure of 1.0 GPa upon magnetic field variation from 0 to 5 T (solid lines). Dashed lines are theoretical calculations at ambient pressure.

In Fig. 62, is plotted the total entropy in $ErCo_2$ calculated for an applied pressure of 1.0 GPa and $B = 0$ (solid circles) and for $B = 5$ T (open circles). In this figure, solid and open triangles represent the corresponding calculations at ambient pressure P_0. In Figs. 63 and 64 are plotted the isothermal entropy change and the adiabatic temperature change in $ErCo_2$, $HoCo_2$ and $DyCo_2$ calculated at an applied pressure of 1.0 GPa upon magnetic field variation from 0 to 5 T (solid lines). For the sake of comparison, also plotted in these figures are the corresponding calculations at ambient pressure (dashed lines) for the same magnetic field variation. From these figures, it can be observed that the applied pressure shifts the magnetic ordering temperature and consequently the peaks of the magnetocaloric potentials ΔS_{iso} and ΔT_{ad} to lower temperatures. However, the magnitudes of the peaks of the magnetocaloric potential are almost unchanged.

We also use the present model to calculate the magnetocaloric effect under simultaneous variation of magnetic field and pressure. In this case, the magnetocaloric potentials ΔS_{iso} and ΔT_{ad} are calculated by Eqs. (40) and (41). In Figs. 65 and 66 are plotted ΔS_{iso} and ΔT_{ad} in $ErCo_2$ upon magnetic field variation from 0 to 2 T and pressure variation from 0 to 1.0 GPa. In these figures, the dashed lines represent the corresponding calculations in which the pressure is kept fixed at ambient pressure. Notice that this particular pressure and magnetic field variation produces a table-like behavior in the ΔS_{iso} curve. Although the table-like behavior is not observed in the calculated ΔT_{ad} curve, its values are also much larger than the ones obtained at fixed pressure. The behavior of the magnetocaloric potentials shown in Figs. 65 and 66 are interesting for practical application in magnetic refrigeration and should be further investigated.

We also used the present model to calculate the barocaloric effect in RCo_2. To this end, we calculate the entropy as a function of temperature for a fixed magnetic field and two different values of applied pressure. In Fig. 67, is plotted the total entropy in the compound $ErCo_2$ for $B = 1$ T at ambient pressure (solid circles) and for an applied pressure of 1.0 GPa (open circles). The barocaloric potentials ΔS_{iso}^{bar} and ΔT_{ad}^{bar} in the compound $ErCo_2$, for a fixed magnetic field of 1 T and pressure variation from 1.0 to 0 GPa were calculated from Eqs. (38) and (39), using the total entropy shown in Fig. 67. The obtained

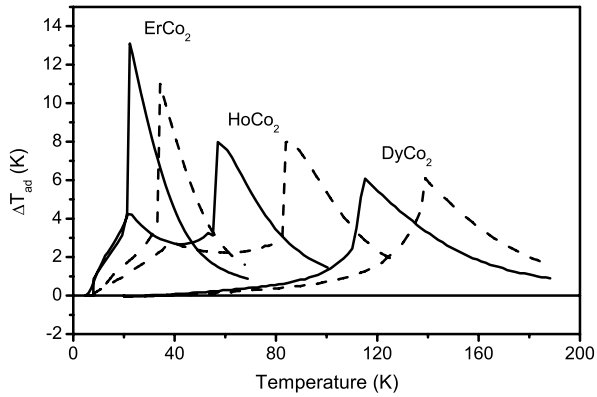

Fig. 64. ΔT_{ad} calculated at an applied pressure of 1.0 GPa upon magnetic field variation from 0 to 5 T (solid lines). Dashed lines are calculations at ambient pressure.

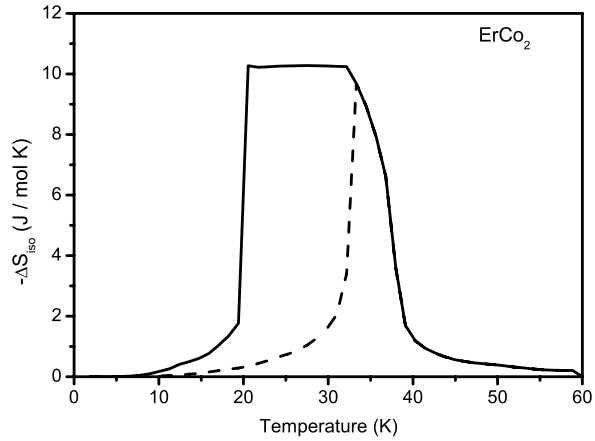

Fig. 65. ΔS_{iso} calculated under magnetic field variation from 0 to 2 T and a linear pressure variation from 0 to 1.0 GPa (solid lines). Dashed lines are calculations at ambient pressure.

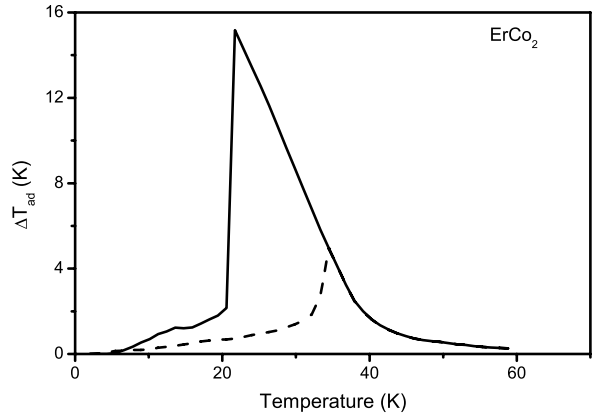

Fig. 66. ΔT_{ad} calculated under magnetic field variation from 0 to 2 T and a linear pressure variation from 0 to 1.0 GPa (solid lines). Dashed lines are calculations at ambient pressure.

results for ΔS_{iso}^{bar} and ΔT_{ad}^{bar} are shown by the solid line in Figs. 68 and 69. For the sake of comparison, also plotted in these figures are the corresponding magnetocaloric potentials ΔS_{iso} and ΔT_{ad} calculated at ambient pressure and magnetic field variation from 0 to 1 T (dashed lines). It can be observed from these figures that: (i) the barocaloric potentials ΔS_{iso}^{bar} and ΔT_{ad}^{bar} exhibit sizeable values in a wider range of temperatures in comparison with the magnetocaloric potentials ΔS_{iso} and ΔT_{ad} at ambient pressure. (ii) the magnitudes of the peaks of the barocaloric potentials upon pressure variation from 1 to 0 GPa are somewhat larger than the magnitudes of the peaks of the magnetocaloric potentials at ambient pressure upon magnetic

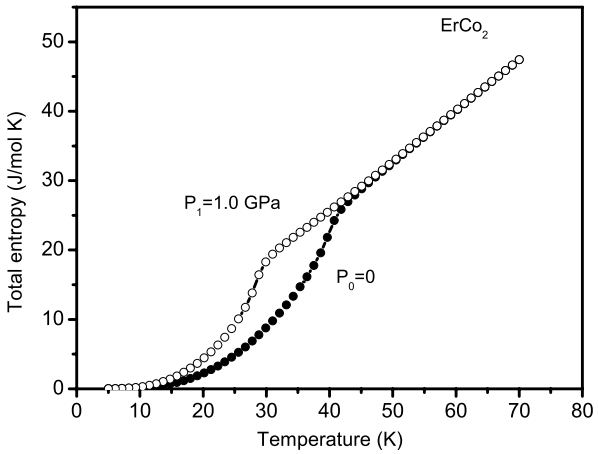

Fig. 67. Total entropy in $ErCo_2$ for $B = 1$ T calculated at ambient pressure (solid circles) and for an applied pressure of 1.0 GPa (open circles).

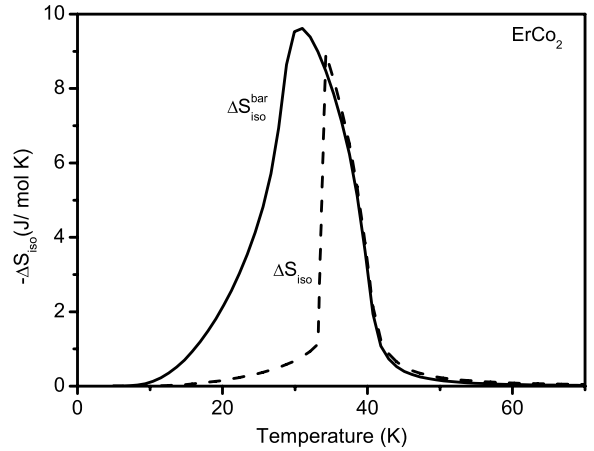

Fig. 68. Barocaloric potential ΔS_{iso}^{bar} in $ErCo_2$, calculated for a fixed magnetic field of 1 T and pressure variation from 1.0 to 0 GPa (solid line). Dashed line represents the magnetocaloric potential ΔS_{iso} calculated at ambient pressure and magnetic field variation from 0 to 1 T.

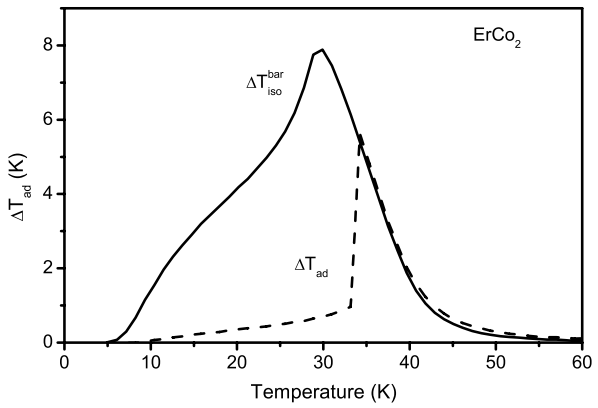

Fig. 69. Barocaloric potential ΔT_{ad}^{bar} in $ErCo_2$, calculated for a fixed magnetic field of 1 T and pressure variation from 1.0 to 0 GPa (solid line). Dashed line represents the magnetocaloric potential ΔT_{ad} calculated at ambient pressure and magnetic field variation from 0 to 1 T.

field variation from 0 to 1 T. These outstanding results point out that applied pressure can be an important mechanism to yield large values of the caloric potentials, which can be useful for the development of magnetic refrigeration. Apart from the possible technological application, further study in this direction can reveal important aspects of the physical mechanism of the entropy change in metals.

The model discussed in this section can be applied to calculate the magnetocaloric effect in other rare earth cobalt based compounds such as Er_3Co, RCoAl and $Nd_7Co_6Al_7$. However, in order to calculate the magnetocaloric effect in rare earth iron based compounds the model should be improved to treat the interaction between itinerant electrons beyond the mean field approximation.

7. Magnetocaloric effect in rare earth doped compounds

The magnitude of the magnetocaloric potentials ΔS_{iso} and ΔT_{ad} can be tuned by doping the sample with impurities [17,34,43,53,260,288–290]. In fact the impurities modify the magnetic interactions in the compound and consequently their magnetocaloric properties. The theoretical description of the magnetocaloric effect in doped compounds is somewhat more complex than the one in pure compounds. As a matter of fact, in the theoretical formulation of a disordered problem the nature of the host ions and the type of impurities are introduced into the host should be considered. For instance, rare earth based compounds doped with non magnetic impurities entering substitutionally at the non rare earth sites, such as: $R(Al_{1-c}Ni_c)_2$ can be considered as an effective rare earth metal. The magnetism and the magnetocaloric properties of this type of doped compound can be described by the formalism developed in Section 4 with an effective exchange interaction parameter renormalized by the impurities. The theoretical description of the magnetocaloric effect in compounds doped with transition elements, such as $R(Ni_{1-c}Fe_c)_2$, is much more complex and is not discussed in this report. In this section, we only consider rare earth doped compounds, in which the impurities (magnetic or not) enter at the rare earth sites such as: $(R^{\lambda}_c R^{\eta}_{1-c})_y Al_2$ and $(R^{\lambda}_c R^{\eta}_{1-c})_y Ni_2$. The simplest way to discuss the magnetocaloric effect in this type of doped compounds, is through the virtual crystal approximation. In this approximation, the doped compound $(R^{\lambda}_c R^{\eta}_{1-c})$ is replaced by a virtual crystal, with an effective angular momentum determined by $J_{eff} = (1-c)J^{\lambda} + cJ^{\eta}$, where J^{λ} and J^{η} are the angular momenta of rare earth ions R^{λ} and R^{η} respectively. This approximation provides averages values of the physical quantities that are compatible with experiments. However, it is not able to provide local values of the magnetization. Another way to discuss the magnetocaloric effect in the doped compound $(R^{\lambda}_c R^{\eta}_{1-c})$ is through the classical Monte Carlo simulation [186–191]. In the Monte Carlo method, the individuality of the rare earth ions is preserved, so that both average and local values of the physical quantities can be calculated. However, the drawback of the classical Monte Carlo simulation is that the crystalline electrical field interaction, sometimes so important in rare earth compounds, can not be properly included, because it has a pure quantum nature. Another problem involving the classical Monte Carlo simulations is the large computer time necessary to calculate the averages of the physical quantities. In this report, we theoretically discuss the magnetocaloric properties of rare earth doped compounds with more than one type of rare earth ion, by using an alternative formulation, based on an extension of the conventional mean field approach [291–293].

7.1. Theoretical formulation

In this subsection, we present a general formulation suitable to describe the magnetocaloric effect in rare earth doped compounds such as $(R^{\lambda}_c R^{\eta}_{1-c})_y T_z$, where R stands for rare earth ions and T for sp or transition metal ions. In order to theoretically discuss the magnetocaloric effect in this kind of doped compounds, we use a model Hamiltonian including both the localized moments from the rare earth ions and the itinerant electrons from the transition element. We also included the conduction electrons and the crystalline lattice. Thus, the model Hamiltonian reads:

$$\mathcal{H} = \mathcal{H}^{spd}_{el} + \mathcal{H}^{4f}_{mag} + \mathcal{H}^{d}_{mag} + \mathcal{H}_{lat}, \tag{154}$$

where:

$$\mathcal{H}^{spd}_{el} = \sum_k \tilde{\varepsilon}_k c^+_k c_k, \tag{155}$$

$$\mathcal{H}_{lat} = \sum_q \hbar\tilde{\omega}_q a^+_q a_q, \tag{156}$$

$$\mathcal{H}^{d}_{mag} = \sum_{i\sigma} \varepsilon_{0\sigma} d^+_{i\sigma} d_{i\sigma} + \sum_{il\sigma} T_{il\sigma} d^+_{i\sigma} d_{l\sigma} + U^d \sum_{i\sigma} n^d_{i\uparrow} n^d_{i\downarrow} - \frac{1}{2}\sum_i \mathcal{J}_{df} \vec{J}^f_i \vec{s}^d_i - \sum_i g^d_i \mu_B \vec{B}.\vec{s}^d_i, \tag{157}$$

$$\mathcal{H}^{4f}_{mag} = -\sum_{il} \mathcal{J}^{ab}_{il}(r) \vec{J}^{f,a}_i . \vec{J}^{f,b}_l - \sum_i g^{f,a}_i \mu_B \vec{B}.\vec{J}^{f,a}_i - \frac{1}{2}\sum_i \mathcal{J}_{df} \vec{J}^{f,a}_i . \vec{s}^d_i + \sum_i \mathcal{H}^a_{i(CF)}. \tag{158}$$

The Hamiltonian $\mathcal{H}^{spd}_{el}$ describes the s, p and 5d conduction electrons and $\mathcal{H}_{lat}$ describes the phonons in the crystalline lattice. These two Hamiltonians have already been discussed in the previous section. The magnetic Hamiltonian $\mathcal{H}^{d}_{mag}$ describes the subsystem of itinerant d-electrons associated with T ions and coupled with the R sublattice. Notice that the Hamiltonian $\mathcal{H}^{d}_{mag}$ is very similar to the one discussed in the previous section. Notice that, in the case of rare earth doped compounds without transition elements, such as $(R^{\lambda}_c R^{\eta}_{1-c})_y Al_2$, the Hamiltonian $\mathcal{H}^{d}_{mag}$ can be neglected, so that the formulation is much

simplified. The magnetic Hamiltonian $\mathcal{H}^{4f}_{mag}$ describes the localized moments of the rare earth ions. In this Hamiltonian, the first term describes the interaction between rare earth magnetic moments, where $J^{f,a}_i$ is the total angular momentum of the rare earth ions, which can be of different types ($a = \lambda$ or η and $b = \lambda$ or η), and $\mathcal{J}^{ab}$ is the exchange interaction integral. As has already been discussed, this exchange interaction integral may be written as $\mathcal{J}^{ab}(r) = \alpha^{ab}_0 \mathcal{J}^{ab}_0(r_0) + \alpha^{ab}_1 \mathcal{J}^{ab}_1(r_0) J_i J_l$, where the parameters α^{ab}_0 and α^{ab}_1 were introduced to simulate the effect of applied pressure. The second term represents the Zeeman interaction between the rare earth magnetic moments and the external magnetic field, where $g^{f,a}_i$ is the Landé factor of rare earth ions, which also depends on the type of rare earth ion which is occupying the site. The third term describes the coupling between rare earth magnetic moments and itinerant d-electrons from the T sublattice, where $\mathcal{J}_{df}$ is the exchange coupling parameter. The last term ($\mathcal{H}^a_{i(CF)}$) describes the crystalline electrical field effect on the 4f ground multiplet of a given rare earth ion. For cubic and hexagonal symmetry, the crystalline electrical field Hamiltonian is given by Eqs. (59) and (60) respectively. For the sake of clarity, we rewrite the magnetic Hamiltonian $\mathcal{H}^{4f}_{mag}$ in the form $\mathcal{H}^{4f}_{mag} = \mathcal{H}^{4f(\lambda)}_{mag} + \mathcal{H}^{4f(\eta)}_{mag}$ where:

$$\begin{aligned}\mathcal{H}^{4f(\lambda)}_{mag} &= -\sum_{il} \hat{\mathcal{J}}^{\lambda\lambda}_0 \vec{J}^{\lambda}_i . \vec{J}^{\lambda}_l - \sum_{il} \hat{\mathcal{J}}^{\lambda\eta}_0 \vec{J}^{\lambda}_i . \vec{J}^{\eta}_l - \sum_{il} \hat{\mathcal{J}}^{\lambda\lambda}_1 (\vec{J}^{\lambda}_i . \vec{J}^{\lambda}_l)^2 - \sum_{il} \hat{\mathcal{J}}^{\lambda\eta}_1 (\vec{J}^{\lambda}_i . \vec{J}^{\eta}_l)^2 \\ &\quad - \sum_i g^{\lambda}_i \mu_B \vec{B} . \vec{J}^{\lambda}_i - \frac{1}{2} \sum_i \mathcal{J}_{df} \vec{J}^{\lambda}_i . \vec{s}^{\,d}_i + \sum_i \mathcal{H}^{\lambda}_{i(CF)}, \end{aligned} \tag{159}$$

$$\begin{aligned}\mathcal{H}^{4f(\eta)}_{mag} &= -\sum_{il} \hat{\mathcal{J}}^{\eta\eta}_0 \vec{J}^{\eta}_i . \vec{J}^{\eta}_l - \sum_{il} \hat{\mathcal{J}}^{\eta\lambda}_0 \vec{J}^{\lambda}_i . \vec{J}^{\eta}_l - \sum_{il} \hat{\mathcal{J}}^{\eta\eta}_1 (\vec{J}^{\eta}_i . \vec{J}^{\eta}_l)^2 - \sum_{il} \hat{\mathcal{J}}^{\eta\lambda}_1 (\vec{J}^{\eta}_i . \vec{J}^{\lambda}_l)^2 \\ &\quad - \sum_i g^{\eta}_i \mu_B \vec{B} . \vec{J}^{\eta}_i - \frac{1}{2} \sum_i \mathcal{J}_{df} \vec{J}^{\eta}_i . \vec{s}^{\,d}_i + \sum_i \mathcal{H}^{\eta}_{i(CF)}, \end{aligned} \tag{160}$$

where we have defined $\hat{\mathcal{J}}^{ab}_0 = \alpha^{ab}_0 \mathcal{J}^{ab}_0$ and $\hat{\mathcal{J}}^{ab}_1 = \alpha^{ab}_1 \mathcal{J}^{ab}_1$ with $a, b = \lambda$ or η. From now on, we drop the label "f" as the superscript of "J" and "g". The magnetic Hamiltonian $\mathcal{H}^{4f(\lambda)}_{mag}$ describes a subsystem of rare earth ions R^{λ}, in which the neighborhood of a given site can be occupied by either R^{λ} or R^{η}. A similar description holds for $\mathcal{H}^{4f(\eta)}_{mag}$. Taking the mean field approximation to treat the two body interaction term, we get

$$\begin{aligned}\mathcal{H}^{4f(\lambda)}_{mag} &= \sum_i \sum_{\alpha=x,y,z} \big[-\tilde{\mathcal{J}}^{\lambda\lambda}_0 \langle J^{\lambda}_{\alpha} \rangle - \tilde{\mathcal{J}}^{\lambda\eta}_0 \langle J^{\eta}_{\alpha} \rangle - \tilde{\mathcal{J}}^{\lambda\lambda}_1 \langle J^{\lambda}_{\alpha} \rangle^3 - \tilde{\mathcal{J}}^{\lambda\eta}_1 \langle J^{\lambda}_{\alpha} \rangle \langle J^{\eta}_{\alpha} \rangle^2 \\ &\quad - 0.5 \mathcal{J}_{df} \langle s^d \rangle - g^{\lambda} \mu_B B \cos\theta_{\alpha} \big] J^{\lambda}_{i\alpha} + \sum_i \mathcal{H}^{\lambda}_{i(CF)}, \end{aligned} \tag{161}$$

where $\tilde{\mathcal{J}}^{ab}_0 = Z_{ab} \alpha^{ab}_0 \mathcal{J}^{ab}_0$ and $\tilde{\mathcal{J}}^{ab}_1 = Z_{ab} \alpha^{ab}_1 \mathcal{J}^{ab}_1$ ($a, b = \lambda$ or η). A similar relation holds for $\mathcal{H}^{4f(\eta)}_{mag}$ changing λ for η. Here θ_x; θ_y and θ_z are the angles between the applied magnetic field vector and the crystallographic axes x, y and z respectively. The terms Z_{ab} ($a, b = \lambda$ or η) represent the number of nearest neighbors at a given rare earth site. For instance, $Z_{\lambda\lambda}$ represents the number of rare earth ions R^{λ} and are in the neighborhood of a given site occupied by rare earth ions R^{λ}. Similarly, the term $Z_{\lambda\eta}$ represents the number of rare earth ions R^{η} are in the neighborhood of a given site occupied by rare earth ions R^{λ}.

The mean values $\langle J^a_{\alpha} \rangle$ ($a = \lambda$ or η and $\alpha = x, y, z$) are calculated by:

$$\langle J^a_{\alpha} \rangle = \frac{\sum_m \langle \psi^a_m | J^a_k | \psi^a_m \rangle \, e^{-\beta \varepsilon^a_m}}{\sum_m e^{-\beta \varepsilon^a_m}}, \tag{162}$$

where ε^{λ}; $|\psi^{\lambda}\rangle$ and ε^{η}; $|\psi^{\eta}\rangle$ are the energy eigenvalues and eigenvectors of the mean field Hamiltonians $\mathcal{H}^{4f(\lambda)}_{mag}$ and $\mathcal{H}^{4f(\eta)}_{mag}$ respectively. Note that the mean values $\langle J^{\lambda} \rangle$ and $\langle J^{\eta} \rangle$ defined in Eq. (162) depend on the mean value $\langle s^d \rangle$ from the d states of the transition element ions, which should be calculated from the magnetic Hamiltonian $\mathcal{H}^d_{mag}$. Using the procedure of the last section, we can write the magnetic Hamiltonian $\mathcal{H}^d_{mag}$, in the mean field approximation, as:

$$\mathcal{H}^d_{mag} = \sum_{i\sigma} \left(\varepsilon_{0\sigma} + U^d \langle n^d_{-\sigma} \rangle - 0.25\sigma \mathcal{J}_{df} \langle J \rangle - 0.5\sigma g^d \mu_B B \right) d^+_{i\sigma} d_{i\sigma} + \sum_{il\sigma} T_{il\sigma} d^+_{i\sigma} d_{l\sigma}. \tag{163}$$

Here $T_{ij\sigma} = \sum_k \tilde{\varepsilon}^d_{k\sigma} e^{ik(R_i - R_j)}$, where $\tilde{\varepsilon}^d_{k\sigma}$ is the renormalized electron dispersion relation. As a matter of fact, it is given by $\tilde{\varepsilon}^d_{k\sigma} = \varepsilon^d_k \alpha^d [1 - \xi^d (M^d)^2]$, where M^d is the magnetization of the T sublattice, the parameter α^d takes into account the applied pressure effect while the magnetoelastic coupling parameter ξ^d takes into account the lattice vibrations. The mean value $\langle J \rangle$ in the above Hamiltonian is $\langle J \rangle = (1-c)\langle J^{\lambda} \rangle + c \langle J^{\eta} \rangle$ where $\langle J^a \rangle = [\langle J^a_x \rangle^2 + \langle J^a_y \rangle^2 + \langle J^a_z \rangle^2]^{1/2}$ ($a = \lambda$ or η) and the components $\langle J^a_x \rangle$, $\langle J^a_y \rangle$ and $\langle J^a_z \rangle$ are calculated in Eq. (162). The local Green's function, for the magnetic Hamiltonian $\mathcal{H}^d_{mag}$ is given by:

$$g^d_{00\sigma}(z, c, T, B, P) = \int \frac{\rho^d_0(\varepsilon') d\varepsilon'}{z - \alpha^d \left[1 - \xi^d (M^d)^2 \right] \varepsilon' - \varepsilon^{\sigma}_0}, \tag{164}$$

where $\rho_0^d(\varepsilon')$ is a standard paramagnetic density of states, $z = \varepsilon + i0$ and $\varepsilon_0^\sigma = \varepsilon_0 + U^d\langle n_{-\sigma}^d\rangle - 0.25\sigma\mathcal{J}_{df}\langle J\rangle - \sigma\mu_B B$. The spin dependent density of states for d-electrons, is calculated by:

$$\rho_\sigma^d(\varepsilon, c, T, B, P) = -\frac{5}{\pi} Img_{00\sigma}^d(z, c, T, B, P), \tag{165}$$

where the factor 5 accounts for the degeneracy of the d states. The electron occupation number per spin direction is given by:

$$\langle n_\sigma^d\rangle = \int \rho_\sigma^d(\varepsilon, c, T, B, P) f(\varepsilon) d\varepsilon, \tag{166}$$

where $f(\varepsilon)$ is the Fermi distribution function. The magnetization at the transition element sublattice per ion is calculated by:

$$M^d(c, T, B, P) = (\langle n_\uparrow^d\rangle - \langle n_\downarrow^d\rangle)\mu_B. \tag{167}$$

The set of Eqs. (164)–(167) and the Eq. (162) should be self consistently solved. This self-consistency is very similar to the one discussed in the last section, i.e.,: for initial values of $\langle J_x\rangle$; $\langle J_y\rangle$; $\langle J_z\rangle$ and $\langle s^d\rangle$, the energies eigenvalues and eigenvectors $(\varepsilon^\lambda; |\psi^\lambda\rangle)$ and $(\varepsilon^\eta; |\psi^\eta\rangle)$ from the magnetic Hamiltonians $\mathcal{H}_{mag}^{4f(\lambda)}$ and $\mathcal{H}_{mag}^{4f(\eta)}$ are calculated. These values are then used to obtain, new values for $\langle J_\alpha\rangle$, through Eq. (162). After that, using the mean value $\langle J\rangle = (1-c)[\langle J_x^\lambda\rangle^2 + \langle J_y^\lambda\rangle^2 + \langle J_z^\lambda\rangle^2]^{1/2} + c[\langle J_x^\eta\rangle^2 + \langle J_y^\eta\rangle^2 + \langle J_z^\eta\rangle^2]^{1/2}$ in Eqs. (164)–(167), we get the magnetization at transition element sublattice (M^d) and consequently the mean value $\langle s^d\rangle$ through the relation $M^d/g^d\mu_B$. This entire self consistent process is repeated until two consecutive mean values of $\langle J\rangle$ and $\langle s^d\rangle$ are obtained within a numerical precision of 0.001. The total magnetization of the compound $(R_c^\lambda R_{1-c}^\eta)_y T_z$ as a function of impurity concentration is:

$$M(c, T, B, P) = yM^{4f}(c, T, B, P) + zM^d(c, T, B, P), \tag{168}$$

where $M^d(c, T, B, P)$ is given in Eq. (167) and $M^{4f}(c, T, B, P)$ is given by:

$$M^{4f}(c, T, B, P) = (1-c)M^{4f(R_y^\lambda T_z)}(c, T, B, P) + cM^{4f(R_y^\eta T_z)}(c, T, B, P), \tag{169}$$

where $M^{4f(R_y^\lambda T_z)}$ is given by:

$$M^{4f(R_y^\lambda T_z)}(c, T, B, P) = \sqrt{(M_x^\lambda)^2 + (M_y^\lambda)^2 + (M_z^\lambda)^2}. \tag{170}$$

The components of the magnetization are given by: $M_\alpha^\lambda = g^\lambda\mu_B\langle J_\alpha^\lambda\rangle$, where the mean value $\langle J_\alpha^\lambda\rangle$ is calculated in Eq. (162). A similar relation holds for $M^{4f(R_y^\eta T_z)}$. The total entropy in the doped compound $(R_c^\lambda R_{1-c}^\eta)_y T_z$ is calculated from:

$$S(c, T, B, P) = S_{el}^{spd}(c, T) + S_{mag}^{4f}(c, T, B, P) + S_{mag}^d(c, T, B, p) + S_{lat}(c, T, B, P), \tag{171}$$

where $S_{el}^{spd}(c, T) = \gamma T$ is the contribution from the conduction electrons. The contribution from the localized moments $S_{mag}^{4f}(c, T, B, P)$ is given by:

$$S_{mag}^{4f}(c, T, B, P) = (1-c)S_{mag}^{4f(R_y^\lambda T_z)}(c, T, B, P) + cS_{mag}^{4f(R_y^\eta T_z)}(c, T, B, P), \tag{172}$$

where $S_{mag}^{4f(R_y^\lambda T_z)}(c, T, B, P)$ is the contribution from the rare earth ions R^λ given by:

$$S_{mag}^{4f(R^\lambda T_z)}(c, T, B, P) = y\Re\left[\ln\sum_m e^{-\beta\varepsilon_m^\lambda} + \frac{1}{k_B T}\frac{\sum_m \varepsilon_m^\lambda e^{-\beta\varepsilon_m^\lambda}}{\sum_m e^{-\beta\varepsilon_m^\lambda}}\right], \tag{173}$$

where $\Re$ is the gas constant and y is the number of magnetic rare earth ions per unit formula. A similar relation holds for $S_{mag}^{4f(R_y^\eta T_z)}$. The contribution from the itinerant d-electrons is given by:

$$S_{mag}^d(c, T, B, P) = z\Re\left[\sum_\sigma \int_{-\infty}^{\mu} \ln\left[1 + e^{-\beta(\varepsilon-\mu)}\right]\rho_\sigma^d(\varepsilon)d\varepsilon + \frac{1}{k_B T}\sum_\sigma \int_{-\infty}^{\mu} (\varepsilon - \mu)\,\rho_\sigma^d(\varepsilon) f(\varepsilon) d\varepsilon\right], \tag{174}$$

where z is the number of magnetic transition element ions per unit formula. The crystalline lattice entropy is given by:

$$S_{lat}(c, T, B, P) = (1-c)S_{lat}^{R_y^\lambda T_z}(c, T, B, P) + cS_{lat}^{R_y^\eta T_z}(c, T, B, P), \tag{175}$$

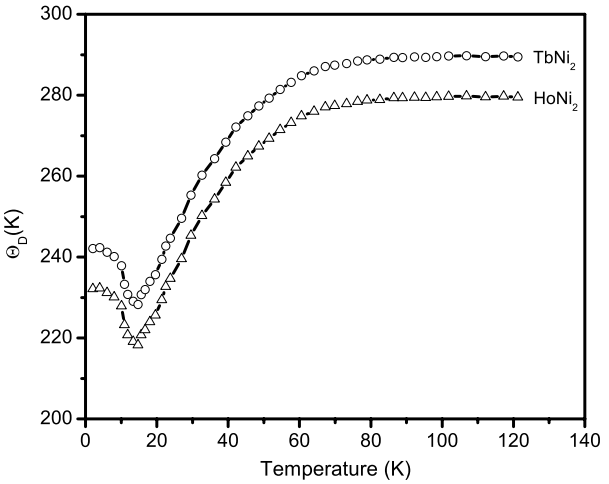

Fig. 70. Temperature dependence of the Debye temperature in $TbNi_2$ and $HoNi_2$.

where $S_{lat}^{R_y^\lambda T_z}(c, T, B, P)$ is given, in the Debye approximation, by:

$$S_{lat}^{R_y^\lambda T_z}(c, T, B, P) = (y+z)\left[-3\Re \ln\left(1-\mathrm{e}^{-\frac{\tilde{\Theta}_D^\lambda}{T}}\right) + 12\Re\left(\frac{T}{\tilde{\Theta}_D^\lambda}\right)^3 \int_0^{\tilde{\Theta}_D^\lambda/T} \frac{x^3}{\mathrm{e}^x - 1}\mathrm{d}x\right], \tag{176}$$

where $y+z$ is the number of ions per unit formula and $\tilde{\Theta}_D^\lambda = \Theta_0^\lambda \alpha_{ph}^\lambda (1 - \xi_{ph}^\lambda M^2)$ is the Debye temperature for the pure compound $R_y^\lambda T_z$, where Θ_0^λ is the bare value of the Debye temperature; M is the total magnetization, ξ_{ph}^λ and α^d are magnetoelastic coupling parameters. A similar relation holds for $S_{lat}^{R_y^\eta T_z}(c, T, B, P)$.

7.2. *Application to* $(Tb_{1-c}Ho_c)Ni_2$

In this subsection, we calculate the magnetocaloric effect in the doped compound $(Tb_{1-c}Ho_c)Ni_2$. In this doped compound, the magnetic moment at Ni site can be neglected, so that is not necessary to include the 3d electrons from the Ni ions in the self consistent calculations. Thus, in this case it is only necessary to self-consistently solve the magnetic state equation for the rare earth ions. In order to perform the numerical calculations, we take $J^{Tb} = 6$; $g^{Tb} = 1.5$ and $J^{Ho} = 8$; $g^{Ho} = 1.25$. The numbers of the nearest neighbors in the pure compounds $HoNi_2$ and $TbNi_2$ were taken as $Z_{HoHo} = 10(1-c)$ and $Z_{TbTb} = 10c$. The numbers Z_{HoTb}, Z_{TbHo} were taken as zero for $c = 0$ and $c = 1$. For intermediate concentrations, these parameters were taken as $Z_{HoTb} = 10(1-c)$ and $Z_{TbHo} = 10c$. In a rigorous description, the exchange interaction parameters [$\mathcal{J}_0^{HoHo}$, $\mathcal{J}_0^{TbTb}$ and $\mathcal{J}_0^{TbHo}$] should be self consistently calculated, in order to incorporate the change in the electron gas due to the presence of impurities. However, this procedure is more complex and is beyond the scope of this report. For the sake of simplicity, we assume that these parameters are almost constant as a function of impurity concentration. Here, we take $\mathcal{J}_0^{HoHo} = 0.006$ meV, $\mathcal{J}_0^{TbTb} = 0.0024$ meV and $\mathcal{J}_0^{TbHo} = \mathcal{J}_0^{HoTb} = 0.013$ meV, in order to reproduce the experimental value of the magnetic ordering temperature as a function of Ho concentration. It should be mentioned that even with the consideration that the exchange parameters $\mathcal{J}_0^{ab}(a, b = \mathrm{Ho}, \mathrm{Tb})$ are constant, the effective exchange interaction parameters $\tilde{\mathcal{J}}_0^{ab}$ depend on the impurity concentration. For instance the effective exchange parameter $\tilde{\mathcal{J}}_0^{TbTb} = Z_{TbTb}\mathcal{J}_0^{TbTb}$ goes from 0.0024 meV to zero and the effective parameter $\tilde{\mathcal{J}}_0^{HoHo} = Z_{HoHo}\mathcal{J}_0^{HoHo}$ goes from 0 to 0.006 meV, as the Ho concentration increases from 0 to 1. The magnetoelastic interaction parameters [$\mathcal{J}_1^{HoHo}$, $\mathcal{J}_1^{TbTb}$, $\mathcal{J}_1^{TbHo}$ and $\mathcal{J}_1^{HoTb}$] were taken as zero, since the magnetic phase transition in the compound $(Tb_{1-c}Ho_c)Ni_2$ is always of second order. The crystalline electrical field parameters [211], [212] were taken as: $x = -0.73$; $W = -0.066$ meV for $TbNi_2$ and $x = -0.44$; $W = 0.021$ meV for $HoNi_2$. The factors F_4 and F_6 were taken as $F_4 = 60$; $F_6 = 13\,860$. The magnetic field was applied along the $\langle 111\rangle$ direction for all Ho concentrations. The Debye temperatures for the compounds $TbNi_2$ and $HoNi_2$ were taken temperature dependent as shown in Fig. 70.

In Fig. 71, is plotted the magnetic part of the entropy for $(Tb_{1-c}Ho_c)Ni_2$ in the absence of an applied magnetic field. From this figure, good agreement can be observed between the calculations and the experimental data for $HoNi_2$ inferred from specific heat capacity [294]. Moreover, it can also be observed that the saturation value of the magnetic entropy in the pure compound $HoNi_2$ is larger than the one in the pure compound $TbNi_2$. For intermediate concentrations, the saturation values of the magnetic entropy lie in between the values of the pure compounds $TbNi_2$ and $HoNi_2$.

In Figs. 72 and 73, we present the isothermal entropy change and the adiabatic temperature change in the compound $(Tb_{1-c}Ho_c)Ni_2$ under magnetic field variation from 0 to 5 T. From the analysis of Fig. 72, it can be observed that increasing Ho concentration pushes the peak of ΔS_{iso} to lower temperatures without significant changes in its magnitude.

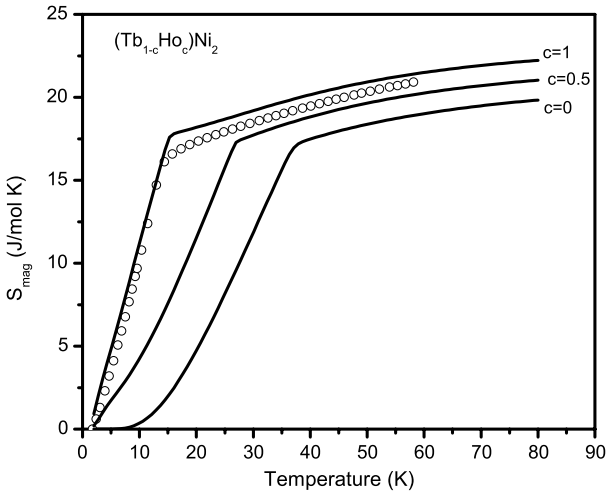

Fig. 71. Calculated magnetic entropy in the compound $(Tb_{1-c}Ho_c)Ni_2$ for $B = 0$ (solid lines). Open circles represent experimental data for $HoNi_2$ inferred from specific heat capacity [294].

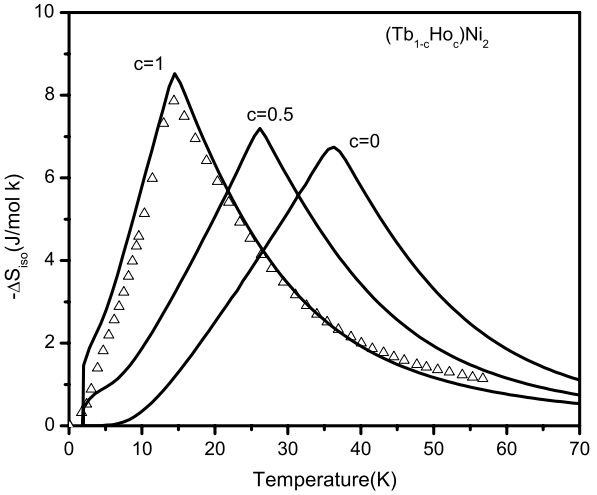

Fig. 72. ΔS_{iso} in $(Tb_{1-c}Ho_c)Ni_2$ under magnetic field variation from 0 to 5 T. Solid lines are theoretical calculations while open triangles represent experimental data for $HoNi_2$ [295].

This fact can be useful to make composite materials using samples of the doped compound $(Tb_{1-c}Ho_c)Ni_2$ with different impurity concentration. With this observation in mind, we theoretically simulate the following composite material: $[A]_{0.407}[B]_{0.057}[C]_{0.070}[D]_{0.026}[E]_{0.440}$, where $A = HoNi_2$, $B = (Tb_{0.25}Ho_{0.75})Ni_2$, $C = (Tb_{0.5}Ho_{0.5})Ni_2$, $D = (Tb_{0.75}Ho_{0.25})Ni_2$ and $E = TbNi_2$ represent each constituent of the composite material with molar compositions of 0.407; 0.057; 0.070; 0.026; 0.440 respectively. The isothermal entropy change in this composite material is calculated by: [214–217]

$$\Delta S_{iso} = \sum_i^n y_i \Delta S_{iso}^i, \tag{177}$$

where ΔS_{iso}^i is the isothermal entropy change of each constituent compound and y_i is its molar composition, which should fulfill the condition $\sum_i^n y_i = 1$.

In Fig. 74, is plotted the calculated isothermal entropy change under magnetic field variation from 0 to 5 T for the mentioned composite material. Notice that the isothermal entropy change in the composite material $[A]_{0.407}[B]_{0.057}[C]_{0.070}[D]_{0.026}[E]_{0.440}$ exhibits an almost constant value of ΔS_{iso} around 4.5 (J/mol K) in a temperature range from 15 to 35 K.

7.3. *Application to* $(Ho_{1-c}Er_c)Co_2$

We also apply the model discussed in this section to calculate the magnetocaloric effect in the doped compound $(Ho_{1-c}Er_c)Co_2$. In this case is necessary to consider the 3d electrons from the Co ions in the self consistent calculations. The

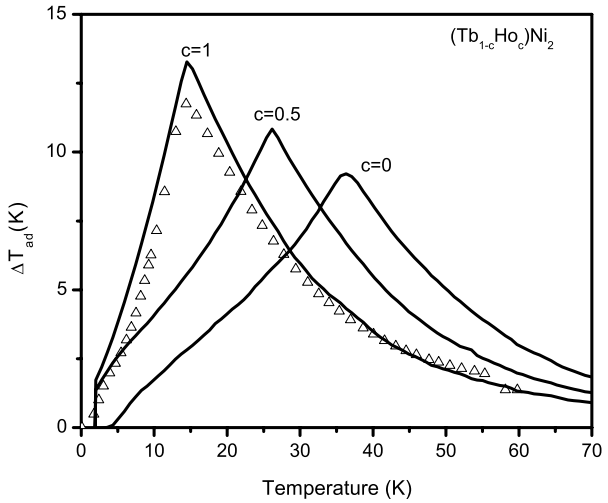

Fig. 73. ΔT_{ad} in $(Tb_{1-c}Ho_c)Ni_2$ under magnetic field variation from 0 to 5 T. Solid lines are theoretical calculations while open triangles represent experimental data $HoNi_2$ [295].

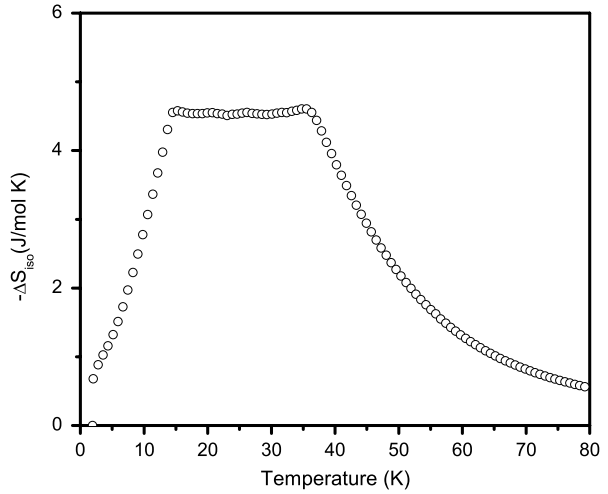

Fig. 74. Calculated ΔS_{iso} in the composite material $[A]_{0.407}[B]_{0.057}[C]_{0.070}[D]_{0.026}[E]_{0.440}$ for ΔB from 0 to 5 T. Here $A = HoNi_2$, $B = (Tb_{0.25}Ho_{0.75})Ni_2$, $C = (Tb_{0.5}Ho_{0.5})Ni_2$, $D = (Tb_{0.75}Ho_{0.25})Ni_2$ and $E = TbNi_2$.

total angular momentum and the Landé factor were taken from Hund's rule as $J^{Ho} = 8$; $g^{Ho} = 1.25$; $J^{Er} = 15/2$ and $g^{Er} = 1.2$. The crystalline electrical field parameters were taken as [283,284]: [$x = -0.24$; $W = -0.04214$ meV] for $ErCo_2$ and [$x = -0.4687$; $W = 0.051702$ meV] for $HoCo_2$. The parameters F_4 and F_6 were taken as $F_4 = 60$; $F_6 = 13\,860$. The number of nearest neighbors in the pure compounds $HoCo_2$ and $ErCo_2$ were respectively taken as $Z_{HoHo} = 10(1-c)$ and $Z_{ErEr} = 10c$. The number nearest neighbors Z_{HoEr}, Z_{ErHo} were taken as zero for $c = 0$ and $c = 1$. For intermediate concentrations, we take $Z_{HoEr} = 10c$ and $Z_{ErHo} = 10(1-c)$. Here we also assume, for the sake of simplicity, that the bare values of the exchange interaction parameters [$\mathcal{J}_0^{HoHo}$, $\mathcal{J}_0^{ErEr}$ and $\mathcal{J}_0^{HoEr}$] are almost constant as a function of impurity concentration. Here we take $\mathcal{J}_0^{HoHo} = 0.0025$ meV, $\mathcal{J}_0^{ErEr} = 0.00155$ meV and $\mathcal{J}_0^{HoEr} = \mathcal{J}_0^{ErHo} = 0.025$ meV. The magnetoelastic interaction parameters were taken as: $\mathcal{J}_1^{HoHo} = 0.0025$ meV, $\mathcal{J}_1^{ErEr} = 0.0013$ meV and $\mathcal{J}_1^{HoEr} = \mathcal{J}_1^{ErHo} = 0.0019$ meV. These parameters were chosen in order to reproduce the experimental value of the magnetic ordering temperature as a function of impurity concentration.

The coupling parameter $\mathcal{J}_{df}$ was taken as $\mathcal{J}_{df} = 0.2$ meV for the whole range of Er concentrations. The bare value of the Debye temperature and the magnetoelastic coupling parameter were taken respectively as $\Theta_0^{Er} = \Theta_0^{Ho} = 230$ K, $\xi^d = \xi_{ph}^{Er} = \xi_{ph}^{Er} = 0.1$. The magnetic field was applied along the $\langle 100 \rangle$ direction for the whole range of Er concentration. The standard paramagnetic 3d-density of states at the Co sublattice was extracted from reference [285]. The number of electrons at the Co site was taken as $n = 8.0$ and the Coulomb interaction parameter was taken as $U^d = 0.25$ in units of the Co 3d-bandwidth. In Figs. 75 and 76, are plotted the isothermal entropy change and the adiabatic temperature change in the doped compound $(Ho_{1-c}Er_c)Co_2$ for a magnetic field variation from 0 to 2 T at ambient pressure. From these figures a good agreement can be observed between the theoretical calculations and the available experimental data [253,287] for the pure

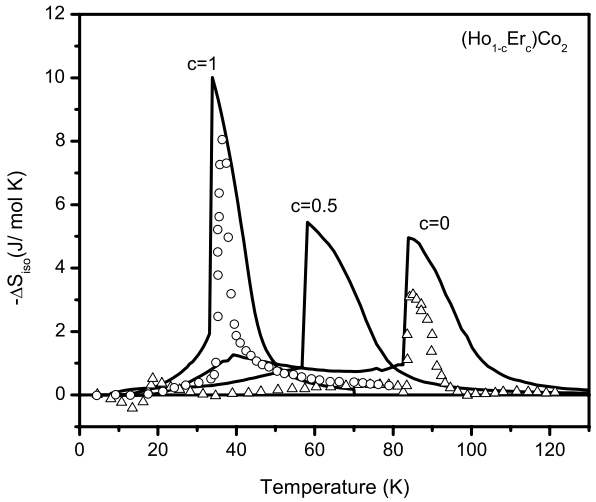

Fig. 75. ΔS_{iso} in $(Ho_{1-c}Er_c)Co_2$ under magnetic field variation from 0 to 2 T. Solid lines are the theoretical calculations while open squares and open triangle represent experimental data [253,287].

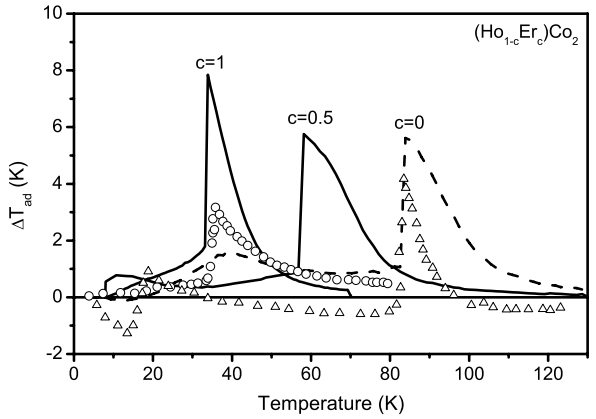

Fig. 76. ΔT_{ad} in $(Ho_{1-c}Er_c)Co_2$ under magnetic field variation from 0 to 2 T. Lines are theoretical calculations while symbols represent experimental data [253,287].

compounds $HoCo_2$ and $ErCo_2$. The results for intermediate concentration are theoretical predictions and need experimental data to be confirmed.

We use Eq. (177) to calculate the isothermal entropy change in the composite material $[(Ho_{0.5}Er_{0.5})Co_2]_{0.501}[(Ho_{0.7}Er_{0.3})Co_2]_{0.203}[HoCo_2]_{0.294}$. The obtained result for a magnetic field variation from 0 to 2 T is shown in Fig. 77. From this figure it can be observed that large values of ΔS_{iso} extend over a wide range of temperatures.

The effect of impurities on the magnetocaloric properties of rare earth doped compounds has been theoretically discussed in this section. It has been shown that doping is a useful mechanism to change the magnitude of the magnetocaloric potentials and the temperature of their peaks. The extended mean field theory discussed in this section can be applied to calculate the magnetocaloric effect in other doped compounds with more than one type of rare earth ion. Moreover, it is expected that the present calculations with a suitable choice of the model parameters is also able to explain the anomalies observed in the magnetocaloric potentials of some doped compounds such as: table-like behavior, inverse magnetocaloric effect and the two peaks structure. All of these aspects are still open questions to be theoretically addressed.

8. Magnetocaloric effect in antiferromagnets and ferrimagnets

Antiferromagnetic materials were described by Néel [296] as formed by two magnetic sublattices with magnetic moments of the same intensity, but aligned antiparallel to each other. Therefore, in the absence of an applied magnetic field, the net magnetization of antiferromagnetic materials should be zero. After Néel's original description, the concept of antiferromagnetic materials has been extended to include materials with more than two magnetic sublattices and other more complex structures, such as triangular, spiral and canted spin arrangements. When the sublattice magnetizations are not equal, a spontaneous magnetization appears giving rise to the ferrimagnetic state [297]. The theoretical description

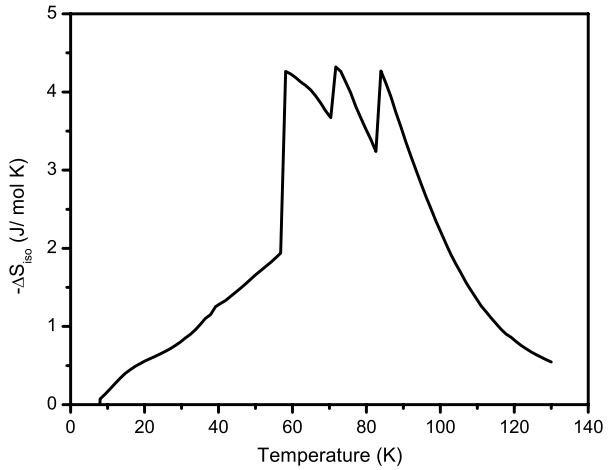

Fig. 77. ΔS_{iso} in the composite material formed by $[(Ho_{0.5}Er_{0.5})Co_2]_{0.501}[(Ho_{0.7}Er_{0.3})Co_2]_{0.203}[HoCo_2]_{0.294}$ for ΔB from 0 to 2 T.

of the magnetocaloric effect in antiferromagnetic and ferrimagnetic compounds is somewhat more complex than the one used for ferromagnetic compounds. This is because it is necessary to consider in the calculations at least two magnetic sublattices [298].

In this report, we discuss the magnetocaloric effect in antiferromagnetic and ferrimagnetic systems, considering a model Hamiltonian with two coupled sublattices of localized magnetic moments. In the model, the existence of the antiferromagnetic, ferrimagnetic and even the ferromagnetic state, depends on the set of model parameters.

8.1. Theoretical formulation

In this subsection, we present a theoretical formulation of the magnetocaloric effect in antiferromagnetic and ferrimagnetic materials in thermodynamic equilibrium. To this end, we consider the following model Hamiltonian

$$\mathcal{H} = \mathcal{H}_{el} + \mathcal{H}_{lat} + \mathcal{H}_{mag}, \tag{178}$$

where the Hamiltonians $\mathcal{H}_{el}$ and $\mathcal{H}_{lat}$ describing respectively conduction electrons and the crystalline lattice, have already been discussed in the previous sections. Here $\mathcal{H}_{mag}$ given by:

$$\mathcal{H}_{mag} = -\sum_{ij} \mathcal{J}_{ab}^{(ij)} J_i^a J_j^b - \sum_{ij\delta} \mathcal{J}_{\delta\delta}^{(ij)} J_i^\delta J_j^\delta - \mu_B B \sum_{i\delta} g_\delta J_i^\delta, \tag{179}$$

describes two sublattices of localized magnetic moments under the action of external magnetic field. For the sake of simplicity, the crystalline electric field interaction is neglected. In the magnetic Hamiltonian $\mathcal{H}_{mag}$, the first term describes the interaction between magnetic ions of different sublattices, where $\mathcal{J}_{ab}^{(ij)}$ is the inter-sublattice exchange interaction parameter; J^a and J^b represent the total angular momentum operators of magnetic ions into the "a" or "b" sublattice. The second term describes the interaction between magnetic ions of same sublattice "δ", where $\mathcal{J}_{\delta\delta}^{(ij)}$ ($\delta = a, b$) is the intra-sublattice exchange interaction parameter. The last term gives the Zeeman interaction, where B is the applied magnetic field, μ_B is the Bohr magneton and g_δ is the Landé factor. The single ion Hamiltonian for the nearest and next nearest neighbors pairs can be explicitly written as:

$$\mathcal{H}_{mag} = -\mathcal{J}_{ab} J_i^a \sum_{j=1}^{Z_{ab}} J_j^b - \mathcal{J}_{ab} J_i^b \sum_{j=1}^{Z_{ba}} J_j^a - \mathcal{J}_{aa} J_i^a \sum_{j=1}^{Z_{aa}} J_j^a - \mathcal{J}_{bb} J_i^b \sum_{j=1}^{Z_{bb}} J_j^b - \mu_B B \sum_{i\delta} g_\delta J_i^\delta. \tag{180}$$

Here Z_{ab} represents the number of nearest-neighbors ions of the "b"-sublattice around the ions of "a"-sublattice; Z_{ba} represents the number of nearest-neighbors ions of the "a"-sublattice around the ions of the "b"-sublattice. Similarly, Z_{aa} (Z_{bb}) represents the number of nearest-neighbors ions of the "a"-sublattice ("b"-sublattice) around the ions of the "a"-sublattice ("b"-sublattice). Considering that all ions in the "a"-sublattice are identical and equivalents, and taking a similar assumption for the ions in the "b"-sublattice, the magnetic Hamiltonian, in the mean field approximation, turns out to be:

$$\mathcal{H}_{mag} = -\mathcal{J}_{ab} Z_{ab} \langle J^b \rangle J_i^a - \mathcal{J}_{ab} Z_{ba} \langle J^a \rangle J_i^b - \mathcal{J}_{aa} Z_{aa} \langle J^a \rangle J_i^a - \mathcal{J}_{bb} Z_{bb} \langle J^b \rangle J_i^b - \mu_B B \left(g_a J_i^a + g_b J_i^b \right). \tag{181}$$

The averages $\langle J^\delta \rangle$ ($\delta = a, b$) are directly related to magnetization in the δ-sublattice through the expression $M^\delta = N_\delta g_\delta \mu_B \langle J^\delta \rangle$, where N_δ is the number of ions into the δ-sublattice. The number of ions in the "a" and "b" sublattice can be written as $N_a = pN$ and $N_b = qN$ respectively, where N is the total number of magnetic ions, p is the fraction of magnetic

ions in the "a"-sublattice and q is the fraction of magnetic ions in the "b"-sublattice under the condition $p + q = 1$. The magnetic Hamiltonian in Eq. (181) can be written as:

$$\mathcal{H}_{mag} = -\mu_B g_a B_a J_i^a - \mu_B g_b B_b J_i^b, \tag{182}$$

where B_a and B_b are effective magnetic fields given by:

$$B_a = B + \gamma_{ab} M_b + \gamma_{aa} M_a \tag{183}$$

$$B_b = B + \gamma_{ba} M_a + \gamma_{bb} M_b, \tag{184}$$

where $\gamma_{ab} = \mathcal{J}_{ab} Z_{ab}/(N_b g_a g_b \mu_B^2)$, $\gamma_{ba} = \mathcal{J}_{ab} Z_{ba}/(N_a g_a g_b \mu_B^2)$, $\gamma_{aa} = \mathcal{J}_{aa} Z_{aa}/(N_a g_a^2 \mu_B^2)$ and $\gamma_{bb} = \mathcal{J}_{bb} Z_{bb}/(N_b g_b^2 \mu_B^2)$ are normalized exchange interaction parameters. Using the energy eigenvalues and eigenvectors of the magnetic Hamiltonian in Eq. (182), we obtain the following coupled magnetic state equations for the "a" and "b" sublattices:

$$M_a = pNg_a \mu_B J_a B_J \left(\mu_B g_a J_a B_a / k_B T\right) \tag{185}$$

$$M_b = qNg_b \mu_B J_b B_J \left(\mu_B g_b J_b B_b / k_B T\right), \tag{186}$$

where B_J is the Brillouin function and k_B is the Boltzmann constant. In the model, the existence of the ferrimagnetic (FI), antiferromagnetic (AF) and ferromagnetic (FM) configurations depends on the choice of the exchange interaction parameters [γ_{aa}, γ_{bb}, γ_{ab}, γ_{ba}], ionic parameters [g_a, J_a, g_b, J_b,] and the fraction of magnetic ions in the "a" and "b"-sublattice [p, q]. In the general case, the transition temperature from the ferrimagnetic phase to the paramagnetic phase can be obtained analytically from the magnetic state equations and is given by

$$T_{FI} = \frac{1}{2}\left[pC_a\gamma_{aa} + qC_b\gamma_{bb}\right] + \sqrt{\left(pC_a\gamma_{aa} - qC_b\gamma_{bb}\right)^2 + 2pqC_aC_b\gamma_{ab}^2} \tag{187}$$

where $C_a = g_a^2 \mu_B^2 J_a(J_a + 1)/3k_B$ and $C_b = g_b^2 \mu_B^2 J_b(J_b + 1)/3k_B$ are the Curie constants. In the particular case where $p = q = 1/2$, $C_a = C_b = C$ and $\gamma_{aa} = \gamma_{bb}$ the model predicts the existence of an antiferromagnetic phase. In this case, the previous relation for the transition temperature turns out to be:

$$T_{FI} = T_N = \frac{C\left(\gamma_{aa} + |\gamma_{ab}|\right)}{2}, \tag{188}$$

which is the well known Néel temperature for antiferromagnets. If we consider $\gamma_{aa} = \gamma_{ab} = \gamma$ in the previous equation, we get:

$$T_{FI} = T_C = C\gamma, \tag{189}$$

which is the well known Curie temperature, that describes the transition from the ferromagnetic state to the paramagnetic state.

Following the standard procedure used in Section 4, for the ferromagnetic case with only one magnetic lattice, we get that the partition function of the δ-sublattice ($\delta = a$ or b) is given by:

$$Z_{mag}^{\delta}(T, B) = \frac{\sinh\left[\left(\frac{2J_\delta + 1}{2J_\delta}\right) y_\delta\right]}{\sinh\left[\left(\frac{1}{2J_\delta}\right) y_\delta\right]}, \tag{190}$$

where $y_\delta = \mu_B g_\delta J_\delta B_\delta / k_B T$. The magnetic free energy per ion is obtained from:

$$F_{mag}(T, B) = -k_B T\left\{N_a \ln Z_{mag}^a + N_b \ln Z_{mag}^b\right\}. \tag{191}$$

The magnetic entropy per mol, calculated from $S_{mag} = -(\partial F_{mag}/\partial T)_B$ is given by:

$$S_{mag}(T, B) = \Re\left\{p\left[\ln Z_{mag}^a - y_a B_J(y_a)\right] + q\left[\ln Z_{mag}^b - y_b B_J(y_b)\right]\right\}, \tag{192}$$

where $\Re$ is the gas constant. It is worth noticing that, for high temperatures the Brillouin function goes to zero and the partition functions Z_{mag}^a and Z_{mag}^b go to the total number of quantum magnetic states in each sublattice, i.e., $(2J_a + 1)$ and $(2J_b + 1)$ respectively. Therefore, the maximum value of the magnetic entropy of the system formed by two sublattices of localized magnetic moments J_a and J_b is given by:

$$S_{mag}^{\max} = \Re\left[p \ln(2J_a + 1) + q \ln(2J_b + 1)\right]. \tag{193}$$

The total entropy is the sum of the contributions from the conduction electrons taken as $S_{el} = \gamma T$, from the magnetic ions calculated in Eq. (192) and from the crystalline lattice given in the Debye approximation by Eq. (86) with Θ_D replacing $\tilde{\Theta}_D$.

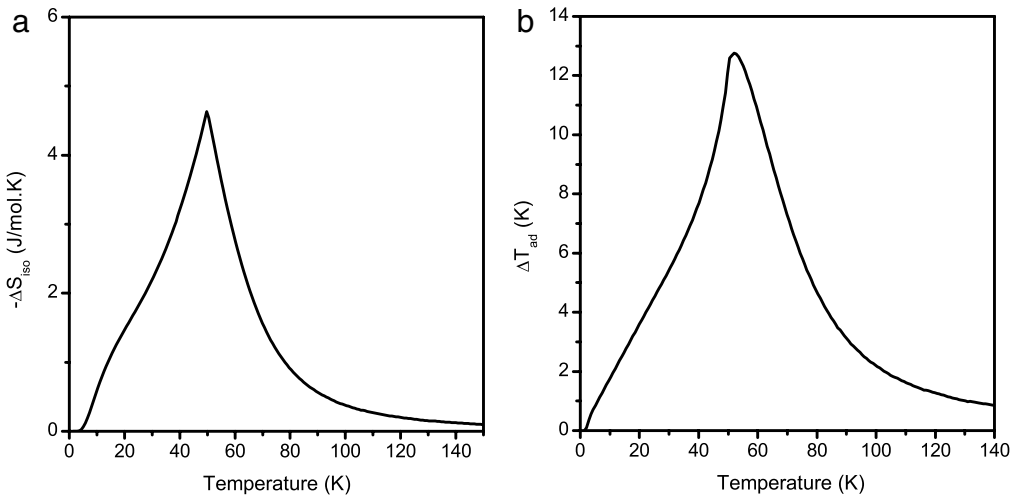

Fig. 78. Isothermal entropy change (a) and adiabatic temperature change (b) for ferromagnetic spins configuration upon magnetic field variation from 0 to 5 T, calculated using the model parameters: $p = q = 1/2, g_a = g_b = 2, J_a = J_b = 7/2, \gamma_{aa} = \gamma_{bb} = \gamma_{ab} = 61.1T^2/\text{meV}$ and $\Theta_D = 300$ K.

Table 5
Model parameters for magnetic configurations. The last column shows the critical temperature, which is T_N for the AF-PM transition, T_C for the FM-PM transition and T_{FI} for the FI-PM transition.

Magnetic phase	γ_{ab} (T^2/meV)	γ_{aa} (T^2/meV)	γ_{bb} (T^2/meV)	p	q	T_{crit} (K)
Antiferromagnetic	−122.2	61.1	61.1	1/2	1/2	75
Ferromagnetic	61.1	61.1	61.1	1/2	1/2	50
Ferrimagnetic (A)	−200	150	230	2/3	1/3	194.3
Ferrimagnetic (B)	−80	10	400	2/3	1/3	117.6

8.2. Systematic study

In this subsection, we illustrate the model with the calculations of the magnetocaloric potentials for ferromagnetic, antiferromagnetic and ferrimagnetic configurations. To this end, we take the following model parameters $J_a = J_b = 7/2$ and $g_a = g_b = 2$, which are common to all spins configurations. The type of the spin configuration is determined by the exchange interaction parameters γ_{aa}, γ_{bb}, γ_{ab} and by the numbers p and q that gives the fraction of ions are in the "a" and "b"-sublattices. In order to simulate a ferromagnetic spin configuration, we adopt the following model parameters: $\gamma_{aa} = \gamma_{bb} = \gamma_{ab} = 61.1\ T^2/\text{meV}$ and $p = q = 1/2$. With these parameters we get a ferromagnetic arrangement with Curie temperature at 50 K (see Table 5). The obtained results for the magnetocaloric potentials ΔS_{iso} and ΔT_{ad} for this ferromagnetic spin configuration upon magnetic field variation from 0 to 5 T are plotted in Fig. 78. The ΔT_{ad} curve was obtained using the Debye temperature $\Theta_D = 300$ K. From this figure, we can observe the usual behavior of the magnetocaloric potentials, which has already been discussed in the previous sections of this report.

In order to simulate an antiferromagnetic spins configuration, we adopt the following model parameters $\gamma_{aa} = \gamma_{bb} = 61.1\ T^2/\text{meV}$ and $\gamma_{ab} = -122.2\ T^2/\text{meV}$ and $p = q = 1/2$. With these parameters we get an antiferromagnetic configuration with a Néel temperature of 75 K (see Table 5).

Fig. 79 shows the temperature dependence of the isothermal entropy change for this antiferromagnetic spin configuration upon magnetic field variation from 0 to 5 T (dotted line), from 0 to 10 T (solid line) and from 0 to 15 T (dashed line). The corresponding curves for the adiabatic temperature change, for the same magnetic field variation is shown in Fig. 80.

From these figures, negative values can be observed for the magnetocaloric potentials $-\Delta S_{iso}$ and ΔT_{ad} below the Néel temperature. This type of behavior, called the inverse magnetocaloric effect, is expected to occur in any antiferromagnetic material. Above the Néel temperature, the usual behavior of the magnetocaloric potentials is observed. It is also worth noticing that at low temperatures the modulus of the magnetocaloric potential $-\Delta S_{iso}$ increases in a non-linear fashion up to the Néel temperature in the presence of an applied magnetic field, $T_{AF}(B)$. In the temperature interval $T_{AF}(B) < T < T_{AF}(B = 0)$, ΔS_{iso} varies linearly with temperature and changes sign in this interval. Comparing the curves of ΔS_{iso} in the antiferromagnetic and ferromagnetic regimes, we can observe that much more magnetocaloric effect is extracted at the ferromagnetic-paramagnetic phase transition than at the antiferromagnetic-paramagnetic phase transition. However, for antiferromagnetic materials the magnetocaloric effect occurs in a broad temperature range, which can be of practical interest for magnetic refrigeration.

Now we discuss the magnetocaloric effect in ferrimagnetic arrangements. In the two sublattice model discussed in this report, there are several schemes that can lead to ferrimagnetic arrangements. Here, we consider ferrimagnetic arrange-

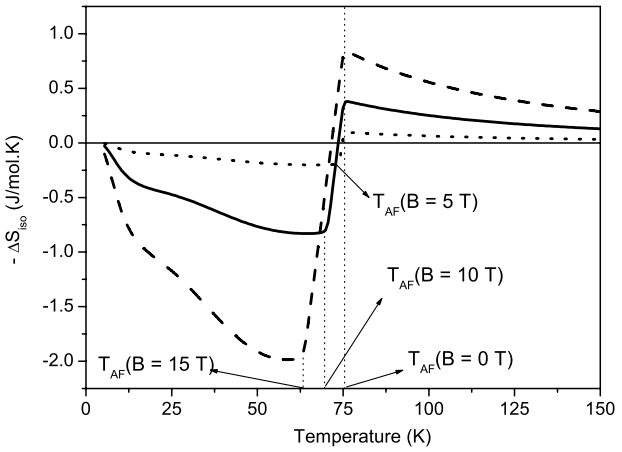

Fig. 79. Isothermal entropy changes for antiferromagnetic spins configuration with ΔB from 0 to 5 T (dotted line), from 0 to 10 T (solid line) and from 0 to 15 T (dashed line), calculated using the model parameters: $p = q = 1/2, g_a = g_b = 2, J_a = J_b = 7/2, \gamma_{aa} = \gamma_{bb} = 61.1\,\mathrm{T}^2/\mathrm{meV}$, and $\gamma_{ab} = -122.2T^2/\mathrm{meV}$.

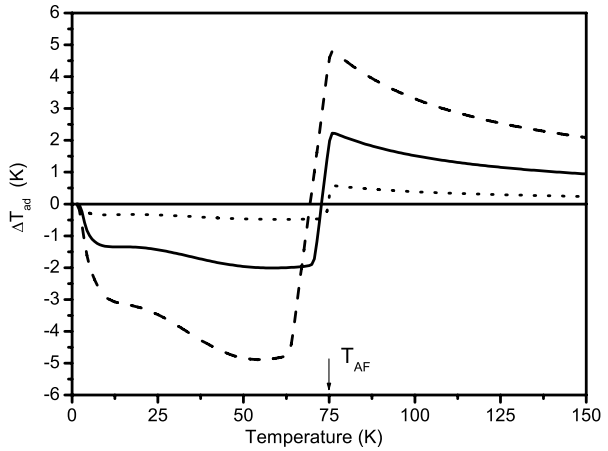

Fig. 80. Adiabatic temperature changes for antiferromagnetic spins configuration with ΔB from 0 to 5 T (dotted line), from 0 to 10 T (solid line) and from 0 to 15 T (dashed line), calculated using the model parameters: $p = q = 1/2, g_a = g_b = 2, J_a = J_b = 7/2, \gamma_{aa} = \gamma_{bb} = 61.1T^2/\mathrm{meV}$, and $\gamma_{ab} = -122.2T^2/\mathrm{meV}$ and $\Theta_D = 300$ K.

ments, in which the magnetic moments of the ions in the "a"-sublattice with up spins have the same magnitude of the magnetic moments of the ions in the "b"-sublattice with down spins, but with a different fraction, i.e., $p \neq q$. In order to simulate ferrimagnetic spin configurations, we use two set of model parameters shown in Table 5. For the first set of parameters, we get a ferrimagnetic state with a transition temperature at $T_{Fl} = 194.36$ K and without compensation temperature. We call this arrangement ferrimagnetic state A. For the second set of parameters, we get a ferrimagnetic state with a transition temperature $T_{Fl} = 117.6$ K and a compensation temperature $T_{comp} = 43$ K. We call this arrangement ferrimagnetic state B. The temperature dependence of the magnetization of these two ferrimagnetic arrangements is shown in Fig. 81.

Notice that the magnetization curve of the ferrimagnetic state A increases with temperature up to $T = 90$ K. This unusual behavior in the magnetization curve occurs when the molecular field in the "b"-sublattice is smaller than the one in the "a"-sublattice. In this scenario, the magnetization M_b at a given temperature decreases faster than the magnetization M_a, so that the net magnetization $M = M_a + M_b = |M_a| - |M_b|$ increases. The magnetization curve of the ferrimagnetic state B exhibits the so-called ferrimagnetic compensation temperature (T_{comp}), where the net magnetization vanishes due to the fact that the magnitude of the magnetizations in both sublattice are equal, i.e., $|M_a| = |M_b|$. The magnetization curve of the ferrimagnetic state B presents $T_{comp} = 43$ K and $T_{Fl} = 117.6$ K and the maximum magnetization value around $0.8\mu_B$ between T_{comp} and T_{Fl}. Fig. 82 shows the isothermal entropy change for the ferrimagnetic state A upon magnetic field variation from 0 to 2 T (dotted line), 0 to 5 T (solid line) and 0 to 10 T (dashed line). Notice that the inverse magnetocaloric effect, i.e., negative values for the magnetocaloric potential $-\Delta S_{iso}$, occurs below the temperature $T_k = 95$ K indicated by the arrow in Fig. 82. For temperatures greater than 95 K, the magnetocaloric potential $-\Delta S_{iso}$ exhibits positive values that increase up to the critical temperature $T_{Fl} = 194.3$ K. Above this temperature, a smooth decrease in $-\Delta S_{iso}$ is observed. The negative values of the magnetocaloric potential $-\Delta S_{iso}$, calculated via Eq. (18), occur because the temperature derivative of the magnetization below $T_k = 95$ K is positive (see Fig. 81). Above the temperature of 95 K the derivative of the magnetization is negative leading to positive values

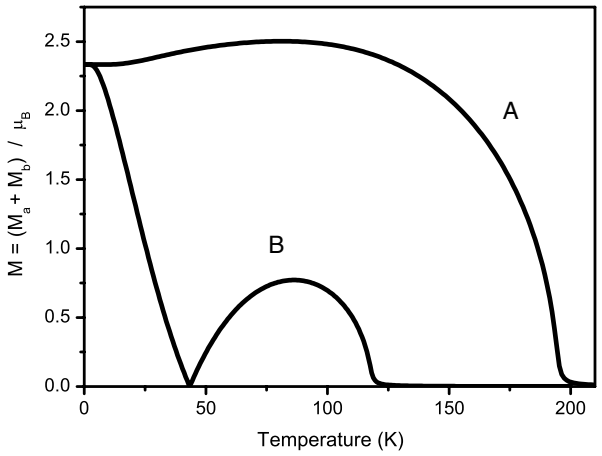

Fig. 81. Temperature dependence of the magnetization for ferrimagnetic states A and B calculated using the model parameters given in Table 5.

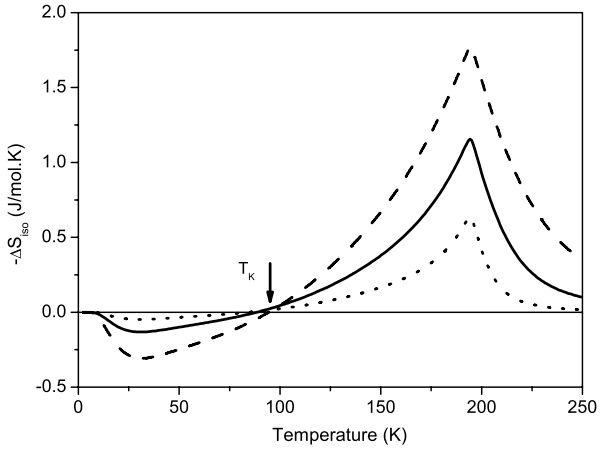

Fig. 82. Isothermal entropy changes for the ferrimagnetic state A upon magnetic field variation from 0 to 2 T (dotted line), from 0 to 5 T (solid line) and from 0 to 10 T (dashed line), calculated using the model parameters: $p = 2/3$, $q = 1/3$, $g_a = g_b = 2$, $J_a = J_b = 7/2$, $\gamma_{aa} = 300$, $\gamma_{bb} = 0$, and $\gamma_{ab} = -200T^2/\text{meV}$.

for the magnetocaloric potential $-\Delta S_{iso}$. The minimum values in the $-\Delta S_{iso}$ curves around $T = 30.3$ K, occur because the temperature derivative of the magnetization in the temperature interval between $T = 0$ K and $T_k = 95$ K is maximum. These minimum values of $-\Delta S_{iso}$, which depend on the magnetic field variations, are $-\Delta S_{iso} = -0.05$, -0.13 and -0.3 J/mol K for ΔB from 0 to 2, 0 to 5 and 0 to 10 T, respectively.

Now we present the results obtained for the second set of model parameters, which leads to the ferrimagnetic state B with compensation temperature. The temperature dependence of the magnetic entropy in this ferrimagnetic arrangement without magnetic field (dotted line) and with a magnetic field of 7 T (solid line), obtained from relation (192), is shown in Fig. 83.

Fig. 84 shows the isothermal entropy change for the ferrimagnetic state B upon magnetic field variation from 0 to 3 T (dotted line), 0 to 5 T (solid line) and 0 to 7 T (dashed line). From this figure, it can be observed that the ΔS_{iso} curves exhibit two peaks: the first one occurs at low temperature around 13 K, which is associated with the large magnetization changes around $2.4\mu_B$, below the compensation temperature (see curve B in Fig. 81). The second and smaller peak is observed at the ferrimagnetic-paramagnetic phase transition $T_{FI} = 117.6$ K. Notice that the magnitudes of the peaks at low temperature are much larger than the ones at higher temperatures, for the corresponding magnetic field change. In addition, the curves of ΔS_{iso} vanish at the temperature $T_0 = 82$ K between T_{comp} and T_{FI}, where the maximum magnetization values appear, (see curve B in Fig. 81). This temperature T_0 separates the normal magnetocaloric effect from the inverse one. The corresponding adiabatic temperature changes for the same magnetic field variations calculated using $\Theta_D = 300$ K are shown in Fig. 85.

The two sublattice model discussed in this section enables us to calculate the magnetocaloric effect in metallic systems of localized magnetic moments with ferromagnetic, antiferromagnetic and ferrimagnetic spin configurations. Here, we only present systematic calculations of the magnetocaloric effect as a function of the model parameters. In order to describe the magnetocaloric effect in real compounds, a fixed set of model parameters should be adjusted by using experimental data of magnetic ordering temperature. A similar model, in the framework of the band theory, can also be developed to discuss

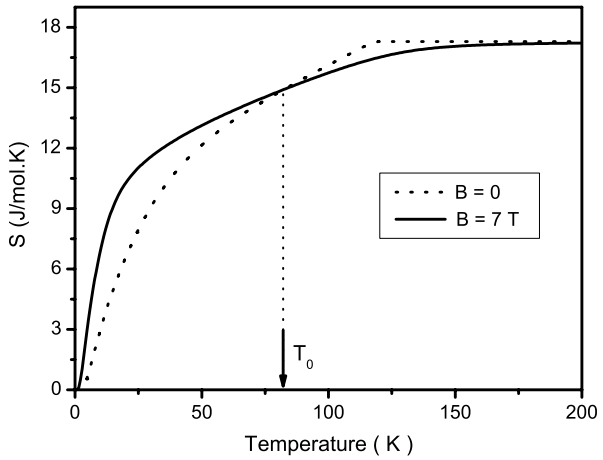

Fig. 83. Temperature dependence of the magnetic entropy of the ferrimagnetic state B for $B = 0$ (dotted line) and for $B = 7$ T (solid line).

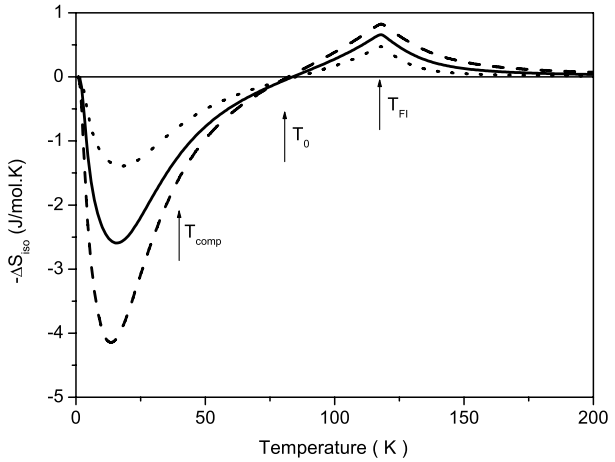

Fig. 84. Isothermal entropy changes for the ferrimagnetic state B, upon magnetic field variation from 0 to 3 T (dotted line), from 0 to 5 T (solid line) and from 0 to 7 T (dashed line), calculated using the model parameters: $p = 2/3, q = 1/3, g_a = g_b = 2, J_a = J_b = 7/2, \gamma_{aa} = 10, \gamma_{bb} = 400, \gamma_{ab} = -80T^2/\text{meV}$.

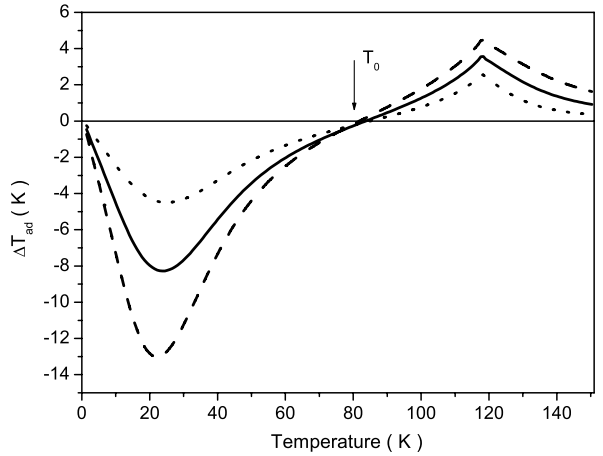

Fig. 85. Adiabatic temperature changes for the ferrimagnetic state B, upon magnetic field variation from 0 to 3 T (dotted line), from 0 to 5 T (solid line) and from 0 to 7 T (dashed line), calculated using the model parameters: $p = 2/3, q = 1/3, g_a = g_b = 2, J_a = J_b = 7/2, \gamma_{aa} = 10, \gamma_{bb} = 400, \gamma_{ab} = -80T^2/\text{meV}$ and $\Theta_D = 300$ K.

the magnetocaloric effect in antiferromagnetic and ferrimagnetic compounds, in which the magnetization has an itinerant character. However, this kind of calculation is somewhat more complex and is not in the scope of the present report.

9. Conclusions and perspectives

In this report, we theoretically discuss the magnetocaloric effect in rare earth metals and their alloys and in transition metal based compounds. The theoretical models discussed in this report explained much experimental data of the magnetocaloric effect. For instance, we were able to describe the effects of impurities, pressure, crystalline electric field and magnetoelastic coupling on the magnetocaloric potentials ΔS_{iso} and ΔT_{ad} observed in many metallic compounds, undergoing both second and first order phase transition. Apart from the theoretical description of the experimental data itself, this report discusses important aspects of the magnetocaloric effect. For instance, it is clearly shown that the relation $\Delta S_{iso} = \int (\partial M/\partial T)\mathrm{d}B$ should not be used to determine the isothermal entropy change around a first order phase transition. It is also shown in this report that the barocaloric effect, not much explored in the literature, can provide large values for the caloric potentials. Another important discussion points out that the simultaneous variation of pressure and magnetic field can be an important mechanism to produce large values of the magnetocaloric potentials in a wide range of temperatures. The theoretical discussion in this report also predicts the possibility to extract more entropy change from the crystalline lattice, so that the isothermal entropy change could overcome the limit of the magnetic entropy.

Despite the theoretical achievements presented in this report, further aspects of the magnetocaloric effect should still be discussed. For instance, we can mention that additional effort should be done in order to understand the magnetocaloric effect in amorphous materials. There is also a necessity to develop models to study the magnetocaloric effect associated with the transition from the superconducting phase to the normal one and with the insulator-metal phase transition. Concerning the models already found in the literature, some improvements are also necessary to be implemented. For example, the contribution from the crystalline lattice to the total entropy should be considered beyond the Debye approximation. In a more rigorous treatment, the entropy of the crystalline lattice should be described through a microscopic model, in which phonons and electron–phonon interactions are included. The electron–electron interaction in transition metal based compounds, should also be treated beyond the mean field theory. For instance, it could be treated in the functional integral technique, which incorporates spin fluctuations, which are very important around the magnetic phase transition. It is expected that this kind of treatment of the two-body interactions produces better values for the magnetic ordering temperatures in the transition metal based compounds.

To conclude this report, we can point some perspectives for future studies on the magnetocaloric effect. For instance, the effect of applied pressure on the magnetocaloric properties should be further investigated. Compounds with first order phase transition, Ce based compounds, Heusler alloys and manganites, where pressure can yield substantial changes in the electronic structure, can be good candidates for such an investigation. The barocaloric effect should receive more attention from the researchers. Compounds undergoing a first order phase transition are interesting systems in which to study the barocaloric effect, since it is expected that large values for the barocaloric potentials occur in these compounds. The combined effect of pressure and magnetic field variation should also be investigated, because it could provide large values for the magnetocaloric potentials with small magnetic field variation. Metallic compounds undergoing first order phase transition and ferrofluids are good candidates in which to study this aspect. The anisotropic magnetocaloric effect is worth further investigation, because it can also provide sizeable values for the magnetocaloric potentials, by rotating the sample in a small constant magnetic field. Rare earth intermetallic compounds, in which the crystalline electric field plays an important role, are interesting systems to investigate the anisotropic magnetocaloric effect. All of these three process of heating and cooling mentioned before are interesting because they can eliminate the necessity for large values of the magnetic field and contribute to enhancing the performance of magnetic refrigerators. We want to stress that further theoretical and experimental studies of the magnetocaloric effect are important, not only for technological applications, but also to understand the physical mechanisms behind the magnetic and thermodynamic properties of the materials.

Acknowledgments

We acknowledge financial support from the Brazilian agencies CNPq and FAPERJ. This work would not have been possible without the assistance of many of our colleagues. We want to acknowledge A. Troper, M.A. Continentino, A.P. Guimarães, S. Gama, F.C.G. Gandra, C.M. Chaves, I.S. Oliveira, M.V. Tovar Costa, I.G. de Oliveira, R.S. Sarthour, M.S. Reis, A. Caldas, E.P. Nóbrega and A.M.G. Carvalho, for useful discussions and critical reading of the manuscript. We also want to thank the graduate students who collaborate in the development of the models discussed in this report. N.A. de Oliveira wishes to express his special thanks to A.A. Gomes for many fruitful discussions about magnetism over the last twenty years. P.J. von Ranke thanks K.A. Gschneidner Jr and V.K. Pecharsky for discussions on the magnetocaloric effect.

References

[1] E. Warburg, Ann. Phys. 13 (1881) 141.
[2] A.M. Tishin, Magnetic therapy of malignant neoplasms by injecting material particles with high magnetocaloritic effect and suitable magnetic phase transition temperature, Patent number: EP1897590-A1, 2008.
[3] P. Debye, Ann. Phys. 81 (1926) 1154.
[4] W.F. Giauque, J. Am. Chem. Soc. 49 (1927) 1864.
[5] W.F. Giauque, D.P. MacDougall, Phys. Rev. 43 (1933) 768.
[6] G.V. Brown, J. Appl. Phys. 47 (1976) 3673.

[7] K.A. Gschneidner Jr., V.K. Pecharsky, Annu. Rev. Mater. Sci. 30 (2000) 387.
[8] V.K. Pecharsky, K.A. Gschneidner Jr., Intermetallic compounds for magnetic refrigeration, in: J.H. Westbrook, R.L. Fleischer (Eds.), in: Intermetallic Compounds — Principles and Practice, vol. 3, John wiley & Sons, New York, 2002 (Chapter 25).
[9] A.M. Tishin, Magnetocaloric effect in the vicinity of the phase transition, in: K.H.J. Buschow (Ed.), in: Handbook of Magnetic Materials, vol. 12, North Holland, Amsterdam, 1999, pp. 395–524. (Chapter 4).
[10] A.M. Tishin, Y.I. Spichkin, The Magnetocaloric Effect and its Applications, 1st edition, Institute of Physics, Bristol, Philadelphia, 2003.
[11] K.A. Gschneidner Jr., V.K. Pecharsky, A.O. Tsokol, Rep. Progr. Phys. 68 (2005) 1479.
[12] V.K. Pecharsky, K.A. Gschneidner Jr., Int. J. Refrig. 29 (2006) 1239.
[13] K.A. Gschneidner Jr., V.K. Pecharsky, Int. J. Refrig. 31 (2008) 945.
[14] E. Bruck, J. Physica D: Appl. Phys. 38 (2005) R381.
[15] A.M. Tishin, J. Magn. Magn. Mater. 316 (2007) 351.
[16] V.K. Pecharsky, K.A. Gschneidner Jr., Phys. Rev. Lett. 78 (1997) 4494.
[17] V.K. Pecharsky, K.A. Gschneidner Jr., J. Magn. Magn. Mater. 167 (1997) L179.
[18] V.K. Pecharsky, K.A. Gschneidner Jr., J. Alloys Compounds 260 (1997) 98.
[19] V.K. Pecharsky, K.A. Gschneidner Jr., Appl. Phys. Lett. 70 (1997) 3299.
[20] V.K. Pecharsky, K.A. Gschneidner Jr., Cryog. Eng. 43 (1998) 1729.
[21] V.K. Pecharsky, K.A. Gschneidner Jr., Adv. Mat. 13 (2001) 683.
[22] V. Provenzano, A.J. Shapiro, R.D. Shull, Nature 429 (2004) 853; Nature 429 (2004) 853–857.
[23] R.D. Shull, V. Provenzano, A.J. Shapiro, A. Fu, M.W. Lufaso, J. Karapetrova, G. Kletetschka, V. Mikula, J. Appl. Phys. 99 (2006) 08k908.
[24] J.Q. Li, W.A. Sun, Y.X. Jian, Y.H. Zhuang, W.D. Huang, J.K. Liang, J. Appl. Phys. 100 (2006) 073904.
[25] Y.H. Zhuang, J.Q. Li, W.D. Huang, W.A. Sun, W.Q. Ao, J. Alloys Compounds 421 (2006) 49.
[26] D.M. Raj Kumar, M. Manivel Raja, R. Gopalan, A. Sambasiva Rao, V. Chandrasekaran, J. Magn. Magn. Mater. 321 (2009) 1300.
[27] E. Yüzüak, B. Emre, A. Yücel, Y. Elerman, J. Alloys Compounds 476 (2009) 929.
[28] W. Choe, V.K. Pecharsky, A.O. Pecharsky, K.A. Gschneidner Jr., V.G. Young Jr., G.J. Miller, Phys. Rev. Lett. 84 (2000) 4617.
[29] V.K. Pecharsky, A.P. Holm, K.A. Gschneidner Jr., R. Rink, Phys. Rev. Lett. 91 (2003) 197204.
[30] L. Morellon, P.A. Algarabel, M.R. Ibarra, J. Blasco, B. Garcia-Landa, Z. Arnold, F. Albertini, Phys. Rev. B 58 (1998) R14721.
[31] C. Magen, Z. Arnold, L. Morellon, Y. Skorokhod, P.A. Algarabel, M.R. Ibarra, J. Kamarad, Phys. Rev. Lett. 91 (2003) 207202.
[32] C. Magen, L. Morellon, P.A. Agarabel, M.R. Ibarra, Z. Arnold, J. Kamarad, T.A. Lograsso, D.L. Schlagel, V.K. Pecharsky, A.O. Tsokol, K.A. Gschneidner Jr., Phys. Rev. B 72 (2005) 024416.
[33] L. Morellon, Z. Arnold, P.A. Algarabel, C. Magen, M.R. Ibarra, Y. Skorokhod, J. Phys. C. 16 (2004) 1623.
[34] Y.I. Spichkin, V.K. Pecharsky, K.A. Gschneidner Jr., J. Appl. Phys. 89 (2001) 1738.
[35] L. Morellon, C. Ritter, C. Magen, P.A. Agarabel, M.R. Ibarra, Phys. Rev. B 68 (2003) 024417.
[36] L. Morellon, Z. Arnold, C. Magen, C. Ritter, O. Prokhnenko, Y. Skorokhod, P.A. Agarabel, M.R. Ibarra, J. Kamarad, Phys. Rev. Lett. 93 (2004) 137201.
[37] L. Morellon, C. Magen, P.A. Algarabel, M.R. Ibarra, C. Ritter, Appl. Phys. Lett. 79 (2001) 1318.
[38] A.O. Pecharsky, K.A. Gschneidner Jr., V.K. Pecharsky, J. Appl. Phys. 93 (2003) 4722.
[39] F. Casanova, A. Labarta, X. Batlle, E. Vives, J. Marcos, L. Mañosa, A. Planes, Eur. Phys. J. B. 40 (2004) 427.
[40] F. Casanova, X. Batlle, A. Labarta, J. Marcos, L. Mañosa, A. Planes, Phys. Rev. B 66 (2002) 212402.
[41] F. Casanova, X. Batlle, A. Labarta, J. Marcos, L. Mañosa, A. Planes, J. Appl. Phys. 93 (2003) 8313.
[42] A.M. Tishin, Cryogenics 30 (1990) 127.
[43] H. Wada, Y. Tanabe, Appl. Phys. Lett. 79 (2001) 3302.
[44] H. Wada, K. Taniguchi, Y. Tanabe, Mater. Trans. 43 (2002) 73.
[45] H. Wada, T. Morikawa, K. Taniguchi, T. Shibata, Y. Yamada, Y. Akishige, Physica B 328 (2003) 114.
[46] S. Gama, A.A. Coelho, A. de Campos, A.M.G. Carvalho, F.C.G. Gandra, P.J. von Ranke, N.A. de Oliveira, Phys. Rev. Lett. 93 (2004) 237202.
[47] A. de Campos, D.L. Rocco, A.M.G. Carvalho, L. Caron, A.A. Coelho, S. Gama, L.M. da Silva, F.C.G. Gandra, A.O. dos Santos, L.P. Cardoso, P.J. von Ranke, N.A. de Oliveira, Nature Mat. 5 (2006) 802.
[48] M. Balli, D. Fruchart, D. Gignoux, C. Dupuis, A. Kedous-Lebouc, R. Zach, J. Appl. Phys. 103 (2008) 103908.
[49] O. Tegus, E. Brück, K.H.J. Buschow, F.R. de Boer, Nature 415 (2002) 150.
[50] E. Brück, O. Tegus, X.W. Li, F.R. de Boer, K.H.J. Buschow, Physica B 327 (2003) 431.
[51] O. Tegus, E. Brück, X.W. Li, L. Zhang, W. Dagula, F.R. de Boer, K.H.J. Buschow, J. Magn. Magn. Mater. 272–276 (2004) 2389.
[52] F. Hu, B. Shen, J. Sun, Z. Cheng, G. Rao, X. Zhang, Appl. Phys. Lett. 78 (2001) 3675.
[53] A. Fujita, S. Fujieda, Y. Hasegawa, K. Fukamichi, Phys. Rev. B 67 (2003) 104416.
[54] A. Yan, K.H. Muller, O. Gutfleisch, J. Appl. Phys. 97 (2005) 036102.
[55] O. Gutfleisch, A. Yan, K.H. Muller, J. Appl. Phys. 97 (2005) 10M305.
[56] Y. Sun, Z. Arnold, J. Kamarad, Guang-Jun Wang, Bao-Gen Shen, Zao-Hua Cheng, Appl. Phys. Lett. 89 (2006) 172513.
[57] E.C. Passamani, C. Larica, J.R. Proveti, A.Y. Takeuchi, A.M. Gomes, L. Ghivelder, J. Magn. Magn. Mater. 312 (2007) 65.
[58] A.M. Gomes, J.R. Proveti, A.Y. Takeuchi, E.C. Passamani, C. Larica, A.P. Guimarães, J. Appl. Phys. 99 (2006) 116107.
[59] J. Lyubina, K. Nenkov, L. Schultz, O. Gutfleisch, Phys. Rev. Lett. 101 (2008) 177203.
[60] M. Balli, M. Rosca, D. Fruchart, D. Gignoux, Appl. Phys. Lett. 92 (2008) 232505.
[61] M. Balli, M. Rosca, D. Fruchart, D. Gignoux, J. Magn. Magn. Mater. 321 (2009) 123.
[62] T. Krenke, E. Duman, M. Acet, E.F. Wassermann, X. Moya, L. Manosa, A. Planes, Nature Mater. 4 (2005) 450.
[63] T. Krenke, E. Duman, M. Acet, E.F. Wassermann, X. Moya, L. Mañosa, A. Planes, E. Suard, B. Ouladdiaf, Phys. Rev. B 75 (2007) 104414.
[64] X. Moya, L. Mañosa, A. Planes, S. Aksoy, M. Acet, E.F. Wassermann, T. Krenke, Phys. Rev. B 75 (2007) 184412.
[65] A.K. Nayak, K.G. Suresh, A.K. Nigam, J. Phys D: Appl. Phys. 42 (2009) 035009.
[66] S. Stadler, M. Khan, J. Mitchell, N. Ali, A.M. Gomes, I. Dubenko, A.Y. Takeuchi, A.P. Guimarães, Appl. Phys. Lett. 88 (2006) 192511.
[67] T. Tang, K.M. Gu, Q.Q. Cao, D.H. Wang, S.Y. Zhang, Y.W. Du, J. Magn. Magn. Mater. 222 (2000) 110.
[68] W. Chen, W. Zhong, D.L. Hou, R.W. Gao, W.C. Feng, M.G. Zhu, Y.W. Du, J. Phys.: Condens. Matter 14 (2002) 11889.
[69] M.S. Reis, A.M. Gomes, J.P. Araújo, P.B. Tavares, I.S. Oliveira, V.S. Amaral, J. Magn. Magn. Mater. 272–276 (2004) 2393.
[70] A.M. Gomes, M.S. Reis, A.P. Guimarães, P.B. Tavares, J.P. Araújo, V.S. Amaral, J. Magn. Magn. Mater. 272–276 (2004) 2385.
[71] Manh-Huong Phan, Seong-Cho Yu, J. Magn. Magn. Mater. 308 (2007) 325.
[72] M. Foldeaki, R. Chahine, B.R. Gopal, T.K. Bose, X.Y. Liu, J.A. Barclay, J. Appl. Phys. 83 (1998) 2727.
[73] T.D. Shen, R.B. Schwarz, J.Y. Coulter, J.D. Thompson, J. Appl. Phys. 91 (2002) 5240.
[74] L. Si, J. Ding, Y. Li, B. Yao, H. Tan, Appl. Phys. A 75 (2002) 535.
[75] J. Sánchez Marcos, J. Rodríguez Fernández, B. Chevalier, J.L. Bobet, J. Etourneau, J. Mag. Magn. Mat. 272–276 (2004) 579.
[76] F. Johnson, R.D. Shull, J. Appl. Phys. 99 (2006) 08K909.
[77] N. Chau, N.D. The, N.Q. Hoa, C.X. Huu, N.D. Tho, S.C. Yu, Mat. Sci. Eng. A 449–451 (2007) 360.
[78] S.G. Min, K.S. Kim, S.C. Yu, Y.C. Kim, K.Y. Kim, K.W. Lee, J.R. Rhee, S.Y. Cha, Y.S. Kim, J. Magn. Magn. Mat. 310 (2007) 2820.
[79] V. Franco, C.F. Conde, J.S. Blázquez, A. Conde, P. Švec, D. Janičkovič, L.F. Kiss, J. Appl. Phys. 101 (2007) 093903.
[80] V. Franco, J.S. Blázquez, M. Millán, J.M. Borrego, C.F. Conde, A. Conde, J. Appl. Phys. 101 (2007) 09C503.
[81] S. Gorsse, G. Orveillon, B. Chevalier, J. Appl. Phys. 103 (2008) 044902.
[82] T.B. Zhang, V. Provenzano, Y.G. Chen, R.D. Shull, Solid State Commun. 147 (2008) 107.
[83] A.K. Burian, M. Kowalczyk, R. Kolano, R. Szymczak, H. Szymczak, M. Polak, J. Alloys Compounds 479 (2009) 71.

[84] R.D. McMichael, J.J. Ritter, R.D. Shull, J. Appl. Phys. 73 (1993) 6946.
[85] D.Y. Chen, S. Patel, D.T. Shaw, J. Magn. Magn. Mater. 146 (1995) 175.
[86] Y. Shao, J. Zhang, J.K.L. Lai, C.H. Shek, J. Appl. Phys. 80 (1996) 76.
[87] Y.Z. Shao, J.K.L. Lai, C.H. Shek, J. Magn. Magn. Mat. 163 (1996) 103.
[88] F. Torres, J.M. Hernández, X. Bohigas, J. Tejada, Appl. Phys. Lett. 77 (2000) 3248.
[89] Y.I. Spichkin, A.K. Zvezdin, S.P. Gubin, A.S. Mischenko, A.M. Tishin, J. Physica D: Appl. Phys. 34 (2001) 1162.
[90] P.J. von Ranke, V.K. Pecharsky, K.A. Gschneidner Jr., B.J. Korte, Phys. Rev. B 58 (1998) 14436.
[91] A. Kirste, M. von Ortenberg, A.A. Demidov, Z.A. Kazei, N.P. Kolmakova, V.V. Platonov, A.A. Sidorenko, O.M. Tatsenko, Physica B 336 (2003) 335.
[92] Z.A. Kazei, V.V. Snegirev, J.-M. Broto, H. Rakoto, JETP Lett. 87 (2008) 687.
[93] T. Samanta, I. Das, S. Banerjee, Appl. Phys. Lett. 91 (2007) 152506.
[94] K.G. Sandeman, R. Daou, S. Özcan, J.H. Durrell, N.D. Mathur, D.J. Fray, Phys. Rev. B 74 (2006) 224436.
[95] Y.Q. Zhang, Z.D. Zhang, J. Alloys Compounds 365 (2004) 35.
[96] M.K. Chattopadhyay, M.A. Manekar, S.B. Roy, J. Physica D: Appl. Phys. 39 (2006) 1006.
[97] B.J. Korte, V.K. Pecharsky, K.A. Gschneidner Jr., J. Appl. Phys. 84 (1998) 5677.
[98] A. Biswas, T. Samanta, S. Banerjee, I. Das, J. Appl. Phys. 103 (2008) 013912.
[99] V.K. Pecharsky, K.A. Gschneidner Jr., S. Yu. Dan'kov, A.M. Tishin, Cryocoolers 10 (1999) 639.
[100] P.J. von Ranke, V.K. Pecharsky, K.A. Gschneidner Jr., Phys. Rev. B 58 (1998) 12110.
[101] P.J. von Ranke, N.A. de Oliveira, S. Gama, J. Magn. Magn. Mater. 277 (2004) 78.
[102] H. Yamada, T. Goto, Phys. Rev. B 68 (2003) 184417.
[103] H. Yamada, T. Goto, Physica B 346–347 (2004) 104.
[104] D. Paudyal, V.K. Pecharsky, K.A. Gschneidner Jr., B.N. Harmon, Phys. Rev. B 73 (2006) 144406.
[105] P.J. von Ranke, E.P. Nóbrega, I.G. de Oliveira, A.M. Gomes, R.S. Sarthour, Phys. Rev. B 63 (2001) 184406.
[106] P.J. von Ranke, N.A. de Oliveira, M.V. Tovar Costa, E.P. Nóbrega, A. Caldas, I.G. de Oliveira, J. Magn. Magn. Mater. 226–230 (2001) 970.
[107] P.J. von Ranke, I.G. de Oliveira, A.P. Guimarães, X.A. da Silva, Phys. Rev. B 61 (2000) 447.
[108] P.J. von Ranke, A.L. Lima, E.P. Nóbrega, X.A. da Silva, A.P. Guimarães, I.S. Oliveira, Phys. Rev. B 63 (2001) 024422.
[109] A.L. Lima, I.S. Oliveira, A.M. Gomes, P.J. von Ranke, Phys. Rev. B 65 (2002) 172411.
[110] P.J. von Ranke, Daniel F. Grangeia, A. Caldas, N.A. de Oliveira, J. Appl. Phys. 93 (2003) 4055.
[111] P.J. von Ranke, M.A. Mota, D.F. Grangeia, A. Magnus, G. Carvalho, F.C.G. Gandra, A.A. Coelho, A. Caldas, N.A. de Oliveira, S. Gama, Phys. Rev. B 70 (2004) 134428.
[112] I.G. de Oliveira, A. Caldas, E.P. Nobrega, N.A. de Oliveira, P.J. von Ranke, Solid State Commun. 114 (2000) 487491.
[113] P.J. von Ranke, N.A. de Oliveira, S. Gama, Phys. Lett. A 320 (2004) 302.
[114] P.J. von Ranke, A. de Campos, L. Caron, A.A. Coelho, S. Gama, N.A. de Oliveira, Phys. Rev. B 70 (2004) 094410.
[115] P.J. von Ranke, N.A. de Oliveira, C. Mello, A. Magnus, G. Carvalho, S. Gama, Phys. Rev. B 71 (2005) 054410.
[116] O. Tegus, G.X. Linb, W. Dagula, B. Fuquana, L. Zhanga, E. Brück, F.R. de Boer, K.H.J. Buschow, Physica B 290–291 (2005) 658.
[117] I.G. de Oliveira, Pedro J. von Ranke, M. El Massalami, C.M. Chaves, Phys. Rev. B 72 (2005) 174420.
[118] P.J. von Ranke, Sergio Gama, A.A. Coelho, A de Campos, A. Magnus, G. Carvalho, F.C.G. Gandra, N.A. de Oliveira, Phys. Rev. B 73 (2006) 014415.
[119] M.B. Gomes, N.A. de Oliveira, Solid State Commun. 137 (2006) 431.
[120] M.B. Gomes, N.A. de Oliveira, J. Magn. Magn. Mater. 301 (2006) 503.
[121] P.J. von Ranke, N.A. de Oliveira, C. Mello, D.C. Garcia, V.A. de Sousa, A. Magnus, G. Carvalho, Phys. Rev. B 74 (2006) 054425.
[122] P.J. von Ranke, N.A. de Oliveira, V.S.R. de Sousa, D.C. Garcia, Isaias G. de Oliveira, A. Magnus, G. Carvalho, S. Gama, J. Magn. Magn. Mater. 313 (2007) 176.
[123] N.A. de Oliveira, Eur. Phys. J. B 40 (2004) 259.
[124] N.A. de Oliveira, J. Alloys Compounds 403 (2005) 4548.
[125] N.A. de Oliveira, P.J. von Ranke, J. Phys. Condens. Matter 17 (2005) 3325.
[126] L.G. de Medeiros Jr., N.A. de Oliveira, J. Magn. Magn. Mater. 306 (2006) 265.
[127] L.G. de Medeiros Jr., N.A. de Oliveira, J. Alloys Compounds 424 (2006) 41.
[128] L.G. de Medeiros Jr., N.A. de Oliveira, A. Troper, J. Appl. Phys. 103 (2008) 113909.
[129] M.L. Boas, Mathematical Methods in the Physical Sciences, second edition, John Wiley & Sons, New York, 1966, p. 152.
[130] N.A. de Oliveira, P.J. von Ranke, Phys. Rev. B 77 (2008) 214439.
[131] See chapter 2 of Ref. [10].
[132] A. Giguere, M. Foldeaki, B. Ravi Gopal, R. Chahine, T.K. Bose, A. Frydman, J.A. Barclay, Phys. Rev. Lett. 83 (1999) 2262.
[133] K.A. Gschneidner Jr., V.K. Pecharsky, E. Bruck, H.G.M. Duijn, E.M. Levin, Phys. Rev. Lett. 85 (2000) 4190.
[134] J.R. Sun, F.X. Hu, B.G. Shen, Phys. Rev. Lett. 85 (2000) 4191.
[135] G.J. Liu, J.R. Sun, J. Shen, B. Gao, H.W. Zhang, F.X. Hu, B.G. Shen, Appl. Phys. Lett. 90 (2007) 032507.
[136] F. Reif, Fundamental of Statistical and Thermal Physics, McGraw-Hill, London, 1965, p. 296.
[137] D. Gignoux, J.C. Peuzin, Magnetostatique, in: Magnétistme - fondements, vol. I, 2000, pp. 69–71. Collection Grenoble Sciences EDP sciences.
[138] V. Basso, C.P. Sasso, M. LoBue, J. Magn. Magn. Mater. 316 (2007) 262.
[139] V. Basso, M. Kuepferling, C. Paolo Sasso, M. LoBue, IEEE Trans. Magn. 44 (2008) 3177.
[140] J.S. Amaral, V.S. Amaral, Appl. Phys. Lett. 94 (2009) 042506.
[141] A.M.G. Carvalho, A.A. Coelho, S. Gama, F.C.G. Gandra, P.J. von Ranke, N.A. de Oliveira, Eur. Phys. J. B 68 (2009) 67.
[142] V.S. Amaral, J.S. Amaral, J. Magn. Magn. Mater. 272–276 (2004) 2104.
[143] J.S. Amaral, N.J.O. Silva, V.S. Amaral, Appl. Phys. Lett. 91 (2007) 172503.
[144] P.J. von Ranke, N.A. de Oliveira, D.C. Garcia, V.S.R. de Sousa, V.A. de Souza, A. Magnus, G. Carvalho, S. Gama, M.S. Reis, Phys. Rev. B 75 (2007) 184420.
[145] P.J. von Ranke, N.A. de Oliveira, V.S.R. de Sousa, A. Magnus, G. Carvalho, S. Gama, M.S. Reis, J. Magn. Magn. Mater. 320 (2008) e143.
[146] K.A. Müller, F. Fauth, S. Fischer, M. Koch, A. Furrer, P. Lacorre, Appl. Phys. Lett. 73 (1998) 1056.
[147] Th. Strässle, A. Furrer, P. Lacorre, K.A. Müller, J. Alloys Compounds 303 (2000) 228.
[148] Th. Strässle, A. Furrer, K.A. Müller, Physica B 276 (2000) 944.
[149] Th. Strässle, A. Furrer, F. Altorfer, K. Mattenberger, M. Böhm, H. Mutka, J. Alloys Compounds 323 (2001) 392.
[150] Th. Strässle, A. Furrer, A. Dönni, T. Komatsubara, J. Appl. Phys. 91 (2002) 8543.
[151] Th. Strässle, A. Furrer, Z. Hossain, Ch. Geibel, Phys. Rev. B 67 (2003) 054407.
[152] N.A. de Oliveira, Appl. Phys. Lett. 90 (2007) 052501.
[153] J.D. Childress, J. Appl. Phys. 33 (1962) 1793.
[154] E. Fatuzzo, H. Kiess, R. Nitsche, J. Appl. Phys. 37 (1966) 510.
[155] P.D. Thacher, J. Appl. Phys. 39 (1968) 1996.
[156] A.S. Mischenko, Q. Zhang, J.F. Scott, R.W. Whatmore, N.D. Mathur, Science 311 (2006) 1270.
[157] A. Mishchenko, R.W. Whatmore, Patent Number: WO2007099279-A1; GB2438895-A.
[158] G. Akcay, S.P. Alpaya, J.V. Mantese, G.A. Rossetti, Appl. Phys. Lett. 90 (2007) 252909.
[159] H. Ohno, D. Chiba, F. Matsukura, T. Omiya, E. Abe, T. Dietl, Y. Ohno, K. Ohtani, Nature 408 (2000) 944.
[160] D. Chiba, M. Yamanouchi, F. Matsukura, H. Ohno, Science 301 (2000) 943.
[161] N. Hur, S. Park, P.A. Sharma, J.S. Ahn, S. Guha, S.-W. Cheong, Nature 429 (2004) 392.
[162] M. Weisheit, S. Fähler, A. Marty, Y. Souche, C.P oinsignon, D. Givord, Science 315 (2007) 349.

[163] I. Pomeranchuk, Zh. Eksp. Teor. Fiz. 20 (1950) 919.
[164] R.C. Richardson, Rev. Modern Phys. 69 (1997) 683.
[165] M.A. Continentino, A.S. Ferreira, Phys. Rev. B 69 (2004) 233104.
[166] M.A. Continentino, A.S. Ferreira, Cryogenics 45 (2005) 331.
[167] M.A. Continentino, A.S. Ferreira, P.G. Pagliuso, C. Rettori, J.L. Sarrao, Physica B 359–361 (2005) 744.
[168] See chapter 11 of Ref. [10].
[169] W.A. Steyert, J Appl. Phys. 49 (1978) 1216.
[170] L.D. Kirol, M.W. Dacus, Adv. Cryog. Eng. 33 (1987) 757.
[171] C.B. Zimm, A. Jastrab, A. Sternberg, V.K. Pecharsky, K.A. Gschneidner Jr., M. Osborne, I. Anderson, Adv. Cryog. Eng. 43 (1998) 1759.
[172] V.K. Pecharsky, K.A. Gschneidner Jr., J. Magn. Magn. Mater. 200 (1999) 44.
[173] B.F. Yu, Q. Gao, B. Zhang, X.Z. Meng, Z. Chen, Int. J. Refrig. 26 (2003) 622636.
[174] J. Chen, Z. Yan, J. Appl. Phys. 69 (1991) 6245.
[175] Z. Yan, J. Chen, J. Appl. Phys. 72 (1992) 1.
[176] W. Dai, J. Appl. Phys. 71 (1992) 5272.
[177] M.A. Ruderman, C. Kittel, Phys. Rev. 96 (1954) 99.
[178] K. Yosida, Phys. Rev. 106 (1957) 893.
[179] N.W. Aschroft, N.D. Mermin, Solid State Physics, Saunders College 187 Publishing, 1976, p. 47.
[180] M.T. Hutchings, Solid State Phys. 16 (1964) 227.
[181] W.H. Stevens, Proc. Phys. Soc. London, Sect. A 65 (1952) 209.
[182] H.G. Purwins, A. Lesson, Adv. Phys. 39 (1990) 309.
[183] K. Andres, S. Darack, H.R. Ott, Phys. Rev. B 19 (1979) 5475.
[184] K.R. Lea, M.J.M. Leask, W.P. Wolf, J. Phys. Chem. Sol. 23 (1962) 1381.
[185] C. Kittel, Phys. Rev. 120 (1960) 335.
[186] E.P. Nóbrega, N.A. de Oliveira, P.J. von Ranke, A. Troper, Phys. Rev. B 72 (2005) 134426.
[187] E.P. Nóbrega, N.A. de Oliveira, P.J. von Ranke, A. Troper, J. Phys. Condens. Matter 18 (2006) 1275.
[188] E.P. Nóbrega, N.A. de Oliveira, P.J. von Ranke, A. Troper, J. Appl. Phys. 99 (2006) 08Q103.
[189] E.P. Nóbrega, N.A. de Oliveira, P.J. von Ranke, A. Troper, Physica B 378–380 (2006) 716.
[190] E.P. Nóbrega, N.A. de Oliveira, P.J. von Ranke, A. Troper, Phys. Rev. B 74 (2006) 144429.
[191] E.P. Nóbrega, N.A. de Oliveira, P.J. von Ranke, A. Troper, J. Magn. Magn. Mater. 310 (2007) 2805.
[192] E.P. Nóbrega, N.A. de Oliveira, P.J. von Ranke, A. Troper, J. Magn. Magn. Mater. 320 (2008) e147.
[193] V.D. Buchelnikov, P. Entel, S.V. Taskaev, V.V. Sokolovskiy, A. Hucht, M. Ogura, H. Akai, M.E. Gruner, S.K. Nayak, Phys. Rev. B. 78 (2008) 184427.
[194] See for instance Ref. [136] page 202.
[195] N.W. Aschroft, N.D. Mermin, Solid State Physics, Saunders College 187 Publishing, 1976, p. 461.
[196] A.M. Tishin, K.A. Gschneidner Jr., V.K. Pecharsky, Phys Rev. B 59 (1999) 503.
[197] V.K. Pecharsky, K.A. Gschneidner Jr., Cryocoolers 10 (1999) 629. ed. by R. G. Ross, Jr. Kluwer (Academic/Plenum Publishers 1999).
[198] V.K. Pecharsky, K.A. Gschneidner Jr., J. Appl. Phys. 86 (1999) 565.
[199] K.A. Gschneidner Jr., V.K. Pecharsky, A.O. Pecharsky, C.B. Zimm, Mat. Sci. Forum 315–317 (1999) 69.
[200] N. Kaplan, E. Dormann, K.H.J. Buschow, D. Lebenbaum, Phys. Rev. B 7 (1973) 40.
[201] G.J. Cock, L.W. Roeland, H.G. Purwins, E. Walker, A. Furrer, Solid State Commun. 15 (1974) 845.
[202] B. Barbara, M.F. Rossignol, H.G. Purwins, E. Walker, in: A. Furrer (Ed.), Crystal Field Effects in Metals and Alloys, Plenum, New York, 1977, p. 148.
[203] H.G. Purwins, Z. Phys. 233 (1970) 27.
[204] C. Deenadas, A.W. Thompson, R.S. Graig, W.E. Wallace, J. Phys. Chem. Solids 32 (1971) 1843.
[205] T. Inoue, S.G. Sankar, R.S. Graig, W.E. Wallace, K.A. Gschneidner Jr., J. Phys. Chem. Solids 38 (1997) 487.
[206] A.L. Lima, A.O. Tsokol, K.A. Gschneidner Jr., V.K. Pecharsky, T.A. Lograsso, D.L. Schlagel, Phys. Rev. B 72 (2005) 024403.
[207] M.E. Wood, W.H. Potter, Cryogenics 25 (1985) 66.
[208] K.H.J. Buschow, in: E.P. Wohlfarth (Ed.), Ferromagnetic Materials, Vol. 1, North Holland, Amsterdam, 1980, p. 297.
[209] E. Burzo, J. Laforest, Acad. Sci. (France) 27 (AB) (1972) 114.
[210] A. Andreeff, Th. Frauenheim, E.A. Goremychkin, H. Griessmann, B. Lippold, W. Matz, O.D. Chistyakov, E.M. Savitskii, Phys. Status Solidi (b) 111 (1982) 507.
[211] E.A. Goremychkin, I. Natkaniec, E. Mühle, O.D. Chistyakov, J. Magn. Magn. Mater. 81 (1989) 63.
[212] E. Gratz, E. Goremychkin, M. Latroche, G. Hilscher, M. Rotter, H. Muller, A. Lindbaum, H. Michor, V. Paul-Boncour, T Fernandez-Diaz, J. Phys.: Condens. Matter 11 (1999) 7893.
[213] Tiezhong Ma, K.A. Gschneidner Jr., V.K. Pecharsky (unpublished).
[214] T. Hashimoto, T. Kuzuhara, M. Sahashi, K. Inomata, A. Tomokiyo, H. Yayama, J. Appl. Phys. 62 (1987) 3873.
[215] T. Hashimoto, T. Kuzuhara, K. Matsumoto, M. Sahashi, K. Inomata, A. Tomokiyo, H. Yayama, IEEE Trans. Magb. 23 (1987) 2847.
[216] A. Smaili, R. Chahine, Adv. Cryog. Eng. 42 (1996) 445.
[217] A. Smaili, R. Chahine, J. Appl. Phys. 81 (1997) 824.
[218] K.H.J. Buschow, A.S. van der Goot, Acta Crystallogr. Sect. B: Struct. Crystallogr. Cryst. Chem. 27 (1971) 1985.
[219] N. Marzouk, R.S. Graig, W.E. Wallace, J. Phys. Chem. Solids 34 (1973) 15.
[220] V.M.T.S. Barthem, D. Gignoux, A. nait-Saada, D. Schmitt, A.Y. Takeuchi, J. Magn. Magn. Mater. 80 (1989) 142.
[221] F.Y. Zhang, D. Gignoux, D. Schmitt, J.J.M. Franse, F.E. Kayzel, N.H. Kim-Ngan, R.J. Radwanski, J. Magn. Magn. Mater. 130 (1994) 108.
[222] L. Morellon, P.A. Algarabel, M.R. Ibarra, A. del Moral, D. Gignoux, D. Schmitt, J. Magn. Magn. Mater. 153 (1996) 17.
[223] D. Gignoux, D. Givord, A. del Moral, Solid State Commun. 19 (1976) 891.
[224] A. Andreeff, V. Valter, H. Grissmann, L.P. Kaun, B. Lipold, V. Mats, T. Franzkhaim, Joint Institute for Nuclear Research, Dubna, U.S.S.R., Commun. P14-11324 (1978).
[225] R.J. Radwansky, N.H. Kim-Ngan, F.E. Kayzel, J.J.M. France, D. Gignoux, D. Schmitt, F.Y. Zhang, J. Phys.: Condens. Matter 4 (1992) 8853.
[226] A.F. Devonshire, Phil. Mag. 40 (1949) 1040.
[227] B. Teng, M. Tu, Y. Chen, J. Tang, J. Phys. Condens. Matter 14 (2002) 6501.
[228] C.P. Bean, D.S. Rodbell, Phys. Rev. 126 (1962) 104.
[229] E.Z. Valiev, J. Exp. Theoret. Phys. 108 (2009) 279.
[230] J. Hubbard, Proc. R. Soc. London A 276 (1963) 238.
[231] N.H. Duc, D. Givord, C. Lacroix, C. Pinettes, Eur. Phys. Lett. 20 (1992) 47.
[232] F. Gautier, Itinerant magnetism, in: Cyrrot (Ed.) Magnetism of Metals and Alloys, pp. 1–244 (Chapter 1).
[233] T. Moriya, J. Magn. Magn. Mater. 14 (1979) 1.
[234] T. Moriya, J. Magn. Magn. Mater. 100 (1991) 261.
[235] T. Moriya, Spin fluctuations and a unified picture of magnetism, in: Electron Correlation and Magnetism in Narrow Band System, in: T. Moriya (Ed.), Springer Series in Solid State Sciences, vol. 29, Springer, 1981.
[236] T. Moriya, Spin Fluctuations in Itinerant Electron Magnetism, in: Springer Series in Solid State Sciences, vol. 56, Springer, 1985.
[237] N.A. de Oliveira, A.A. Gomes, J. Magn. Magn. Mater. 114 (1992) 269.
[238] C.A.M. da Silva, A.A. Gomes, Introduction to the physics of metallic systems, MO00194-CBPF1994, available online at www.biblioteca.cbpf.br./index_2.html.

[239] Philip L. Taylor, A Quantum Approach to the Solid State, Prentice Hall, New Jersey (Chapter 5).
[240] E.N. Economou, Green's Functions in Quantum Physics, in: Springer Series in Solid State Science, vol. 7, Springer-Verlag, Berlin, 1979.
[241] See for instance Ref. [136] page 225.
[242] H. Ido, S. Yasuda, G. Kido, J. Appl. Phys. 69 (1991) 4621.
[243] H. Ido, S. Yasuda, M. Kido, G. Kido, T. Miyakawa, J. Phys. (Paris) Colloq. 49 (1988) C8-167.
[244] H. Ido, T. Susuzi, I. Iguchi, J. Magn. Magn. Mater. 31–34 (1983) 159.
[245] Kazuko Motizuki, Keiko Katoh, J. Phys. Soc. Japan 53 (1984) 735.
[246] K. Maki, T. Kaneko, H. Hiroyoshi, K. Kamigaki, J. Magn. Magn. Mater. 177–181 (1998) 1361.
[247] O. Nashima, T. Suzuki, H. Ido, K. Kamishima, T. Goto, J. Appl. Phys. 79 (1996) 4647.
[248] T. Goto, M.I. Bartashevich, K. Kondo, K. Terao, H. Yamada, H. Ido, J. Alloys Compounds 325 (2001) 18.
[249] V.A. Chernenko, L. Wee, P.G. McCormick, R. Street, J. Appl. Phys. 85 (1999) 7833.
[250] S.A. Niktin, A.M. Tishin, Cryogenics 31 (1991) 166.
[251] H. Wada, S. Tomekawa, M. Shiga, Cryogenics 39 (1999) 915.
[252] H. Wada, S. Tomekawa, M. Shiga, J. Magn. Magn. Mater. 196–197 (1999) 689.
[253] H. Wada, Y. Tanabe, M. Shiga, H. Sugawara, H. Sato, J. Alloys Compounds 316 (2001) 245.
[254] A. Giguere, M. Foldeaki, W. Schnelle, E. Gmelin, J. Phys.: Condens. Matter 11 (1999) 6969.
[255] J. Herrero-Albillos, F. Bartolomé, L.M. García, F. Casanova, A. Labarta, X. Batlle, Phys. Rev. B 73 (2006) 134410.
[256] M. Forker, S. Muller, P. de la Presa, A.F. Pasquevich, Phys. Rev. B 68 (2003) 014409.
[257] A.M. Gomes, M.S. Reis, I.S. Oliveira, A.P. Guimarães, A.Y. Takeuchi, J. of Magn. Magn. Mater. 242–245 (2002) 870.
[258] K. Gu, J. Li, W. Ao, Y. Jian, J. Tang, J. Alloys Compounds 441 (2007) 39.
[259] R. Kuentzler, A. Tari, J. Magn. Magn. Mater. 61 (1986) 29.
[260] N.K. Singh, P. Kumar, K.G. Suresh, A.A. Coelho, S. Gama, A.K. Nigam, J. Phys. D: Appl. Phys. 40 (2007) 1620.
[261] N.K. Singh, P. Kumar, K.G. Suresh, A.K. Nigam, A.A. Coelho, S Gama, J. Phys.: Condens. Matter 19 (2007) 036213.
[262] N.H. Duc, D.T.K. Anh, J. Magn. Magn. Mater. 242–245 (2002) 873.
[263] N.H. Duc, D.T.K. Anh, P.E. Brommer, Physica B 319 (2002) 1.
[264] N.A. de Oliveira, P.J. von Ranke, M.V. Tovar Costa, A. Troper, Phys. Rev. B 66 (2002) 094402.
[265] N.A. de Oliveira, P.J. von Ranke, M.V. Tovar Costa, A. Troper, J. Appl. Phys. 91 (2002) 8879.
[266] W. Dunhui, T. Shaolong, H. Songling, S. Zhenghua, H. Zhida, D. Youwei, J. Alloys Compounds 360 (2003) 11.
[267] N.A. de Oliveira, P.J. von Ranke, J. Magn. Magn. Mater. 264 (2003) 55.
[268] A. Troper, P.J. von Ranke, N.A. de Oliveira, J. Magn. Magn. Mater. 272–276 (2004) 583.
[269] N.A. de Oliveira, P.J. von Ranke, A. Troper, Phys. Rev. B 69 (2004) 064421.
[270] N.A. de Oliveira, J. Phys.: Condens. Matter 20 (2008) 175209.
[271] N.A. de Oliveira, J. Magn. Magn. Mater. 320 (2008) e150.
[272] N.A. de Oliveira, Eur. Phys. J. B 65 (2008) 207.
[273] N.H. Duc, T. Goto, in: K.A. Gschneidner Jr., L. Eyring (Eds.), Handbook on the Physics and Chemistry of Rare Earths, vol. 26, Elsevier, 1999, p. 177.
[274] N.H. Duc, P.E. Brommer, Formation of 3d-moments and Spin Fluctuations in Some Rare-earth Cobalt Compounds, in: K.H. Buschow (Ed.), Handbook on the Magnetic Materials, vol. 12, Elsevier, 1999 (Chapter 3).
[275] E. Gratz, A.S. Markosyan, J. Phys.: Condens. Matter 13 (2001) R385.
[276] M. Sakoh, D.M. Edwards, Phys. Status Solidi (b) 70 (1975) 611.
[277] D. Bloch, R. Lemaire, Phys. Rev. 2 (1970) 2648.
[278] D. Bloch, D.M. Eduards, M. Shimizu, J. Voiron, J. Phys. F: Met. Phys. 5 (1975) 1217.
[279] J. Inoue, M. Shimizu, J. Phys. F: Met. Phys. 12 (1982) 1811.
[280] M. Shimizu, Rep. Progr. Phys. 44 (1981) 329.
[281] S. Khmeleveskyi, P. Mohn, J. Phys.:Condens. Matt. 12 (2000) 9453.
[282] E. Burzo, E. Gratz, V. Pop, J. Magn. Magn. Mater. 123 (1993) 159.
[283] H. Imai, H. Wada, M. Shiga, J. Magn. Magn. Mater. 140–144 (1995) 835.
[284] D. Gignoux, F. Givord, R. Lemaire, Phys. Rev. B 12 (1975) 3878.
[285] O. Syschenko, T. Fujita, V. Sechovsky, M. Divis, H. Fujii, J. Magn. Magn. Mater. 226–230 (2001) 1062.
[286] N. Pillmayr, G. Hilscher, E. Gratz, V. Sechovsky, J. de Phys. C 8 (1988) 273.
[287] see Ref. [10] pages 232–234.
[288] K.A. Gschneidner Jr., V.K. Pecharsky, S.K. Malik, Adv. Cryog. Eng. 42 (1996) 475.
[289] X.J. Niu, K.A. Gschneidner Jr., A.O. Pecharsky, V.K. Pecharsky, J. Magn. Magn. Mater. 234 (2001) 193206.
[290] J. Ćwik, T. Palewski, K. Nenkov, G.S. Burkhanov, O.D. Chistyakov, J. Klamut, J. Warchulska, J. Alloys Compounds 460 (2008) 41.
[291] N.A. de Oliveira, P.J. von Ranke, J. Magn. Magn. Mater. 320 (2008) 386.
[292] N.A. de Oliveira, P.J. von Ranke, Solid State Commun. 144 (2007) 103.
[293] N.A. de Oliveira, J. Alloys Compounds 455 (2008) 81.
[294] J. Ćwik, T. Palewski, K. Nenkov, G.S. Burkhanov, O.D. Chistyakova, N. Kolchugina, H. Madge, Physica B 358 (2005) 323.
[295] Niraj K. Singh, S. Agarwal, K.G. Suresh, R. Nirmala, A.K. Nigam, S.K. Malik, Phys. Rev. B 72 (2005) 014452.
[296] L. Néel, Ann. Phys. (Paris) 17 (1932) 64.
[297] L. Néel, Ann. Phys. (Paris) 3 (1948) 137.
[298] P.J. von Ranke, N.A. de Oliveira, B.P. Alho, E.J.R. Plaza, V.S.R. de Sousa, L. Caron, M.S. Reis, J. Phys.: Condens. Matter 21 (2009) 056004.